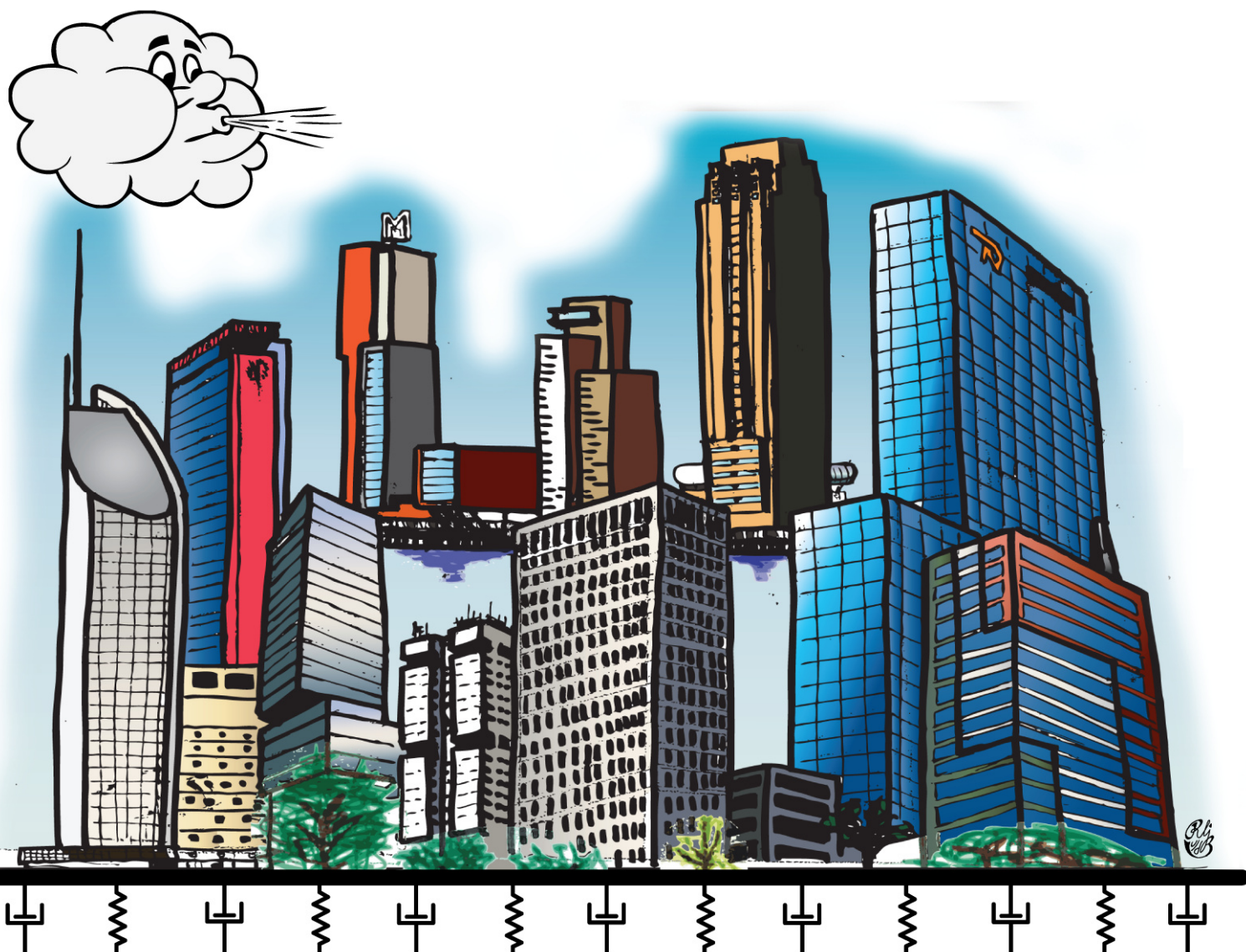


Investigation of damping in high-rise buildings

Identification and prediction of damping in the serviceability limit state for wind-induced vibrations



R.L.J. van den Berg
April 2012

Main report of Graduation project:

Investigation of damping in high-rise buildings
 Identification and prediction of damping in the serviceability limit state for wind-induced vibrations



Faculty of Civil Engineering and Geosciences
 Department: Design and Construction
 Specialization: Building Engineering, Structural Design

A project in cooperation with

TNO innovation
 for life

TNO bouw en ondergrond
 Van Mourik Broekmanweg 6
 Postbus 49
 2600 AA, Delft
 T: 088 866 30 00
 E: wegwijzer@tno.nl

abt

ABT bv
 Delfttechpark 12
 Postbus 458
 2600 AL, Delft
 T: +31(0)15 270 36 11
 E: info@abt.eu

Author:

R.L.J. van den Berg
 +31 639199546
ronaldvdberg@gmail.com
 student ID nr: 1316834

Graduation committee

Chairman:	Prof. R. Nijssse	TU Delft, CitG, Design and Construction
Supervisor:	Prof.dr. A. Metrikine	TU Delft, CitG, Structural mechanics
Supervisor:	Dr. ir. C.R. Braam	TU Delft, Citg, Design and Construction
Supervisor:	Dr. ir. R.D.J.M. Steenbergen	TNO bouw en ondergrond, Delft
Daily Supervisor:	ir. C.J. Scheffer	ABT bv, Delft

Preface

After ten months of work, I'm proud to present this master thesis as the result of my graduation project: *Investigation of damping in high-rise buildings: identification and prediction of damping in the serviceability limit state for wind-induced vibrations*. The project has been executed in order to finish my master education at the faculty of Civil Engineering and Geosciences at the Delft University of Technology. I've followed the specialization Structural Design which is part of the master program: Building Engineering.

This report isn't the only result of ten months of hard work. During the project, I've experienced very fruitful and happy times, but also very hard and frustrating times. I'm very thankful to my parents and my friends how helped me through these hard times. During this project I've got to know myself even better. I'm always expecting the best result and I can lose myself in perfecting the details. This can lead to very good results, but it takes a lot of time and progress is slow. This isn't always manageable. Sometimes it's better to let go of perfectness and go for the best possible result in the available time.

This project could not be completed without the help of several people and companies. Since the beginning of July, ABT offered me a workplace at their office in Delft. For this I'm very thankful. Their office is a good work environment. I would like to give special thanks to ir. C.J. Scheffer. She was my daily supervisor and she has guided me through the process. I'm glad that she was always available for support.

I'm also very thankful for the support of TNO. They provided me with measurements, which has been a key ingredient for this investigation. My special thanks goes to Dr. ir. R.D.J.M. Steenbergen. He made it possible to obtain the measurements and his knowledge about the subject was very useful. His positive attitude to the subject and his helpfulness kept me enthusiastic and motivated.

Next to these two persons of my graduation committee, I would like to thank the other three members. Dr. ir. C.R. Braam, for his practical review and comments on my project. Prof.dr. A. Metrikine for his help on solving the dynamical problems of my model and Prof. R. Nijse for his overview over the project and the leadership during the meetings.

Ronald van den Berg,
Delft, the Netherlands, April 11, 2012

Table of Contents

List of symbols	6
Abstract	8
1. Introduction.....	12
1.1. General	12
1.2. Problem	13
1.3. Objective	14
1.4. Outline of the report	14
2. High-rise Buildings	16
2.1. Definition.....	16
2.2. Important design aspects.....	17
2.3. Types of main load bearing structures.....	24
3. Dynamic response due to wind load	29
3.1. Situation	29
3.2. Wind load	30
3.3. Dynamical systems	36
3.4. Spectral analysis of the response.....	45
3.5. The influence of structural properties on the dynamic response.....	49
4. Damping in high-rise buildings	55
4.1. General	55
4.2. Measured values of damping in high-rise buildings.....	59
4.3. Theoretical mechanism behind damping.....	66
4.4. Prediction of damping	68
4.5. Sources of damping in high-rise building	71
5. Case studies.....	81
5.1. Structural characteristics.....	81
5.2. Influence of structural characteristics on damping.....	87
5.3. Conclusions.....	95
6. Model	99
6.1. Justification of the model.....	99
6.2. The free vibration	101
6.3. Calibration of the mass and stiffness parameters.....	104
7. Simulated dynamic behaviour.....	108
7.1. Assumed wind loading spectrum	109
7.2. The steady state response.....	110
7.3. Calibration of damping and load parameters	113
7.4. Conclusion	118
8. Conclusions and recommendations	119
Literature list	125

List of symbols

Used notations

\bar{x}	=mean of x	
\tilde{x}	=fluctuating part of x	
\hat{x}	=peak value of x	
σ_x	=root mean square (rms)/standard deviation of x	
S_x	=Fourier Transform of x	
S_{xx}	=variance spectrum of x	
X_i	=value of X in i^{th} mode	
$X_{e,i}$	=modal/effective value of X in i^{th} mode	
\dot{x}	=first derivative of x with respect to time (t)	
\ddot{x}	=second derivative of x with respect to time (t)	
x' or x^I	=first derivative of x with respect to the distance (z)	
x'' or x^{II}	=second derivative of x with respect to the distance (z)	
\mathbf{X}	=matrix X	
\underline{x}	=vector x	

Greek symbols

β_i	=ratio of stiffness and mass (i-th mode of vibration)	
γ	=measure for damping	
δ	=logarithmic decrement	-
ρ	=density	kg/m ³
ρA	=distributed mass density of a building	kg/m
$\underline{\phi}$	=eigen mode shape vector (i-th mode of vibration)	-
φ_i	=phase shift (i-th mode of vibration)	rad
χ	=aerodynamic admittance	-
σ	=stress	N/m ²
ω or Ω	=angular frequency of the load	rad/s
$\omega_{n,i}$	=natural angular frequency (un-damped system) for i^{th} mode of vibration	rad/s
$\omega_{1,i}$	=natural angular frequency (damped system) for i^{th} mode of vibration	rad/s
ζ_i	=damping ratio for i^{th} mode of vibration	-

Symbols

a	=acceleration	m/s ²
A	=area	m ²
b	=base width of the building, perpendicular to wind direction	m
c or c_T	=viscous damping	Ns/m

c_{σ}	=critical viscous damping	Ns/m
c_d	=distributed viscous damping	Ns/m ²
c_R	=rotational viscous damping	Nms/rad
C_f	=shape factor	-
C_w	=wind loading factor	N ² /m ²
d	= width of the building at its base, parallel to wind direction	m
d_{eff}	=width of lateral load resisting structure at base, parallel to wind direction	m
E	=modulus of elasticity	N/m ²
EI	=bending stiffness	Nm ²
E^*I	=internal viscous material damping	Nsm ²
f	=frequency	Hz
f_s	=sampling frequency	Hz
$f_{n,i}$	=natural frequency (i-th mode of vibration)	Hz
F	=force	N
GA_s	=shear rigidity	N
h	=building height	m
$h_{r,eff}$	=slenderness of the lateral load resisting structure (h/d_{eff})	-
h_r	=slenderness of the structure (h/d)	-
H_{xF}	=transfer function between x and F	
i	=number of mode	
I	=moment of inertia	m ⁴
k or k_T	=spring stiffness	N/m
k_R	=rotation spring stiffness	Nm/rad
I_v	=wind gust intensity	-
L	=gust length	m
m	=mass	kg
M	=moment	Nm
n	=measure for damping	1/s
n	=number of ...	-
N	=number of degrees of freedom/modes	-
p_w	=wind pressure	N/m ²
q	=distributed load	N/m
t	=time	s
u	=deflection	m
v	=velocity	m/s
z_0	=the aerodynamic roughness length	m
z_s	=reference height	m

Abstract

High-rise buildings are buildings in which the lateral load resisting structure has a slenderness larger than 5. Because of their slenderness the design of these buildings is dominated by the deflection due to horizontal wind forces. Traditionally a minimum stiffness is required to keep the maximum deflection at the top below the maximum allowable deformation of $h/500$. The Eurocode requires calculation of the maximum deformation in the serviceability limit state under a maximum mean wind velocity that occurs once per 50 years. This wind load needs to be enlarged by a factor ($c_s c_d$) to take into account the dynamical effects of the wind load on the structure.

The dynamic wind load will also introduce vibrations of the building. Especially high-rise buildings are sensitive for these vibrations, because in general their natural frequencies (0,1 - 0,5 Hz) correspond with the low frequency region in which the strongest wind gusts appear, causing resonance. Vibrations with large accelerations can be sensible for occupants and to avoid uncomfortable motions, the accelerations must be kept in the admissible area prescribed in ISO 10137

Increasing importance of the uncertain damping parameter

Most conveniently the peak deflection and acceleration can be calculated by considering the along wind response in the weakest direction of a building. The dynamic response can be calculated by making use of a spectral approach. In this approach the response spectrum of the deflection at the top, can be calculated by multiplication of the wind loading spectrum, the aerodynamic admittance function and the transfer function.

$$S_{u_{top}}(\omega) = \left| H_{u_{top},F}(\omega) \right|^2 \chi^2 S_{FF}(\omega) \quad (0.1)$$

Based on this formula, it has been derived that the maximum deflection mainly depends on the stiffness. The peak acceleration depends on: the mass, stiffness and damping ratio of the building.

$$u_{top,max} = \bar{u} + 3,5\sigma_u = \frac{F_{e,mean}}{k_{e,1}} + 3,5 \left[\frac{\sigma_{Fe}}{k_{e,1}} + \sqrt{\chi^2(\omega_{n,1}) S_{FF}(\omega_{n,1}) \cdot \frac{\pi\omega_{n,1}}{4\zeta k_{e,1}^2}} \right] \quad (0.2)$$

$$u_{top,max} \sim k_{e,1}^{-1} + k_{e,1}^{-1} + m_{e,1}^{0,39} \zeta^{-0,5} k_{e,1}^{-1,39}$$

$$a_{top,max} = 3,5\sigma_a = 3,5\omega_{n,1}^2 \sigma_u = 3,5\omega_{n,1}^2 \sqrt{\chi^2(\omega_{n,1}) S_{FF}(\omega_{n,1}) \cdot \frac{\pi\omega_{n,1}}{4\zeta k_{e,1}^2}} \quad (0.3)$$

$$a_{top,max} \sim m_{e,1}^{-0,61} \zeta^{-0,5} k_{e,1}^{-0,39}$$

Due to the application of new building materials and building techniques (high strength building materials and optimisation techniques) less material is needed to achieve the required stiffness. Therefore it can be expected that future high-rise buildings will become higher, more slender and lighter, which makes them more vulnerable to wind-induced vibrations, while the deflection criterion can still be satisfied. As a consequence the comfort criteria will become more governing in the design of future high-rise buildings.

To avoid large accelerations, it's not very practical to increase the mass. An increase of stiffness decreases the maximum allowable acceleration. Therefore an increase of damping is the most

effective and practical parameter to keep accelerations low. However, it is also the most uncertain parameter.

Structural designers normally use the damping values for reinforced concrete and steel buildings that are given in the Eurocode (steel: $\zeta=0,8\%$, concrete: $\zeta=1,6\%$). However most designers are not aware that the actual damping values can deviate a lot from these values (steel up to $\zeta=2-3\%$ and a minimum of $1,0\%$ for concrete buildings). The uncertainty around the damping value can lead to a larger risk for inserviceability or an economical inefficient design. To solve this problem a better identification and prediction of damping is needed.

Prediction of damping

From literature study it has been found that, besides material, many aspects influence the damping. Lagomarsino has given an empirical formula to estimate the damping based on the natural period and the applied building material. Based on the Japanese damping database, an empirical formula (AIJ2000) has been fitted that takes into account the natural frequency, the height, material and amplitude dependency of damping. However, comparison between the predicted values and the actual damping values still show a lot of scatter. This scatter is most probably caused by structural characteristics of the main load bearing structure, the non-structural fit out and the foundation.

Information has been gathered about the structural characteristics of 11 Dutch buildings. The influence of the structural characteristics on damping has been investigated by comparing the damping of different categories. Based on the conclusions from this investigation, a classification method (vdBerg) has been proposed to obtain a better damping prediction. On the basis of the following structural characteristics, buildings can be classified in a high, normal and low damping class. Subsequently, the damping can be estimated by the corresponding empirical function.

Table 1 –classification of a building

Main Load bearing Structure	Foundation	Non Structural Elements	Class	formula
steel structure with bolted braced/rigid frames	low rocking ratio (< 3,5)	many separation walls	high	$\zeta=3,24 \cdot (h/d)^{-0,31}$
(partly) prefabricated structure with rigid frames	low struct. Mass density (< 225 kg/m ³)			
other combinations			normal	$\zeta=2,32 \cdot (h/d)^{-0,22}$
cast in-situ, monolithic concrete, core/shear walls (coupled)	high rocking ratio ($\geq 3,5$) high struct. Mass density (≥ 225 kg/m ³)	few separation walls	low	$\zeta=1,76 \cdot (h/d)^{-0,31}$

In comparison with Lagomarsino's formula and the AIJ2000 formula, this method has resulted in a better estimation of the damping values. Still this estimation method needs to be further verified and improved. The conclusions must be based on the damping values of more buildings. Preferable the newest and most slender buildings must be monitored, because they will give the best reference for the future design. Also the amplitude dependency of damping needs to be determined to take into account as well.

Mathematical model; damping identification and design tool

A simple mathematical model (see Figure 1) has been developed to identify the amount of damping in different parts of the building. By comparison of the structural characteristics of many buildings with the found damping per part, structural characteristics can be linked to low/high values of damping in specific parts. With this information, the model can be used to optimize the design by a prediction of the total damping based on the damping in 4 parts.

The mass (ρA) and stiffness (EI , k_T and k_R) have been determined from design calculations. The unknown damping parameters (c_D , c_R , c_T and E^*I) and wind load parameter (C_w) have been calibrated by the method indicated in the following figure.

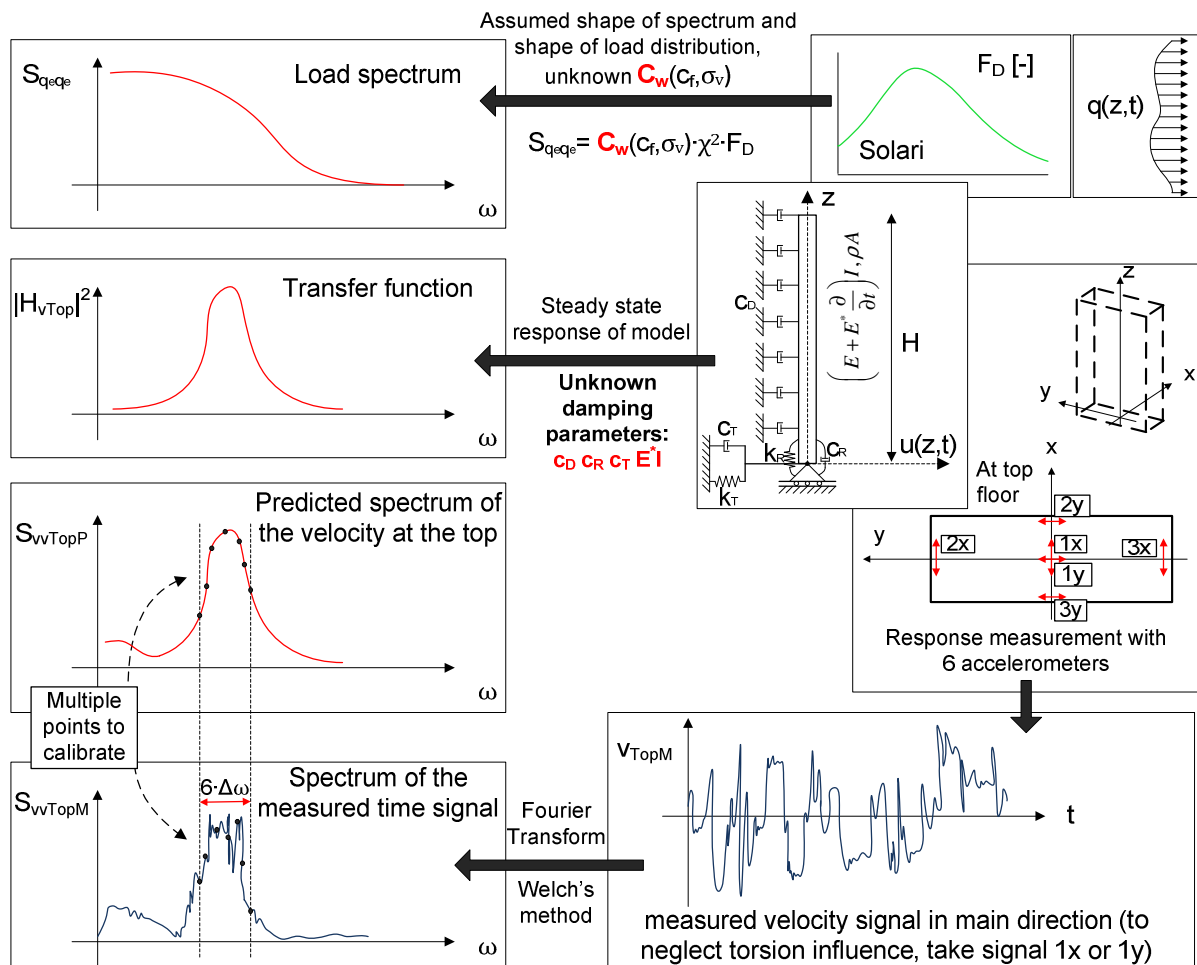


Figure 1 – overview of the method to obtain a spectrum of the predicted and measured velocity

The spectrum of the velocity at the top has been predicted for many values of C_w , c_D , c_R , c_T and E^*I . By comparison with the measured spectrum at the quasi static and the resonance peak of the first natural frequency (Figure 2), values for the best fitted combination have been found.

It is possible to give a reliable estimation of the load factor C_w but it is only possible to estimate the order of magnitude of the damping parameters. The influence of c_T can be neglected. The relative contribution of each damping source to the total damping can't be determined with this method because c_D , c_R and E^*I influence the resonance peak in the same way. Also many different

combinations can lead to a best fit. The measured response at the top is insufficient to determine the contribution of each damping source.

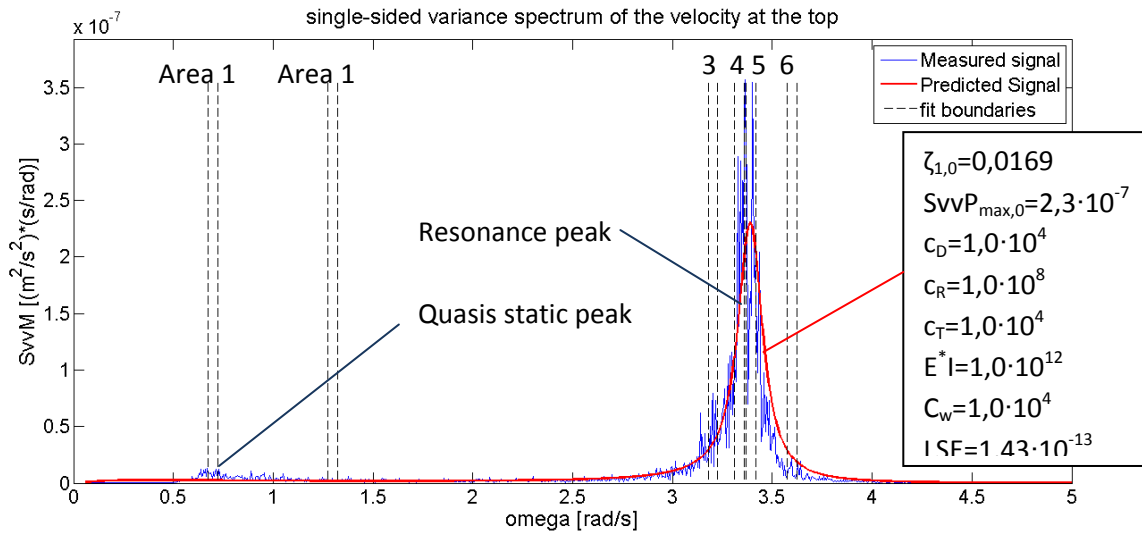


Figure 2 – predicted response from best fitted combination for the New EMC in x-direction

For better identification of the contribution of different damping sources, the method of measurement must be extended. Not only the deflection at the top needs to be monitored. To investigate the contribution of the damping in the foundation, also the rotation of the base must be monitored. The damping of the casco and the completed building must be determined to investigate the influence of the non-structural elements. In order to really investigate the influence of one structural characteristic, it is also advised to perform a serie of dynamic tests on scale models of high-rise buildings in which one structural aspect can be changed and the others are kept constant.

1. Introduction

1.1. General

Already since ages, people are making towers. Even children have a natural need to build a tower. Place a kid in a room with many blocks and it will make a tower, preferably as high as possible.

The history of mankind also shows multiple examples of very high towers. The bible told us the story of the tower of Babylon, the Egyptians created the pyramids, the French built the Eiffel tower and the skyline of Manhattan is crowded with skyscrapers. High buildings were built to reach for the sky, to honor mighty kings, to impress people and were used as a symbol of status. Most recently the highest building in the world has been finished; the Burj Khalifa, in Dubai, has a height of 828 m and is really a symbol of the richness of this small oil state.

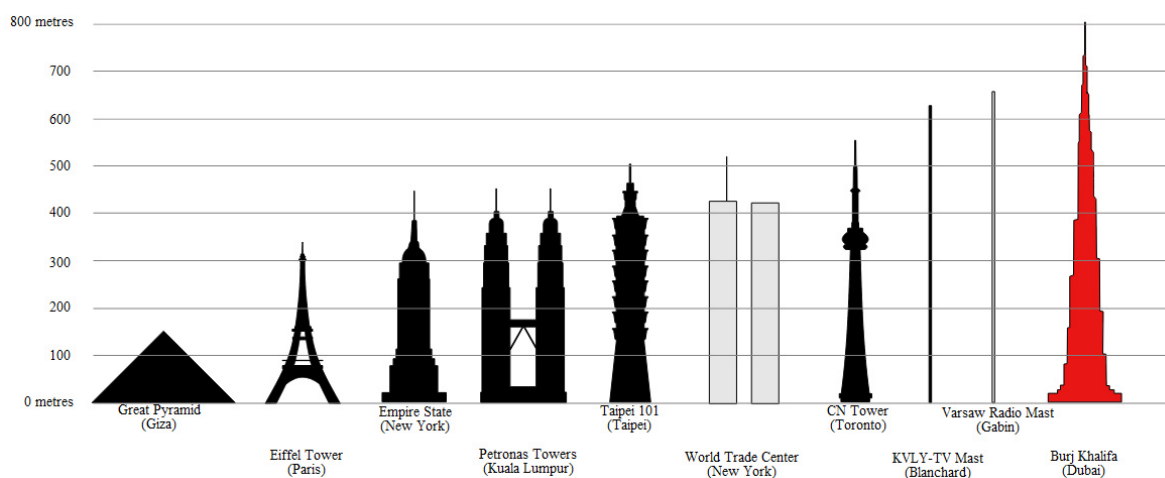


Figure 3 – chart of characteristics high buildings throughout the history of mankind
[Lijst Van Hoogste Gebouwen Ter Wereld, 2012]

High-rise buildings are impressive buildings. But the high-rise buildings are also becoming a necessary need. During the last age, the world has become increasingly urban. At the end of the twentieth century, around 46% of the world population lives in urban areas. This percentage will continue to grow. [Hayden, 2009, pp. 10-29] To create living and work space for more people on a small area of land, more and higher buildings need to be built.

Because of their slenderness, high-rise buildings are sensitive to dynamic horizontal loads like wind and earthquakes. These loads can lead to unpleasant vibrations and the design of high-rise buildings is dominated by dynamic horizontal loads. The new generation of high-rise buildings will become even more sensitive to these loads. In higher buildings, stresses and deflections due to lateral loads will become increasingly larger because the wind loads increase exponentially with the height. Higher buildings will also be more slender because the width of the buildings may be limited (for example because of daylight requirements). The application of new building materials and building techniques results in lighter structures. High-rise buildings of this new generation which are more slender and lighter are more sensitive to dynamic loading, but still need to fulfill their structural requirements. [Oosterhout & Geurts, 2001; Woudenberg & Vambersky, 2003]

In the Ultimate Limit State (ULS), the building must be strong enough to provide structural safety during infrequent severe events such as heavy earthquakes and heavy storms/typhoons. In the

Serviceability Limit State (SLS), the building must be stiff enough to allow functional use of the building during more frequent events such as moderate earthquakes and strong winds. Two serviceability requirements must be met, namely: restrictions to the lateral deflection must be met to provide integrity of structural components and the maximum lateral acceleration is restricted to provide human comfort.

Traditionally, a maximum drift index (the ratio between maximum deflection and building height) of $h/500$ is dominant in the design of the building's lateral load resisting structure. However meeting this requirement, doesn't also imply that the comfort criterion concerning accelerations is met. [B.S. Smith & Coull, 1991, p. 12] Especially for the new generation of high-rise buildings which are more slender and lighter, the comfort criterion may become more governing as can be concluded from the figure below. (The ISO-criterion is the maximum allowable acceleration.)

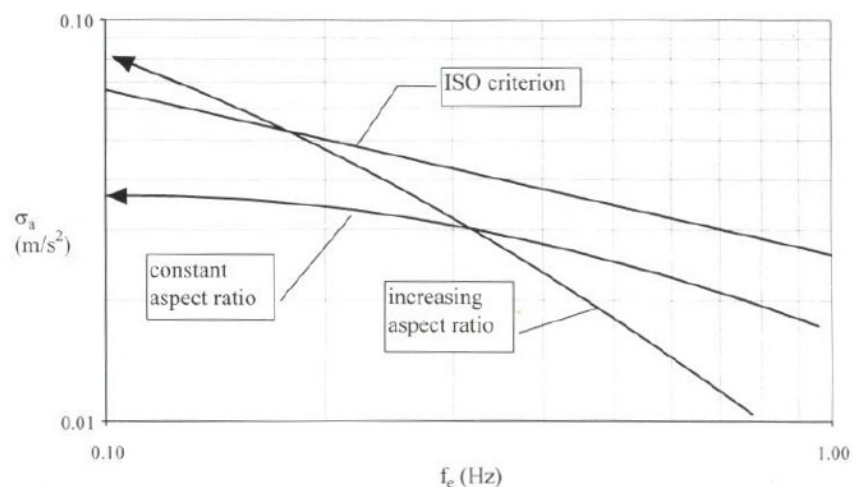


Figure 4 – influence of the slenderness (aspect ratio) on the acceleration in relation to the criterion [Oosterhout, 1996, p. 51]

The dynamic behaviour of high-rise buildings under dynamic loading depends on three parameters: the natural frequency of the building, depending on mass and stiffness and the damping of the building. Concerning accelerations for a slender building, damping is the most important parameter. [Oosterhout, 1996, p. 51]

It can be concluded that for the dynamic behaviour of future high-rise buildings, the importance of damping in the design grows. Therefore this thesis aims at an investigation of damping properties of high-rise buildings.

This study is limited to the Dutch high-rise scene, because of the available measurements and structural information on high-rise buildings. Since no severe earthquakes occur in the Netherlands, only wind-induced vibrations have been considered.

1.2. Problem

The natural frequency and the damping are the most important factors that influence the dynamic behaviour of a high-rise building.

There are multiple empirically based formulae to estimate the natural frequency in the early design phase. It can be determined more accurately when a finite element model of the building and its foundation is available, in which the stiffness and mass of different components is specified. The

stiffness may be influenced by cracking, but modern finite element packages are also able to take this into account. The natural frequency can be estimated with enough accuracy in the design phase.

For damping, it is not possible to give reasonable predictions based on finite elements models because of complex mechanisms and the contribution of non structural elements. Based on full scale measurements, predictors of damping exist. However predictors show significant scatter because the amount of damping depends on many factors which most predictors don't take into account (material, type of structural system, type of foundation, type of non-structural elements, etc.). This makes these estimators unreliable.

For reinforced concrete and steel buildings damping values have been prescribed in the Eurocode. A lower damping value is given for steel buildings because of the lower internal material damping of steel. This doesn't seem right, because damping not only depends on the used material. In fact, there are examples of steel buildings where higher damping has been measured than in reinforced concrete buildings. [Kijewski-Correa & Pirnia, 2007; NNI, 2007a; R.J. Smith, et al., 2010; Steenbergen & Geurts, 2011]

Due to this uncertainty, damping can be overestimated or underestimated in the design phase, leading to undesired effects. At overestimation, the structure may be subjected to large accelerations, leading to discomfort. Also deflections may become larger, leading to damage of non-structural elements. At underestimation, the stiffness of the building has been increased unnecessary in order to fulfill the strength and serviceability requirements. More or stronger material increases costs and larger elements reduce saleable floor space. [R.J. Smith & Willford, 2008]

Estimations of damping are based on used building material and lead to large uncertainty around damping, while it will become an increasingly important parameter for the design of future high-rise buildings. A better estimation is needed to generate more efficient and economical designs and reduces the risk on unwanted dynamic behaviour.

1.3. Objective

Diverse structural characteristics influence the structural damping of a high-rise building, while estimators are only based on material. The goal of this research is to study the influence of structural characteristics on the structural damping. On the basis of this knowledge, it should be possible to give a better prediction of the structural damping in the design phase of a high-rise building in the Netherlands.

1.4. Outline of the report

This report has 3 parts. The results of the literature study (ch. 2 to 4), the case studies (ch. 5) and the development and application of a dynamic model (ch. 6. and 7).

Chapter 2, 3 and 4 contain the results of the literature study. In chapter 2, a definition will be given for high-rise buildings, important aspects in the design of a high-rise will be described and different types of structural systems to construct a high-rise building will be distinguished. Secondly in chapter 3, it will be explained how the dynamic behaviour of high-rise buildings under wind load can be predicted. It will be explained how a dynamic wind load is taken into account and how a building can be schematized in order to calculate the response. From this theory, the influence of important

parameters will be given. Damping is one of these important parameters. Since this study focuses on damping properties of high-rise buildings, and the relation with its structural properties, the most important information available from literature, concerning this subject, is presented in chapter 4. Results of damping measurements from literature have been collected, as well as prediction methods based on these results and theories about the actual mechanisms behind the damping of a high-rise building. In the last two sections it will be described what the sources of damping in a high-rise building are and what structural characteristics have to be investigated because they influence these sources.

Chapter 5 contains the result of 11 case studies. On the basis of the literature study, information about selected structural characteristics of these buildings has been gathered. The natural frequency and damping of these buildings have also been collected from monitoring of their dynamic behaviour. With this information, relations between some structural characteristics and damping can already be observed and described. A new method has been proposed in which damping is estimated on the basis of a high, normal or low damping class, depending on the structural characteristics.

Chapter 6 and 7 describe the dynamical model that has been developed to identify the damping in different parts and to be used as a design tool. In chapter 6 the model will be introduced. An expression for the free vibration will be given and it will be described how the mass and stiffness parameters have been adapted to match the predicted and measured natural frequency. In chapter 7 it will be described how the unknown damping and load parameters in the model have been calibrated and how reliable the results are.

This report ends with the conclusions and recommendations in chapter 8.

2. High-rise Buildings

To start an investigation of damping in high-rise buildings, it is first important to give a definition of a high-rise building. Secondly it is important to investigate the different design aspects to find what are the most important design aspects concerning damping. High-rise buildings can also be designed in different ways, so the most common types of main load bearing structures will be described in the third section to clarify the differences.

2.1. Definition

A high-rise building is a very tall building. Tallness is a relative concept, so no universally measurable definition of tallness can be given. Whether a building is tall depends on someone's own perception and the environment in which the building has been built. However from a structural point of view, a high-rise building can be defined as:

"A tall building may be defined as one that, because of its height, is affected by lateral forces due to wind or earthquake actions to an extent that they play an important role in the structural design."
[B.S. Smith & Coull, 1991, p. 1]

Not only the height plays an important rule, also the width of the building is important. The smaller the width of the lateral load resisting structure, the smaller the lever arm to resist the moment due to wind. Increasing slenderness leads to higher stresses at the base of the building due to horizontal loading.

In this thesis, a building with an slenderness of the lateral load resisting structure larger than 5 is defined as a high-rise building ($h_{r,eff}=h/d_{eff}>5$) because in general the effect of lateral forces will play an important role in the structural design of these buildings. [Hoenderkamp, 2007, p. 2]

Dutch high-rise buildings are relative low in comparison with high-rise buildings in the rest of the world because daylight regulations allow a maximum depth for offices of 7,2 m. The width may be limited to 14,4 m and a corridor, such that buildings of 80 m high can already be defined as high-rise.

Dimensions

The orientation of the building in the coordinate system and the definition of its dimensions are indicated in Figure 5.

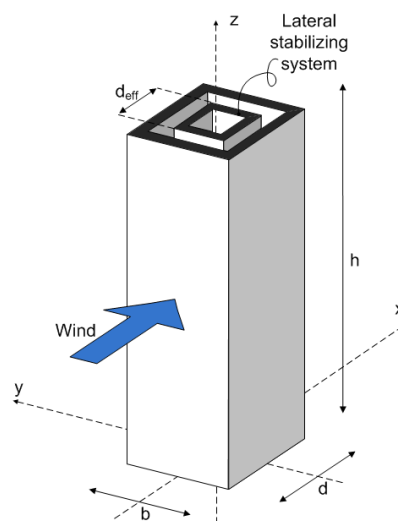


Figure 5 – definition of dimensions

2.2. Important design aspects

Different designs are possible to fulfill structural requirements regarding strength, stiffness and stability. The most important design aspects will be illustrated by considering the most common type of main load bearing structure for a high-rise building: a core structure.

Except for the rigid frame system, the structural behaviour of other systems (shear walls, braced frames, outrigger systems and tube systems, see §2.3) is comparable with a core structure because deformation is mainly caused by bending. Rigid frame systems show also considerable shear deformation. Therefore this system is less applied in high-rise buildings (see Figure 11 and Figure 12) because it is less stiff and not very efficient to stabilize the building.

For simplicity, a building with a rectangular lay-out, constant over height, stabilized by a central (concrete) core is considered in its weak direction to illustrate the most important design aspects.

2.2.1. Stability

The most fundamental requirement for a high-rise building is that the building doesn't tip over as a rigid body, under the applied lateral forces. In order to prevent this, the resisting moment of the dead weight with respect to the edge must be larger than the overturning moment caused by the horizontal wind forces.

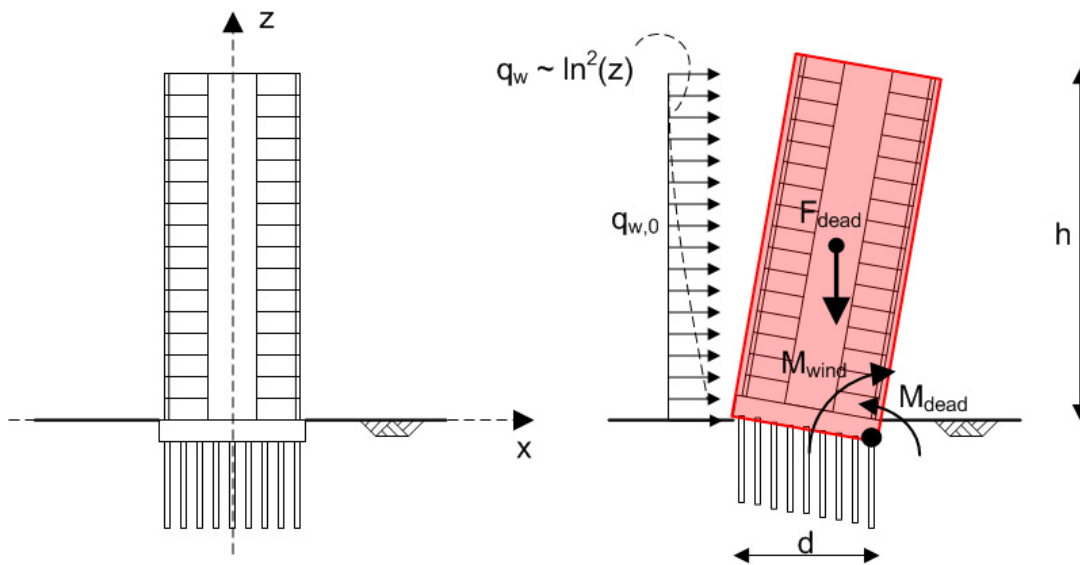


Figure 6 – left: high-rise building with core, right: stability problem

When it is assumed that one pile can provide all the required vertical reactions:

$$M_{wind} = \int_0^h q_w(z) \cdot z \cdot dz = \frac{1}{2} q_{w,0} z^2 \quad (2.1)$$

$$M_{dead} = \frac{1}{2} \cdot d \cdot F_{dead} \quad (2.2)$$

The requirement is:

$$M_{dead} > M_{wind} \quad (2.3)$$

If this requirement is not met, foundation piles must be designed to resist the large tensile forces. This must be prevented as much as possible, because the tensile force in piles is restricted or tensile piles are more expensive.

2.2.2. Strength

The strength requirement demands that the building structure has enough strength to resist the most critical combination of loads in order to avoid failure of the structure and to provide safety for the users. An analysis of the magnitude and location of the highest stresses is needed and the stress must be lower than the allowable stress in the material.

Critical stress under vertical and horizontal load

The load bearing structure must transfer the vertical loads and the horizontal loads to the foundation. The vertical loads consist out of dead and live loads and cause a uniform compressive stress distribution at the bottom. The maximum compressive stress at the base increases linear with increasing building height, Figure 7.

The horizontal wind force causes a moment at the base of the structure, resulting in maximum compressive/tension stress at the edge of the stabilizing structure. The maximum occurring stress at the edge, increases more than quadratic with increasing building height, because at constant wind pressure ($q_{w,0}$) the moment depends on z^2 (see Eq. (2.1)) but the (mean) wind pressure (q_w) also increases over height as a function of $\ln^2(z)$, see appendix B.4.

If the maximum compressive stress due to vertical load is larger than the maximum tensile stress due to the horizontal load, there is no tension at the bottom and the maximum compressive stress is critical. Otherwise, tensile stress occurs in the stabilizing element and especially for concrete which has a low tensile strength, this becomes governing.

As the maximum stress decreases with building height, the required cross sections also decrease. Smaller wall thicknesses and smaller columns can be used in the top part of the building to efficiently use the material.

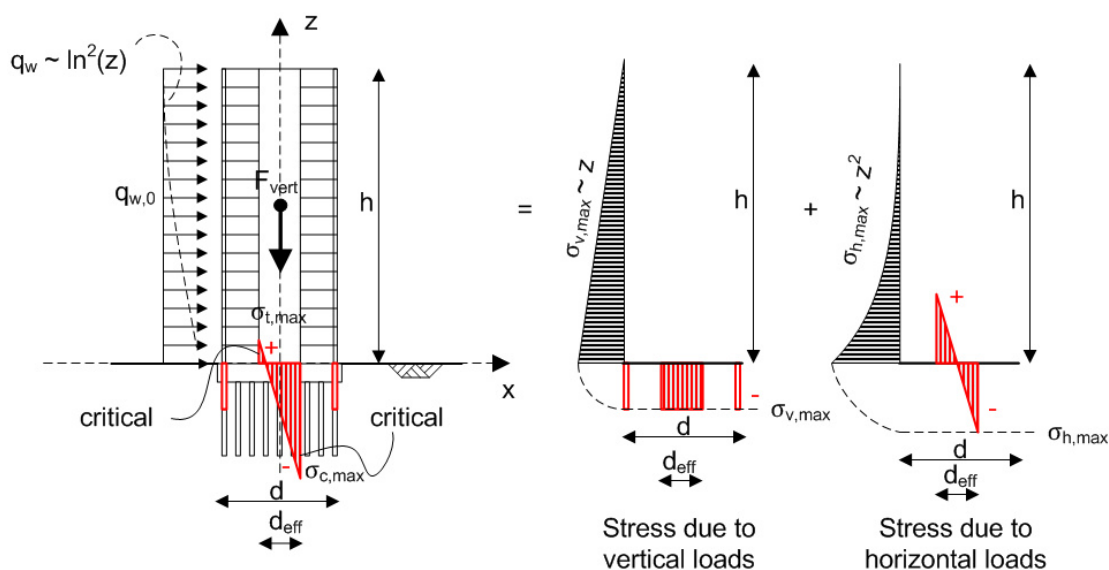


Figure 7 – strength: maximum occurring stresses in a high-rise building due to vertical and horizontal load

Because the core can be modeled as an Euler Bernoulli beam (see page 19) , the maximum stress can be calculated with:

$$\sigma_{h,\max} = \pm \frac{M_{wind} \cdot \frac{1}{2} d_{eff}}{I_{core,xx}} \quad (2.4)$$

$$\sigma_{v,\max} = - \frac{F_{vert}}{A_{core+columns}} \quad (2.5)$$

The maximum compression/tensile stress at the edge of the core is equal to:

$$\sigma_{\max} = - \frac{F_{vert}}{A_{core+columns}} \pm \frac{M_{wind} \cdot \frac{1}{2} d_{eff}}{I_{core,xx}} \quad (2.6)$$

Local stress increasing effects

Besides the horizontal and vertical loads, other effects can locally lead to higher stresses. Because of the height and large vertical loads, shortening in time due to creep, shrinkage and/or elastic deformation is significant and can lead to local stress increase in elements. Elements will also significantly shorten/extend under the influence of temperature differences. These effects should be taken into account and require proper detailing. [B.S. Smith & Coull, 1991, §2.6] Because this thesis focuses on the effect of wind on the total system, these local effects have been neglected.

Other effects

Failure of a critical member can initiate a progressive collapse of part of or an entire building. Special provisions have to be taken to avoid progressive collapse.

During a fire, stiffness and strength of the material decrease due to high temperatures. As a consequence large deflections or collapse can occur when the temperature increases in time. Again, special provisions have to be taken to protect the structural members against fire and secure the structural integrity as long as needed to provide occupants a safe escape.

2.2.3. Stiffness

A high-rise building deforms under the horizontal wind loading. Traditionally the drift index (the ratio between maximum deflection and building height) has been restricted to 1/500 of the structural height to prevent large second order effects, malfunction of nonstructural components (elevators, doors etc.) and cracking of concrete and consequently loss of stiffness. [B.S. Smith & Coull, 1991, p. 12]

Bending and Shear deformation

The deformation of a high-rise building is comparable with the deformation of a clamped beam that deforms due to bending and shear deformation. The differential equation for the bending deformation has been derived by considering an Euler Bernoulli beam, the differential equation for the shear deformation by considering a shear beam. Assuming constant load $q_{w,0}$ and application of the boundary conditions of the clamped beam, the expression for the deflection over height has

been derived [Simone, 2009]. Substituting $z=h$, leads to the well known expressions for the deformation at the top.

Bending deformation:

$$EI \frac{d^4 u}{dz^4} = q(z) \quad (2.7)$$

$$u(z) = \frac{q_{w,0}}{24EI} (z^4 - 4z^3h + 6z^2h^2) \rightarrow u(h) = \frac{q_{w,0}h^4}{8EI} \quad (2.8)$$

Shear deformation:

$$GA_s \frac{d^2 u}{dz^2} = q(z) \quad (2.9)$$

$$u(z) = \frac{q_{w,0}}{2GA_s} (2hz - z^2) \rightarrow u(h) = \frac{q_{w,0}h^2}{2GA_s} \quad (2.10)$$

Total deformation:

$$u(h) = \frac{q_{w,0}h^4}{8EI} + \frac{q_{w,0}h^2}{2GA_s} \quad (2.11)$$

In general, both deformations should be taken into account, but for slender beams (>5), the shear deformation is small compared to the bending deformation and can be neglected. [Blaauwendraad, 2006, p. 45; Simone, 2009, p. 30] Even when openings in the concrete walls introduce some more shear deformation, this deformation can be neglected for concrete cores because this system has enough shear rigidity (GA_s). [Tolsma, 2010]

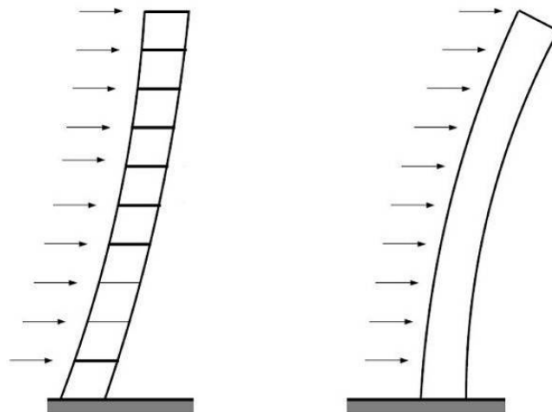


Figure 8 – shear deformation and bending deformation of a clamped beam [Tolsma, 2010]

In rigid frames, shear deformation will be larger and also has to be taken into account for the total deflection. Therefore these systems act less stiff and are less applicable in high-rise buildings. In this thesis, the Euler Bernoulli beam is adopted as a model suited to describe the deflection of a high-rise building.

Total deformation

In reality, the foundation rotates, and must be modeled as a rotation spring. For a constant wind load, the deformation at top can easily be calculated as a summation of the deflection due to rotation of the foundation and bending of the building.

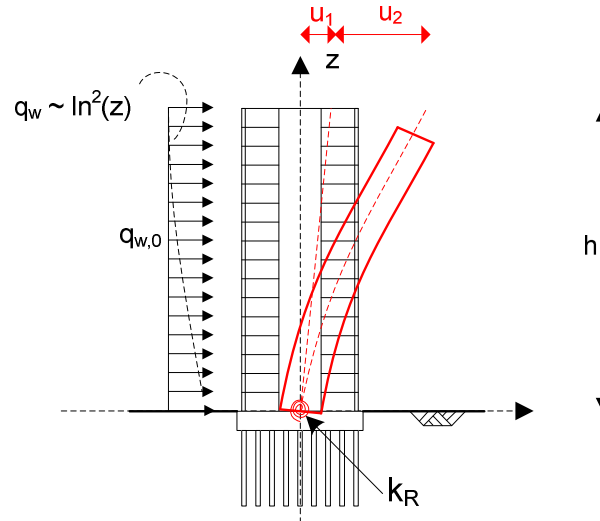


Figure 9 – deformation due to rotation of the foundation and bending of the building

$$u_{tot} = u_1 + u_2 = h \cdot \frac{M_{wind}}{k_R} + \frac{q_{w,d} \cdot h^4}{8 \cdot EI} \leq \frac{h}{500} \quad (2.12)$$

$$h \cdot \frac{\frac{1}{2} q_{w,0} \cdot h^2}{k_R} + \frac{q_{w,0} \cdot h^4}{8 \cdot EI} \leq \frac{h}{500}$$

The minimum required stiffness can be calculated by rearrangement of the terms:

$$EI \geq \frac{500 \cdot q_{w,0} \cdot h^3}{8} - \frac{h \cdot k_R}{4} \quad (2.13)$$

2.2.4. Influence of slenderness

The large (effective) slenderness is characteristic for tall buildings. Doubling the slenderness has the following consequences with respect to the criteria on stability, strength and stiffness. [Hoenderkamp, 2007, pp. 3-4]

- The uniform stress due to vertical loads at ground level, increases with a factor $2^1=2$
- The overturning moment increases to the power two, the dead weight moment increases to the power one because the width of the building remains equal. The unity check for the stability problem increases with a factor $2^1=2$.
- The overturning moment increases to the power two, the maximum stresses due to wind loading increases with a factor $2^2=4$
- The deflection at the top increases to the power 4, so the maximum deflection increase with a factor $2^4=16$

- The drift index is the deflection at the top divided by the height, so the drift index increases to the power 3, thus the drift index increases with a factor $2^3=8$

2.2.5. Governing design aspect

From the consideration in the former subsection, it seems logic to use the drift index as a leading requirement in the design of high-rise buildings, because it increases most with increasing slenderness. However, this consideration doesn't include an increase of maximum wind pressure with increasing height and the dynamic behaviour of high-rise buildings.

An increase of wind pressure affects the overturning moment and the deflection to the same degree because they both depend on the integral of the wind pressure over height. Still the drift index requirement is governing in the design.

So far, only static situations (loads and response don't change in time) have been discussed for the building's design. The response due to this mean wind load depends on height and lateral stiffness.

However, dynamic loads cause changing displacements in time, the building will vibrate. Especially high-rise buildings are sensitive for these vibrations because in general their natural frequencies lie between 0.1 and 0.5 Hz. [Hoenderkamp, 2007, p. 121]. Because the strongest wind gusts also appear in this low frequency region (see Figure 26) resonance occurs, causing dynamic displacements additional to the static deflections.

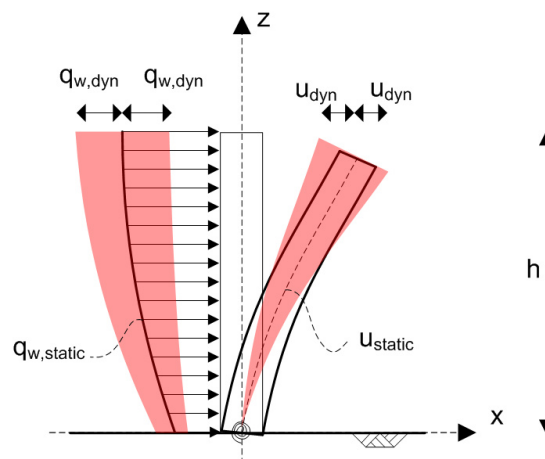


Figure 10 – increasing static (mean) wind load and dynamic bandwidth of loading and displacement.

The dynamic behaviour can't be neglected, but structural building engineers have the tendency to avoid dynamic calculations. Therefore designers multiply the static wind load with a dynamic amplification factor (see appendix A.1 and B.1) to obtain an increased static deflection to take dynamic effects into account. This is called the quasi-static calculation.

However, vibrations with large accelerations can be sensible and uncomfortable for humans. Therefore it is important to study the displacement of the building in time. This behaviour is more complex than the static calculations because the response not only depends on lateral stiffness and height, but also on the mass, the geometry, the damping of the building and the characteristics of the dynamic wind load. For now it can be concluded:

For a high-rise building, satisfaction of the drift index restriction by taking into account a dynamic factor in a quasi-static calculation doesn't automatically imply that human comfort is granted, thus the maximum accelerations have to be studied by a dynamic analysis. [B.S. Smith & Coull, 1991, p. 12]

2.2.6. Acceleration

It is generally agreed that human comfort is related to acceleration. There is however no general accepted restriction. In appendix D an overview is given of three multiple criteria. In this thesis the restriction recommended in the Eurocode 0, ISO 10137 has been adopted. For frequencies below 1 Hz, this criterion is based on the ISO6897, so for high-rise buildings that have natural frequencies below 1 Hz, this can be used as an equivalent.

Both NEN6702 and Eurocode provide a formula to calculate the maximum peak acceleration, (Appendix A.6 and B.5.2) and the accelerations can be checked. The influence of structural parameters behind these formula is unclear because the procedure is complicated. Therefore the theory behind the dynamic behaviour of high-rise buildings will be explained in the next chapter.

It will be made clear that for the new generation of high-rise buildings the human comfort criterion will become more governing for the design of high-rise buildings. It shall also be explained that damping is the most important parameter considering this criterion.

2.3. Types of main load bearing structures

The main load bearing structure (MLBS) of a high-rise building must be designed to transfer the horizontal and vertical loading to the foundation while fulfilling the requirements concerning, strength, stiffness, stability and accelerations. The most used materials in the MLBS of high-rise buildings are reinforced concrete and steel. The different types of construction and their maximum height of application are indicated in the two figures below and their characteristics are described in the following subsections.

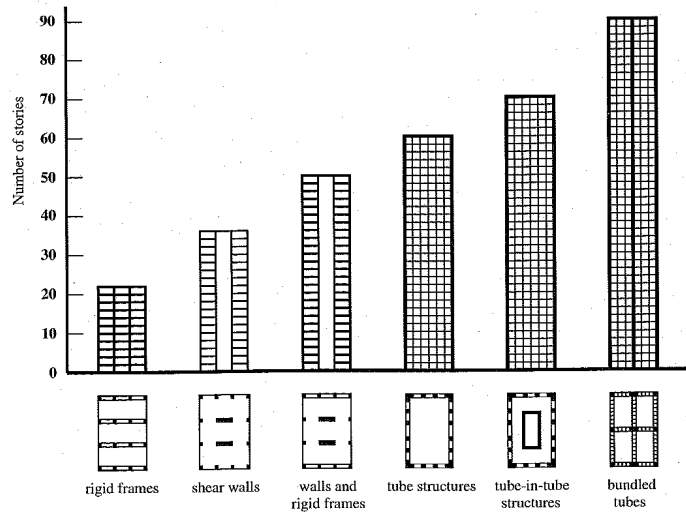


Figure 11 - Lateral load resisting structures in reinforced concrete [Hoenderkamp, 2007]

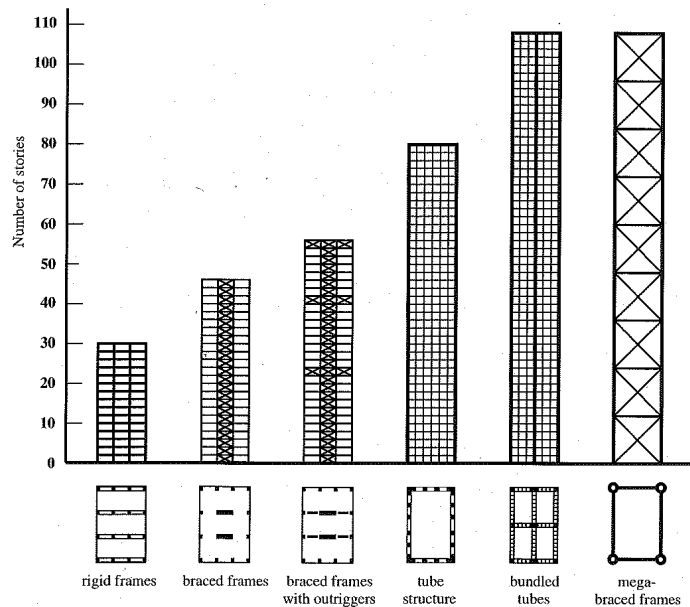


Figure 12 - Lateral load resisting structures in steel [Hoenderkamp, 2007]

Many variations on these types exist. Different types and materials can be combined and in addition extra vertical elements can be needed to transfer the vertical loads to the foundation. In the next subsections, it will be described how these different structural systems transfer the loads to the foundation.

2.3.1. Rigid Frame system

In a rigid frame system, the horizontal stiffness is provided by un-braced frames. Beams and columns are jointed together with moment resistant connections. The horizontal loading is transferred to the foundation by bending action of the columns and beams. Because the horizontal load is transferred by bending in the elements, the shear rigidity (GA_s) is low, causing large shear deformation. Therefore a rigid frame is not very effective in transferring horizontal loads to the foundation. [Hoenderkamp, 2007] An advantage of the system is that the frames provide more open functional space in comparison with shear walls and trussed frames.

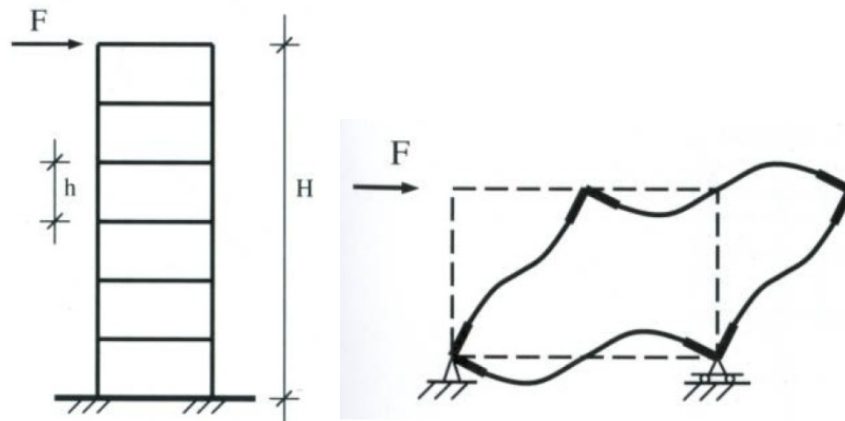


Figure 13 – Un-braced frame system with deformation of one frame [Hoenderkamp, 2007]

2.3.2. Shear wall systems

In a shear wall system, the horizontal stiffness is provided by massive walls. These walls have high in-plane stiffness. The walls are clamped to the foundation and the horizontal forces are transferred to the foundation by bending of the walls. Walls in different directions are necessary to provide stiffness to resist wind loading from different directions.

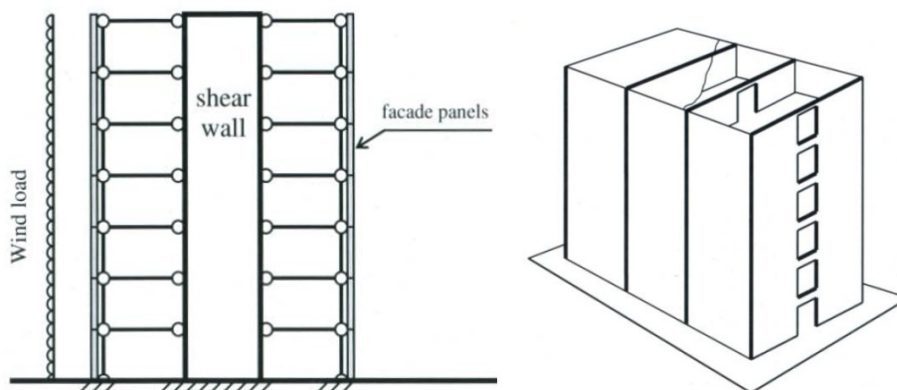


Figure 14 - shear wall system, coupled shear wall system [Hoenderkamp, 2007]

In coupled shear wall systems, the horizontal stiffness is provided by two or more shear walls in different directions that are connected by the floors and the floor beams. The horizontal load is transferred to the foundation by bending of the coupled shear walls. The cooperation between the coupled shear walls depends on the stiffness of the connection.

2.3.3. Core structures

Coupled shear walls are often shaped into three-dimensional core structures. The horizontal stiffness of the building is provided by the bending of the core. Inside the core, elevators, stairs, ducts etc. are situated. Floors are attached to the core and are supported by beams around the perimeter of the building.

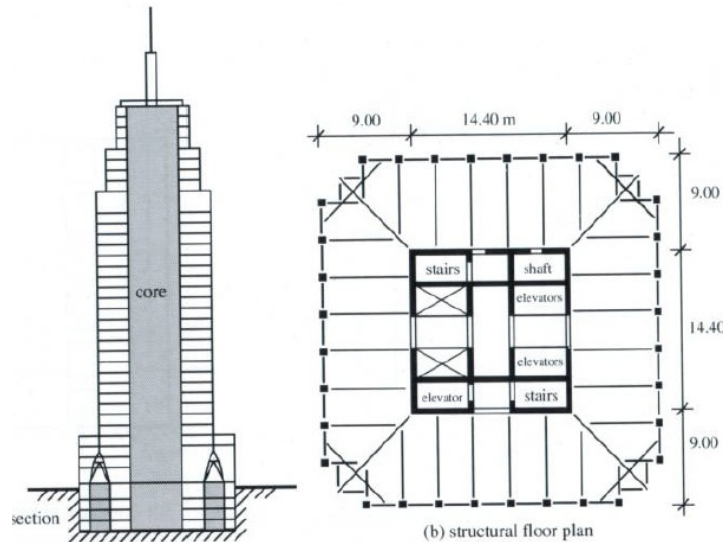


Figure 15 - core system [Hoenderkamp, 2007]

2.3.4. Braced frame systems

In braced frames, the horizontal stiffness is provided by braced frames. Connections between columns, beams and diagonals are hinges. The horizontal load is transferred to the foundation by pure axial deformation of the elements. Bending of the frame activates axial deformation of the vertical members, while the shear mode activates the diagonals.

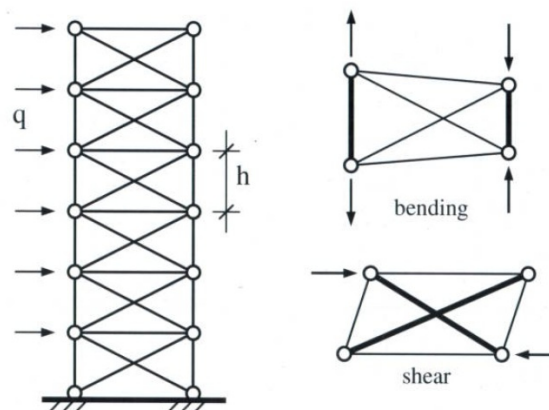


Figure 16 - Trussed frame system, mechanism behind bending and shear. [Hoenderkamp, 2007]

Since elements are very stiff in axial direction, this system is a very efficient way to transfer the horizontal loads to the foundation. However, the diagonal braces in the frames make it difficult to use the space in the frames. [Hoenderkamp, 2007]

2.3.5. Outrigger systems

In an outrigger system the horizontal stiffness is provided by central walls or frames that are connected to columns in the façade by an outrigger. In this way, the façade columns will also participate in resisting the horizontal loads. The axial compression and tension force form a bending moment, opposite to the moment due to horizontal loading. This reduces the maximum lateral moment, located at the base.

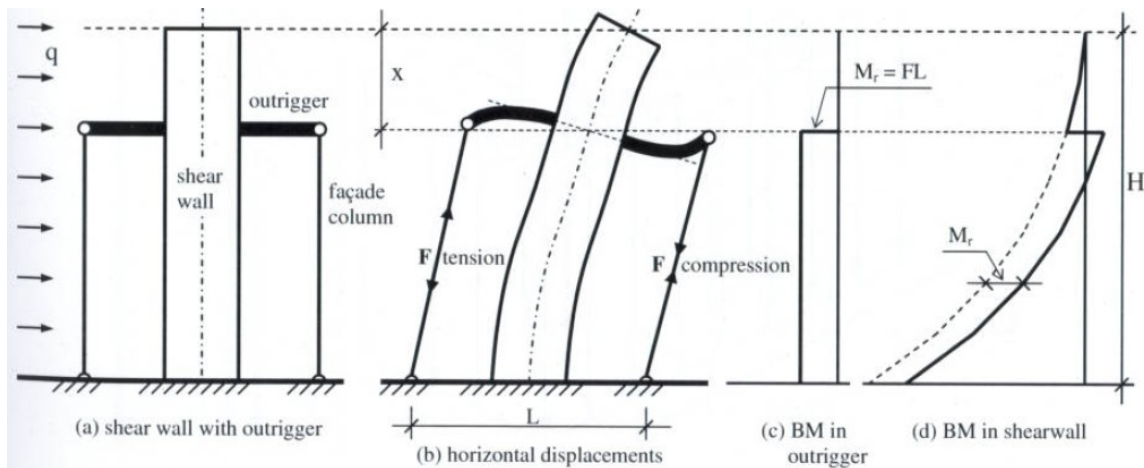


Figure 17 - Shear wall system with outriggers and moment diagrams [Hoenderkamp, 2007]

2.3.6. Tube Structures

In tube structures, the horizontal stiffness is provided by a steel or concrete tube with small openings for windows. The basic idea behind the tube is to place as much as possible material around the perimeter of the building to maximize the moment of inertia. The horizontal loads are transferred to the foundation by the façade that acts like a rigid frame. An ideal stress distribution (according to the Euler Bernoulli bending beam theory) is shown in Figure 18, but because of shear lag, peak stresses occur in the corners of the building. [Hoenderkamp, 2007]

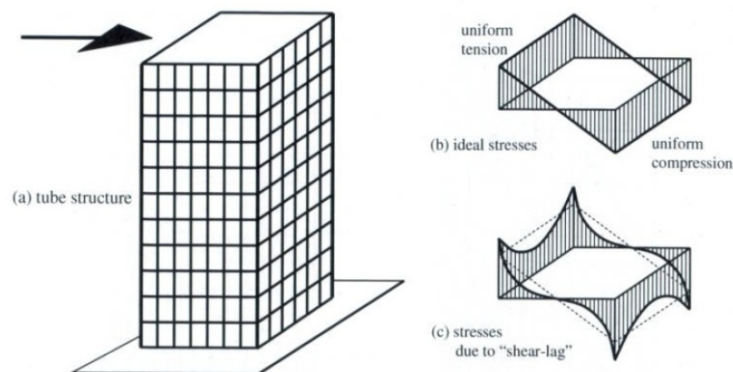


Figure 18 - Tube structure [Hoenderkamp, 2007]

As a consequence of the shear lag, the middle columns aren't used effectively. The shear lag can be minimized by application of mega diagonals in the façade, using belt structures or by division of the tube in smaller tubes.

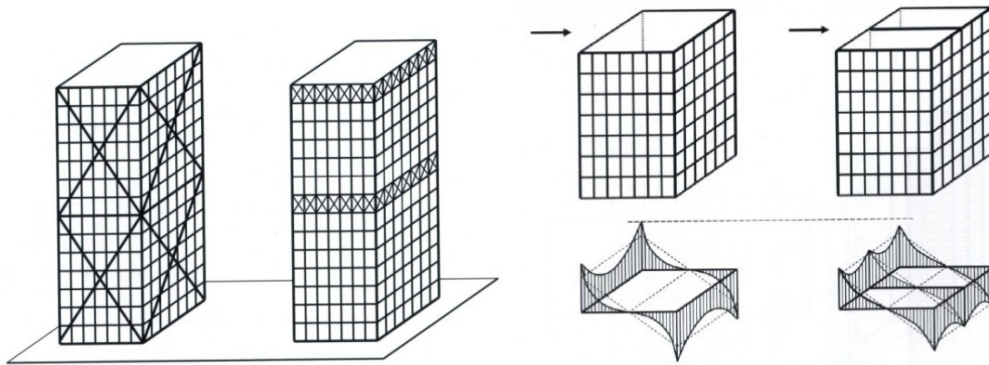


Figure 19 - Provisions to reduce the shear lag: mega diagonals, belt structure and division [Hoenderkamp, 2007]

The lateral stiffness can be further increased by application of a core in the tube. This system is called a tube-in-tube structure.

2.3.7. Conclusion

Different types of main load bearing structures have been defined for high-rise buildings. Two groups will be distinguished in this thesis, that show two main ways of load transfer:

- Cantilever bending/axial shortening action
- Frame action

Shear wall systems, core structures, braced frames, outrigger systems and tube systems belong to the first group because the load is transferred mainly via axial deformation of the material. This results in bending deformation. Rigid frames systems belong to the second group because their deformations are due to shearing and flexure of the frame member and connections, resulting in shear deformation.

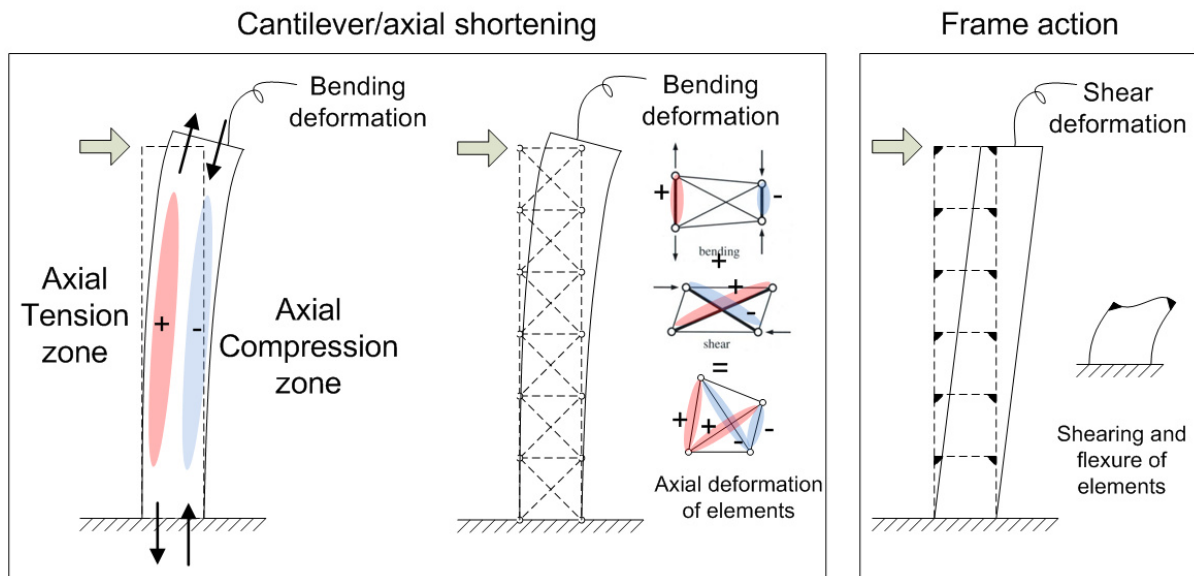


Figure 20 – two categories of load transfer

3. Dynamic response due to wind load

In this chapter it will be explained how the dynamic response due to wind can be calculated. First the situation will be explained and some assumptions have to be made to simplify the analysis. Secondly it will be described how the wind is modeled. The third second will give a brief overview of the theory behind dynamic systems, this theory is necessary to understand the spectral analysis which will be presented in the fourth section. Based on this analysis the peak displacement and accelerations can be calculated and the influence of the structural parameters will be derived.

3.1. Situation

The dynamic problem of time-varying wind load on a tall building is a 3-dimensional problem. The magnitude and direction of the wind velocity changes in time and is different over height and width. As a consequence, the wind pressure has an asymmetric distribution over the surface and introduces torsion, even for a symmetric building. Also a uniform wind flow from certain direction acting on one side, causes loads in three different directions because of vortex shedding. Vortex shedding causes pressure difference between two sides which results in a resulting force perpendicular to the wind direction, the lift force (F_L). The drag force (F_D) acts parallel to the wind direction and Torsion (T) causes a rotation of the structure. [Balendra, 1993, §3.2]

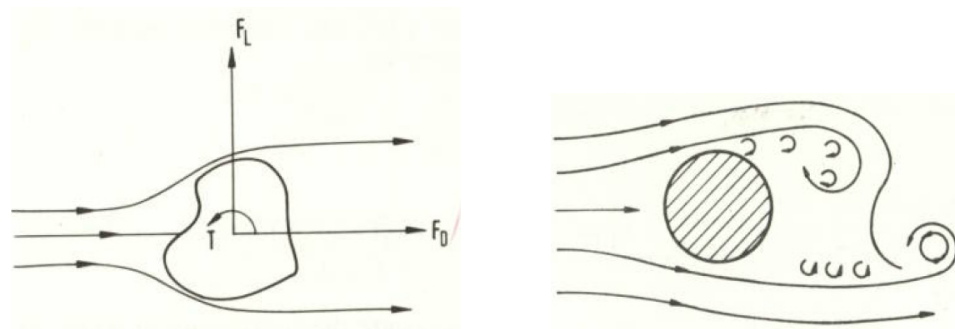


Figure 21 – left: random cross section of a building and the direction of the drag and lift force and the torsion, right: vortex shedding that causes pressure differences. [Balendra, 1993]

Because of these three forces, the response of the structure under turbulent wind flow can be split in three main directions: along-wind response, cross-wind response and torsional response. Cross wind response is of most concern for cylindrical like buildings. Along-wind response is most governing for buildings that have a high b/d ratio. Torsional response plays a major role in buildings with a-symmetrical mass or stiffness distribution. [Oosterhout, 1996]

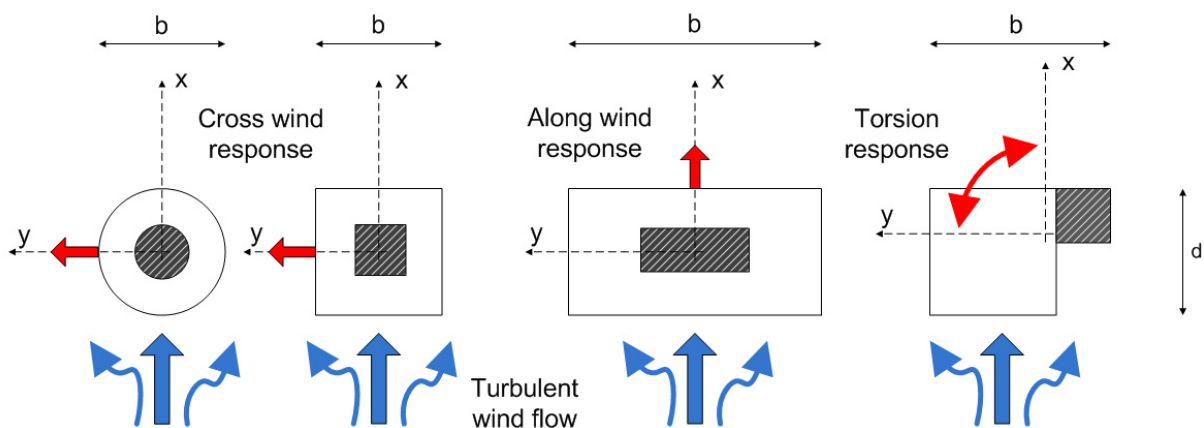


Figure 22 – most governing response under turbulent wind flow for different cross sections.

In Europe (and also for most of our studied buildings, see chapter 5) most tall buildings have high b/d ratio's, in this case the along wind response is mostly governing. Therefore the dynamic behaviour of a high-rise building under a wind load is analyzed by considering the deflection due to a along wind loading in its weakest direction (x -direction). Because most buildings are symmetrical, the deflection of the centre of rotation can be analyzed as a 2-dimensional bending problem because at this point the influence of the rotation due to torsion can be neglected.

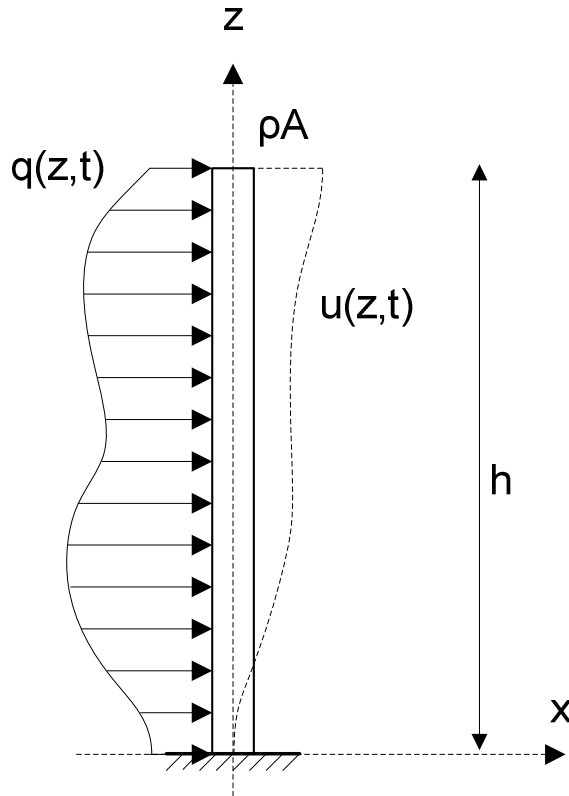


Figure 23 – situation: tall structure subjected to dynamic wind load

A tall building is subjected to a wind load that varies over height and in time, $q(z,t)$ [kN/m]. The response is denoted as $u(z,t)$ [m] and changes in time and over height. The building has height h [m] and constant mass density ρA [kg/m]. To analyze the dynamic behaviour, two aspects need to be modeled: the wind load and the structure.

3.2. Wind load

The wind load on a small area of the building depends on the wind climate and the shape of the building. The total wind force on a surface depends on the wind velocity, the air density, the area and a coefficient to take the shape of the building into account. The wind velocity can be split into a mean and fluctuating part [Vrouwenvelder, 2004, §6.4].

$$F_w = \sum A_i \cdot C_{p,i} \cdot p_{w,i}$$

$$p_w = \frac{1}{2} \rho v^2 = \frac{1}{2} \rho (\bar{v} + \tilde{v})^2 = \left[\frac{1}{2} \rho \bar{v}^2 + \rho \cdot \bar{v} \cdot \tilde{v} \right] \quad (3.1)$$

(in which the term \tilde{v}^2 has been neglected, because it is relative small).

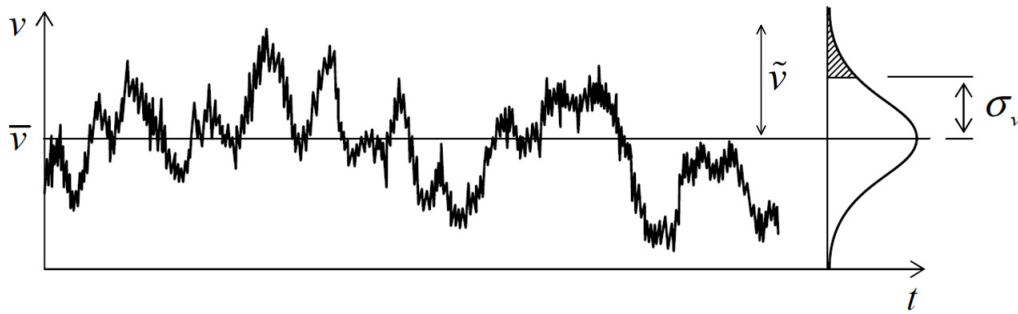


Figure 24 – mean wind velocity, fluctuating part and standard deviation [Vrouwenvelder, 2004]

3.2.1. Mean wind velocity

The hourly mean wind velocity changes over height. The logarithmic wind profile as given in Eurocode EN 1991-1-4 has been adopted in this thesis.

$$\bar{v}(z) = v_b \cdot k_r \cdot \ln\left(\frac{z}{z_0}\right) \quad (3.2)$$

$$k_r = 0,19 \left(\frac{z_0}{0,05}\right)^{0,07} \quad (3.3)$$

v_b is the reference wind speed at height of 10 m, and for $z_0=0,05$ m. z_0 is a measure for the roughness of the terrain. Values are given in standards. For a city centre in area II of the Netherlands, $v_b=27,0$ m/s and $z_0=0,5$ m. (see appendix B.2.3)

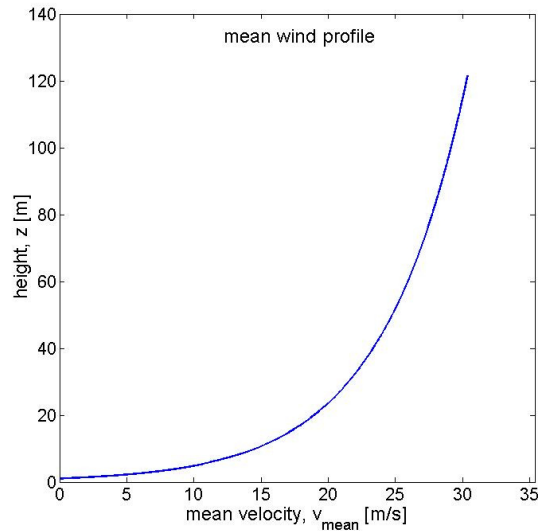


Figure 25 – shape of the mean wind profile

3.2.2. Fluctuating wind velocity

Gusts are the random fluctuating part of the wind speed in time. A spectral description of the turbulence is a convenient tool to account for the energy that is contained in the sequence of gusts. In this thesis the single sided variance spectrum of Solari (S_w) as used in Eurocode EN 1991-1-4, is adopted:

$$S_{vv}(z, f) = \frac{\sigma_v^2}{f} \frac{6,8 \cdot f_L}{(1 + 10,2 f_L)^{5/3}} \left[\left(\frac{m}{s} \right)^2 \frac{1}{s} \right] \quad (3.4)$$

$$f_L(z, f) = \frac{f \cdot L(z)}{\bar{v}(z)}$$

σ_v^2 [(m/s)²] is the standard deviation to the power two, also called the variance, f [Hz] is the frequency and $L(z)$ [m] is the turbulence length scale, that depends on a terrain factor α :

$$L(z) = 300 \left[\frac{z}{200} \right]^\alpha \quad \text{with} \quad \alpha = 0,67 + 0,05 \ln(z_0) \quad (3.5)$$

The spectrum shows how the energy is distributed over gusts with different frequencies and has been defined such that the area under the graph represents the variance. The spectrum will be assumed constant over height with $z=z_s=0,6h$.

The wind velocity that is exceeded once per hour is about equal to the hourly mean wind velocity plus 3,5 times the standard deviation of the wind speed [Vrouwenvelder & Geurts, 2006]. The extreme windpressure is equal to:

$$p_{w,peak} = \left[\frac{1}{2} \rho \bar{v}^2 + \rho \cdot \bar{v} \cdot 3,5 \cdot \sigma_v \right] = \frac{1}{2} \rho \bar{v}^2 [1 + 7 \cdot I_v] \quad (3.6)$$

In which I_v is the turbulence intensity:

$$I_v(z) = \frac{\sigma_v}{\bar{v}} = \frac{1}{\ln\left(\frac{z}{z_0}\right)} \rightarrow \sigma_v = \bar{v} \cdot I_v \quad (3.7)$$

From this an expression for the standard deviation has been derived which shows that it is constant over height.

$$\sigma_v = \bar{v} \cdot I_v = v_b \cdot k_r \cdot \ln\left(\frac{z}{z_0}\right) \cdot \frac{1}{\ln\left(\frac{z}{z_0}\right)} = v_b \cdot 0,19 \left(\frac{z_0}{0,05}\right)^{0,07} \quad (3.8)$$

For a city centre, area II of the Netherland $v_b=27,0$ m/s and $z_0=0,5$ m. This leads to $\sigma_v=6,0$ m/s. The spectrum has been plotted (see Figure 26) as a function of the frequency expressed in rad/s and for $z=0,6h$ and $\sigma_v=6,0$ m/s (for the transformation from f [Hz] to ω [rad/s], see appendix E).

3.2.3. The shape factor

The shape factor C_f takes the shape of the building into account. For the most common shapes values have been determined experimentally and can be found in standards. For irregularly shaped buildings, wind tunnel tests are necessary. A shape factor can be determined from test results by measurement of the drag force in caused by wind and divide this by the measured wind speed, the air density and the area opposed to wind.

$$C_f = \frac{F_D}{\frac{1}{2} \rho (\bar{v}(h))^2 A_{wind}} \quad (3.9)$$

For the along wind response on a rectangular structure the shape factor can be based on the pressure coefficients for a rectangular building, C_p (appendix A.3) or c_f (appendix B.3).

3.2.4. The aerodynamic admittance

On a large surface, the peaks of the wind velocity at different places won't occur at exactly the same time. Thus the total wind load on a larger surface shows less variance. The smoothing effect is mainly caused by the smaller wind gusts at the higher frequencies. [Vrouwenvelder, 2004, §6.4] This phenomenon will be taken into account by the aerodynamic admittance function as given in Eurocode EN 1991-1-4:

$$\chi^2 = R_h R_b \quad [-] \quad (3.10)$$

In which (for R_b take $h=b$):

$$R_h = \frac{1}{\eta} - \frac{1 - e^{-2\eta}}{2\eta^2} \quad (3.11)$$

$$\eta = \frac{4,6 \cdot f \cdot h}{\bar{v}(z_s)} \quad (3.12)$$

3.2.5. The along wind load spectrum

For the description of the dynamic behaviour, only the effect of the fluctuating wind load has to be considered because the mean wind load causes the static deflection around which the dynamic deflection takes place. (see Figure 10)

$$F_{w,static} = A \cdot C_f \cdot \frac{1}{2} \rho \bar{v}^2 \quad (3.13)$$

$$F_{w,dynamic} = A \cdot C_f \cdot \rho \cdot \bar{v} \cdot \tilde{v}$$

Because there is a linear relation between the fluctuating wind velocity and the dynamic force, the spectrum of the wind force must be obtained by:

$$S_{FF}(z_s, \omega) = [C_f \rho \bar{v}(z_s) A]^2 S_{vv}(z_s, \omega) \quad (3.14)$$

In which the aerodynamic admittance function still has to be taken into account and reduces the total variance of the load, leading to an effective wind loading spectrum.

$$S_{F_e F_e}(z_s, b, h, \omega) = \chi^2(z_s, b, h, \omega) S_{FF}(z_s, \omega) \quad (3.15)$$

In the figures below, the spectra are plotted for the New EMC (see ch. 6) ($C_f=1,45$, $\rho=1,25 \text{ kg/m}^3$, $v_b=27,0 \text{ m/s}$, $z_0=0,5 \text{ m}$, $h=121,5 \text{ m}$, $b=44,3 \text{ m}$). The area under the spectrum is equal to the variance (the standard deviation to the power two) of the fluctuating wind velocity.

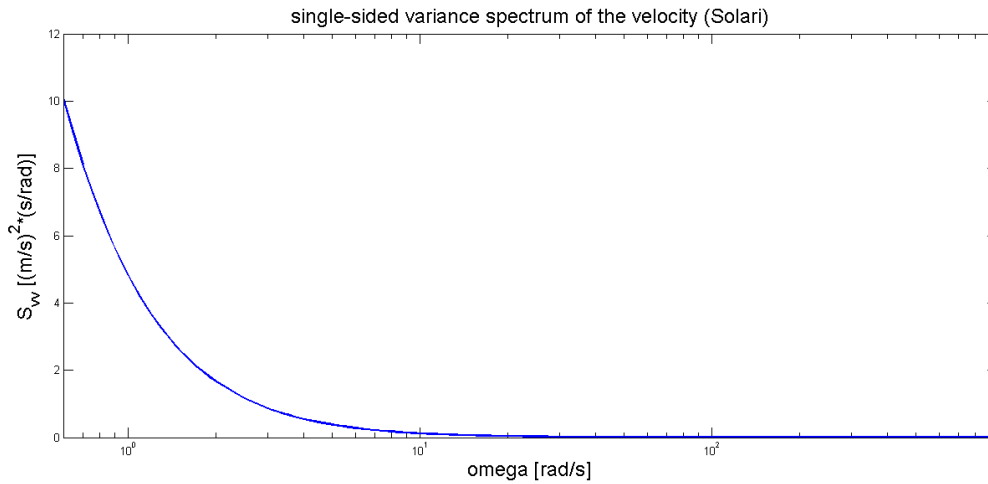


Figure 26 – single sided variance spectrum of the wind velocity, for the NEW EMC with $\sigma_v=6.0$ m/s, at $z=0,6h$

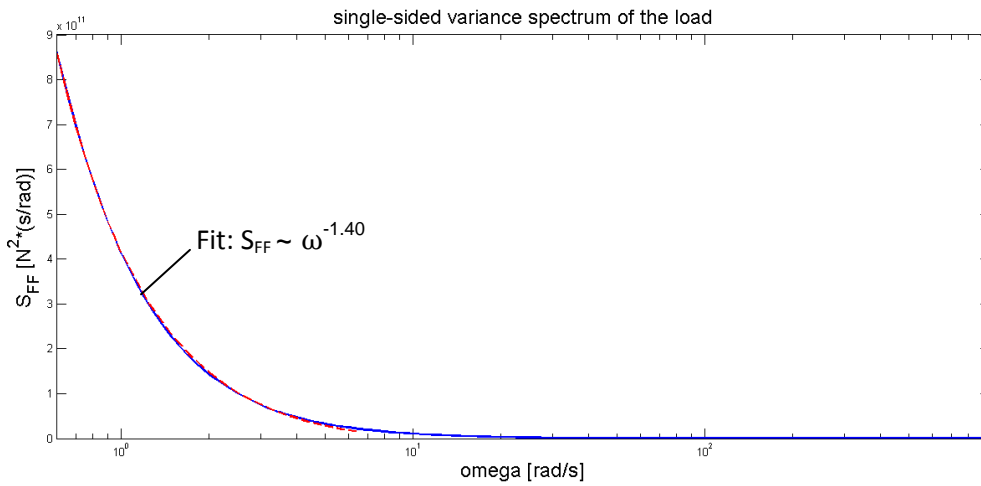


Figure 27 – the single sided variance spectrum of the load, for the NEW EMC with $\sigma_v=6.0$ m/s, at $z=0,6h$

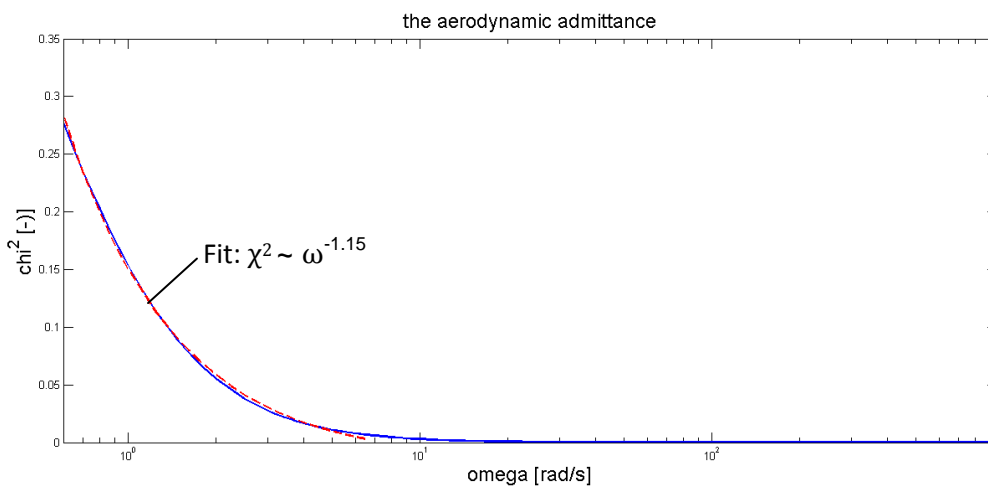


Figure 28 – aerodynamic admittance function, for the NEW EMC with $h=121,5$ m and $b=44,3$

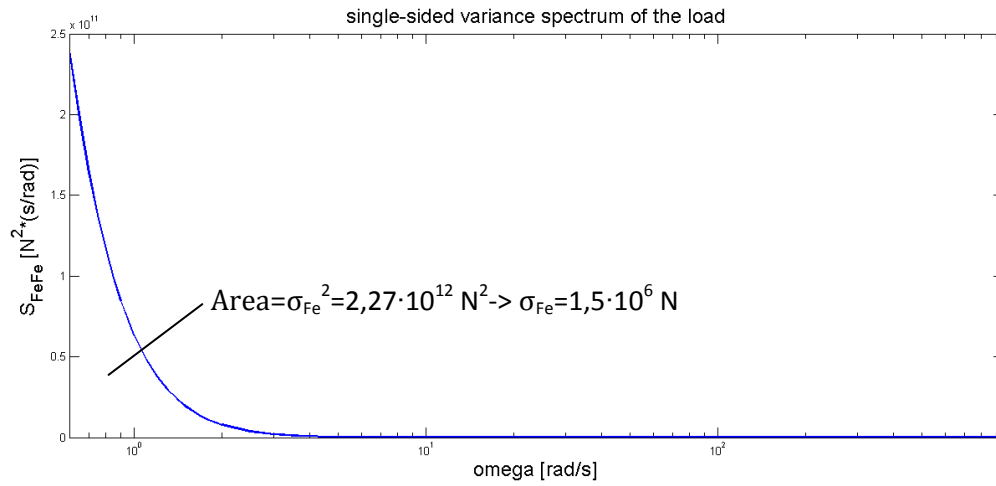


Figure 29 – single sided variance spectrum of the load, for the NEW EMC with $\sigma_v=6.0$ m/s, at $z=0,6h$

3.3. Dynamical systems

To be able to calculate the dynamic response of a high-rise building, the building needs to be modeled. There are three ways to model a tall building:

- Discrete systems with finite degrees of freedom
 - Single-degree-of-freedom system (SDOF)
 - N-degrees-of-freedom system ($N \geq 2$) (NDOF)
- Continuous systems with infinite degrees of freedom

Discrete systems simplify the analysis by replacing the distributed characteristics by discrete characteristics of loading, mass, stiffness and damping. An extensive description of the theory behind each system can be found in appendix F.

In the following subsections it will be summarized how the response to harmonic loading can be obtained according to the modal analysis. Knowledge about this response is needed to determine the response to the wind loading spectrum and will give essential insight in the dynamic behaviour of a high-rise building. To understand the modal analysis, it will first be explained how the dynamic response of a SDOF, NDOF and continuous system can be obtained.

3.3.1. SDOF system

The simplest dynamical system is the single degree of freedom system. In this system a building is represented by a single mass attached to the world by an element that has a certain stiffness and damping. These properties are translated into a spring and viscous damping element in the simple model on the right.

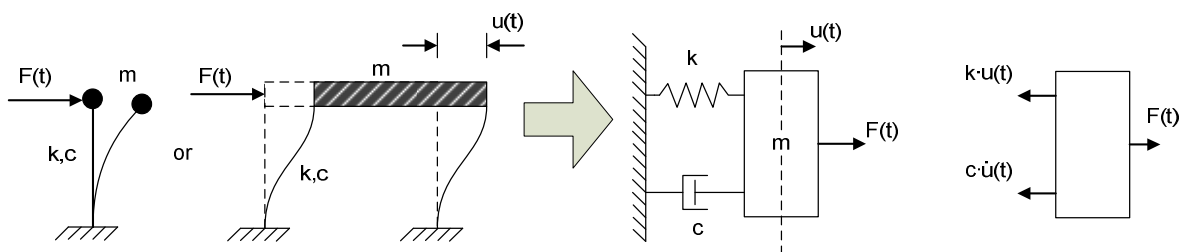


Figure 30 – SDOF system

The equation of motion of the mass attached to the world with a spring, damper and time dependent load is derived by Newton's law.

$$m\ddot{u} + c\dot{u} + ku = F(t) \quad (3.16)$$

In which:

\dot{u} = the first time derivative of the deflection

\ddot{u} = the second time derivative of the deflection

Solution under harmonic loading

When the system is subjected to a harmonic load $F(t) = \hat{F} \cos(\omega t)$, the response of the system can be described by the summation of the homogeneous and particular solution [Metrikine]:

$$u_{tot}(t) = u_{hom}(t) + u_{part}(t) \quad (3.17)$$

$$u_{tot}(t) = e^{-nt} [A_0 \cos(\omega_1 t) + B_0 \sin(\omega_1 t)] + |\hat{U}_{part}| \cos(\omega t - \varphi) \quad (3.18)$$

The homogeneous solution is the free vibration when the system is given an initial displacement or velocity. The free vibration is a damped harmonic function (see Figure 31). n is a value for damping, A_0 and B_0 depend on the initial conditions and ω_1 is the natural frequency for the damped system. This natural frequency is about equal to the natural frequency of the un-damped system, ω_n for low values of the damping ratio: ζ . This is the ratio between the damping and the critical damping. It will be assumed that this damping ratio is small, which is valid for high-rise buildings.

$$\omega_1 = \omega_n \sqrt{1 - \zeta^2} \approx \omega_n \quad \text{for } \zeta < 0,1 \quad (3.19)$$

$$\omega_n = \sqrt{\frac{k}{m}} \quad (3.20)$$

$$n = \zeta \omega_n \rightarrow \zeta = \frac{n}{\omega_n} \quad (3.21)$$

$$\zeta = \frac{c}{c_{kr}} \quad (3.22)$$

$$c_{kr} = 2\sqrt{km} \quad (3.23)$$

The particular solution is the response to the harmonic force. \hat{U}_{part} is the amplitude of the response, ω is the frequency of the harmonic load and φ is the phase lag between load and response. The amplitude and phase lag depend on the frequency of loading:

$$|\hat{U}_{part}| = \frac{\hat{F}}{k} \frac{1}{\sqrt{\left(1 - \frac{\omega^2}{\omega_n^2}\right)^2 + \left(\frac{2n}{\omega_n}\right)^2 \frac{\omega^2}{\omega_n^2}}} = u_{static} \frac{1}{\sqrt{\left(1 - \frac{\omega^2}{\omega_n^2}\right)^2 + (2\zeta)^2 \frac{\omega^2}{\omega_n^2}}} \quad (3.24)$$

$$\varphi = \arctan \left(\frac{2n\omega}{\omega_n^2 - \omega^2} \right) \quad (3.25)$$

The magnification factor has been introduced. This factor is non-dimensional and relates the static deflection to the amplitude of the dynamic deflection.

$$|H_{uF}(\omega)| = \frac{|\hat{U}_{part}|}{u_{static}} = \frac{1}{\sqrt{\left(1 - \frac{\omega^2}{\omega_n^2}\right)^2 + (2\zeta)^2 \frac{\omega^2}{\omega_n^2}}} \quad (3.26)$$

$$u_{static} = \frac{\hat{F}}{k} \quad (3.27)$$

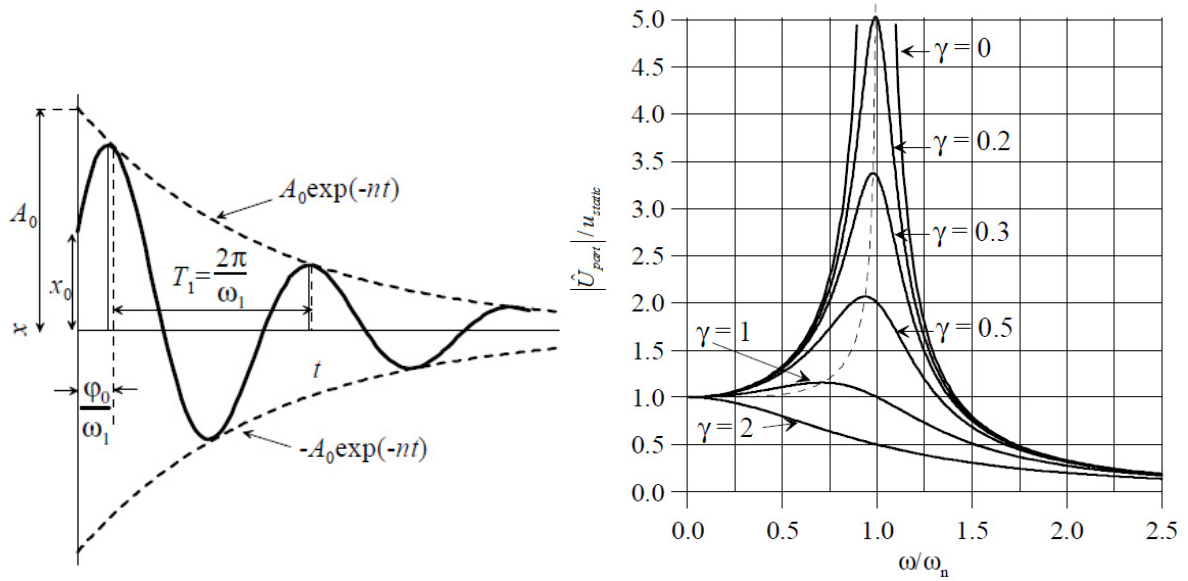


Figure 31 – left: the damped free vibration, right: the frequency response function of the steady state response [Metrikine]

Steady state response under harmonic loading

The damping is assumed to be low for tall buildings, $\zeta \ll 1$ and $n \ll 1$. As a consequence the amplitude of the free vibration (u_{hom}) rapidly vanishes in time because the damping is in the exponent. The remaining particular solution is the steady state response. Since the wind is present over a long time, only the steady state response has to be considered. The amplitude of steady state response depends on the frequency of loading and on the damping. Their influence can be observed in the frequency response function, plotted for different damping values (see Figure 31).

$$\gamma = \frac{2n}{\omega_n} = 2\zeta \tag{3.28}$$

In the steady state response, the relation between the force and displacement is:

$$u(t, \omega) = \left| \hat{U}_{part} \right| \cos(\omega t - \varphi) = \frac{1}{k} \left| H_{uF}(\omega) \right| \hat{F} \cos(\omega t - \varphi) \tag{3.29}$$

The acceleration can be obtained by double differentiation of the function:

$$a(t, \omega) = \ddot{u}(t, \omega) = -\omega^2 \left| \hat{U}_{part} \right| \cos(\omega t - \varphi) = -\omega^2 \frac{1}{k} \left| H_{uF}(\omega) \right| \hat{F} \cos(\omega t - \varphi) \tag{3.30}$$

The maximum displacement and acceleration are:

$$u_{max}(\omega) = \left| \hat{U}_{part} \right| = \frac{1}{k} \left| H_{uF}(\omega) \right| \hat{F} \tag{3.31}$$

$$a_{max}(\omega) = -\omega^2 \left| \hat{U}_{part} \right| = -\omega^2 \frac{1}{k} \left| H_{uF}(\omega) \right| \hat{F} \tag{3.32}$$

3.3.2. NDOF system

A tall building can be represented as a N-DOF system in which the mass has been divided over N degrees of freedom. The masses have been connected with elements that have a certain stiffness and damping that have been translated to a spring and a viscous damping element in the right schematization of Figure 32.

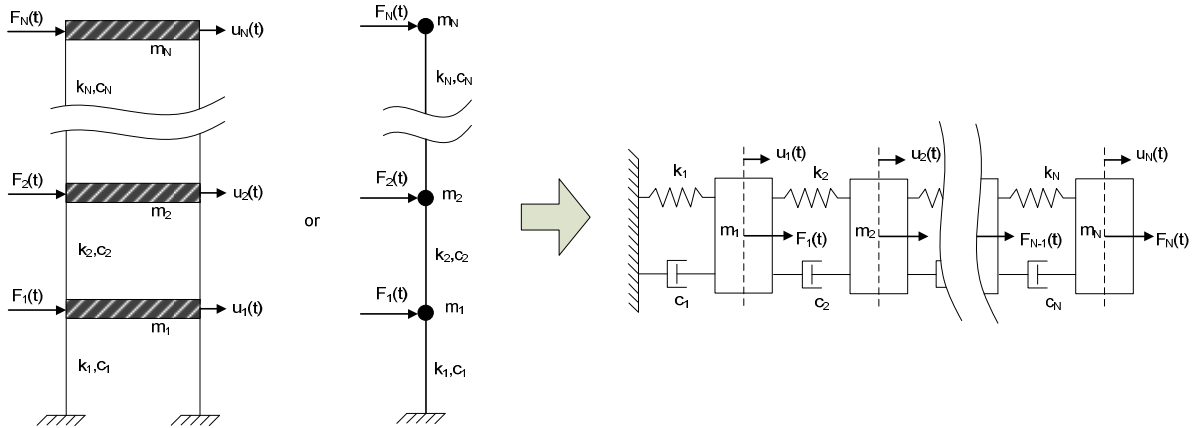


Figure 32 – N-degree of freedom system

When the N-degree-of-freedom system is subjected to a harmonic load $\underline{F}(t) = \hat{F} \cos(\Omega t)$ the equation of motion is:

$$\mathbf{M}\ddot{\underline{u}} + \mathbf{C}\dot{\underline{u}} + \mathbf{K}\underline{u} = \underline{F}(t) \quad (3.33)$$

$\underline{F}(t)$ and $\underline{u}(t)$ are vectors that represent the loading and displacement at the degrees of freedom and \mathbf{M} , \mathbf{C} and \mathbf{K} are the mass, damping and stiffness matrix respectively. The response of the system can be described by the summation of the homogeneous and particular solution.

$$\underline{u}(t) = \underline{u}_{\text{hom}}(t) + \underline{u}_{\text{part}}(t) \quad (3.34)$$

Although it is general not valid for a building, the modal damping matrix is assumed to be diagonal in order to be able to perform the modal analysis (see F.2.5.169).

Homogeneous solution

The homogeneous solution describes the free vibration of the system when no load acts on the system and an initial displacement and/or initial velocity is given to the system. It has been derived (see appendix F.2.1) that a system with N-degrees of freedom has N natural frequencies and each frequency is related to a mode of vibration. The mode of vibration with the lowest natural frequency is called the fundamental mode (of vibration). The free vibration of a damped system is a summation of all possible modes of vibration (see Eq. (F.85)):

$$\begin{aligned} \underline{u}_{\text{hom}}(t) &= \hat{u}_1 e^{(-\zeta_1 \omega_{n,1} t)} \cos(\omega_{1,1} t + \varphi_2) + \dots + \hat{u}_N e^{(-\zeta_N \omega_{n,N} t)} \cos(\omega_{1,N} t + \varphi_1) \\ \underline{u}_{\text{hom}}(t) &= A_1 \underline{\phi}_1 e^{(-\zeta_1 \omega_{n,1} t)} \cos(\omega_{1,1} t + \varphi_2) + \dots + A_N \underline{\phi}_N e^{(-\zeta_N \omega_{n,N} t)} \cos(\omega_{1,N} t + \varphi_2) \end{aligned} \quad (3.35)$$

or

$$\underline{u}_{\text{hom}}(t) = \sum_{i=1}^N A_i \underline{\phi}_i e^{(-\zeta_i \omega_{n,i} t)} \cos(\omega_{1,i} t + \varphi_i)$$

Each mode is described by a damped harmonic function. $\underline{\phi}_i$ is the shape of the eigen vector for the i^{th} mode of vibration and ζ_i is the damping per mode of vibration, the modal damping. Constants A_i and φ_i can be found from the initial conditions: $\underline{u}(0)$ and $\dot{\underline{u}}(0)$. $\omega_{1,i}$ is the natural frequency of the i^{th} mode of the damped system. This natural frequency is about equal to the natural frequency of the un-damped system for low values of ζ_i . (In general, this is valid for high-rise buildings)

$$\omega_{1,i} = \omega_{n,i} \sqrt{1 - \zeta_i^2} \approx \omega_{n,i} \quad \text{for } \zeta_i < 0,1 \quad (3.36)$$

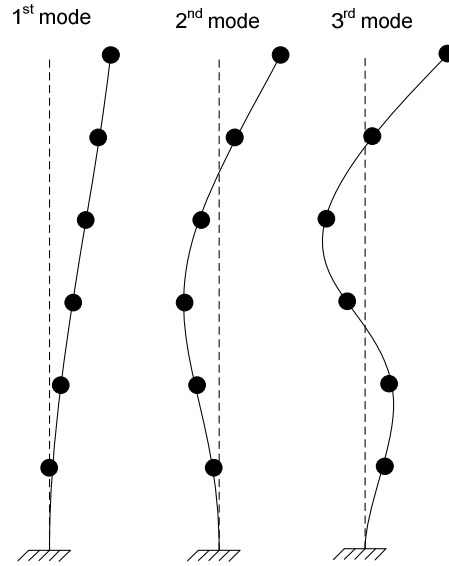


Figure 33 – possible shapes of the eigen vectors ($\underline{\phi}_i$) for the first 3 modes

Particular solution

The solution for the particular solution is found as the superposition of N eigen modes of the free vibrations, multiplied with N unknown functions of time:

$$\underline{u}_{part}(t) = \sum_{i=1}^N \underline{\phi}_i \hat{p}_{i,part} \cos(\Omega t - \varphi_{i,part}) \quad (3.37)$$

In which the amplitude and the phase shift are:

$$\hat{p}_{i,part} = \frac{1}{\sqrt{\left(1 - \frac{\Omega^2}{\omega_{n,i}^2}\right)^2 + 4\zeta_i^2 \frac{\Omega^2}{\omega_{n,i}^2}}} \frac{1}{\omega_{n,i}^2} \frac{\underline{\phi}_i^T \hat{\underline{F}}}{m_{ii}^*} \quad (3.38)$$

$$\tan \varphi_{i,part} = \frac{2\zeta_i \Omega / \omega_{n,i}}{1 - (\Omega / \omega_{n,i})^2} \quad (3.39)$$

Ω is the frequency of the load, $\underline{\phi}_i^T$ is the eigen vector, for the i^{th} mode. $\hat{\underline{F}}$ is the vector with the amplitudes of loading and m_{ii}^* is the effective mass for the i^{th} mode.

The damping causes a phase shift ($\varphi_{i,part}$). If the damping is zero, there is no phase shift. Damping also prevents an infinite amplitude at resonance ($\Omega=\omega_{n,i}$) to occur, because without damping the denominator turns to zero at resonance ($\Omega=\omega_{n,i}$). Eq. (3.38) can be rewritten into a matrix notation:

$$\hat{P}_{part} = H_{pF} \hat{F} \tag{3.40}$$

$$\begin{bmatrix} \hat{P}_{1,part} \\ \hat{P}_{2,part} \\ \hat{P}_{N,part} \end{bmatrix} = \begin{bmatrix} H_{p_1F_1} & H_{p_1F_2} & \cdot & H_{p_1F_N} \\ H_{p_2F_1} & H_{p_2F_2} & \cdot & H_{p_2F_N} \\ \cdot & \cdot & \cdot & \cdot \\ H_{p_NF_1} & H_{p_NF_2} & \cdot & H_{p_NF_N} \end{bmatrix} \begin{bmatrix} \hat{F}_1 \\ \hat{F}_2 \\ \cdot \\ \hat{F}_N \end{bmatrix} \tag{3.41}$$

In which H_{uiFp} is the ratio of the amplitude of the displacement for the i^{th} mode, to the force applied to the degree of freedom p. For a specific degree of freedom q an expression for the displacement due to a harmonic load that only acts at a specific point p can be found:

$$u_{part,q}(t) = \sum_{i=1}^N \phi_{i,q} H_{p_iF_p}(\Omega) \hat{F}_p \cos(\Omega t - \varphi_{i,part}) \tag{3.42}$$

In which

$$H_{p_iF_p} = \frac{1}{\sqrt{\left(1 - \frac{\Omega^2}{\omega_{n,i}^2}\right)^2 + 4\zeta_i^2 \frac{\Omega^2}{\omega_{n,i}^2}}} \frac{1}{\omega_{n,i}^2} \frac{\phi_{i,p}}{m_{ii}^*} \tag{3.43}$$

It can be concluded that: The maximum displacement at q is a summation of the displacement in q from every mode of vibration caused by a load with frequency Ω at degree of freedom p.

Because of a phase lag between the displacements in different modes, the maximum doesn't occur at once. This complicates the derivation. From Eq. (3.42) an expression (see Eq. (3.49)) for the maximum amplitude for the displacement in q to a load in p has been derived [Spijkers, et al., 2005, pp. 54-58] and the frequency response function (FRF) has been plotted in the figure below.

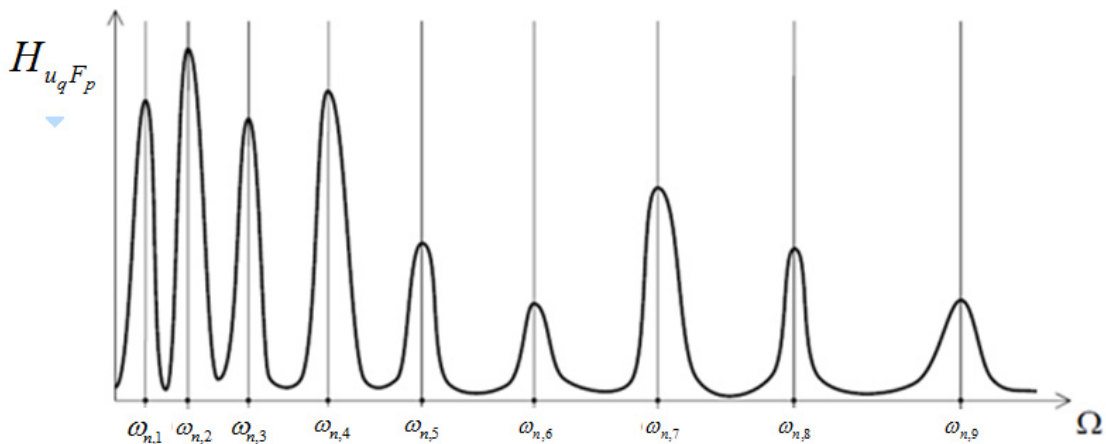


Figure 34 – example of a frequency response function for point q due to a specific load only at point p.

Since the structure now has N-natural frequencies, there are also N-resonance peaks in the frequency response function of degree of freedom q. When Ω is equal to one of the own frequencies, the displacements are enlarged because of resonance. The peaks don't have equal height because the response of a degree of freedom can be different in different modes. (see Figure 33).

Steady state response

The damping is assumed to be low for tall buildings, $\zeta \ll 1$. As a consequence, the amplitude of the free vibration (u_{hom}) rapidly vanishes in time because the damping is in the exponent and the particular solution remains as the steady state response. Since the wind is present over a long time, only the steady state response has to be considered. Thus, the amplitude of a displacement in q can be considered by the frequency response function (see Figure 34) and the following expression:

$$\hat{u}_q = H_{u_q F_p} \cdot \hat{F}_p \quad (3.44)$$

In which:

$$H_{u_q F_p}(\Omega) = \sqrt{\left(\sum_{i=1}^N \phi_{i,q} H_{p_i F_p}(\Omega) \cos(\varphi_{i,part}) \right)^2 + \left(\sum_{i=1}^N \phi_{i,q} H_{p_i F_p}(\Omega) \sin(\varphi_{i,part}) \right)^2} \quad (3.45)$$

Basically to obtain the maximum displacement at a certain point in a building, the response due to a load at all points have to be summed up. (Basically this means a summation of N-frequency response functions). Thus, there is a linear relation between the amplitude of the load and the amplitude of the response:

$$\hat{u}_q(\Omega) = \sum_{p=1}^N H_{u_q F_p}(\Omega) \cdot \hat{F}_p \quad (3.46)$$

Acceleration

The acceleration can be obtained by double differentiation of the displacement. In the former section it has been derived that the maximum acceleration in the steady state response, is equal to the maximum displacement of the steady state response, times the square of the frequency of the harmonic load. So the maximum acceleration at degree of freedom q, caused by a load a degree of freedom p is equal to:

$$a_{\max,q}(\Omega) = \Omega^2 \cdot \hat{u}_q(\Omega) = \sum_{p=1}^N \Omega^2 \cdot H_{u_q F_p}(\Omega) \cdot \hat{F}_p \quad (3.47)$$

3.3.3. Continuous systems

A continuous system is basically a N-degree-of-freedom system with infinite degrees of freedom, infinite natural frequencies and infinite modes of vibration. Consequently, the frequency response function has infinite amount of peaks. The behaviour of a continuous system is comparable with a NDOF system, so the theory won't be summarized in this section. The derivation of the response is different and can be found in appendix F.3.

3.3.4. Modal force, mass, stiffness and damping ratio for a mode

The building can vibrate in three main directions: along wind, cross wind and torsional direction. From the theory of structural dynamics, the vibration in each direction can be modeled by an infinite summation of uncoupled modes of vibration by making use of the modal analysis.

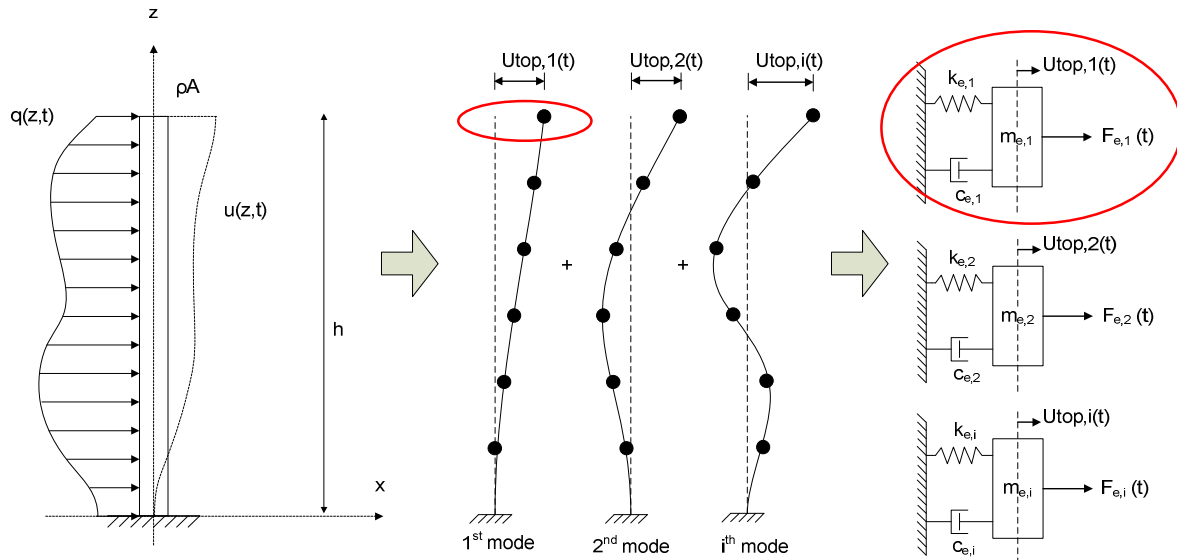


Figure 35 – deflection of total building to governing SDOF system with modal parameters.

From measured natural frequencies in multiple investigations (see a.o. appendix J) it has been observed that in general for tall buildings, the lowest natural frequency is associated with a translational vibration in the main direction with the lowest stiffness (x -axis), the second own frequency is associated with a translational vibration in the other main direction (y -axis) and the third own frequency is associated with the torsional vibration mode. The magnitudes of the frequencies depend on the stiffness and mass, but for tall buildings the first three modes are in the range of the wind loading spectrum (see Figure 29).

Because most buildings have a regular shape, the most governing direction can be considered. For a rectangular cross section, the along wind response will be governing. For a square or circular building, the first two natural frequencies will be close together and it has been stated that the cross wind response will be governing. When non-linear effects in its dynamic behaviour are little or not present, and the vibration modes can be uncoupled, it is sufficient to only study the fundamental (1^{st}) mode of a vibration. [Oosterhout, 1996]

For a tall building, the first mode of a translational vibration is always shaped as the first mode in Figure 35. The largest deflection and acceleration occurs at the top.

Instead of considering the deflection in a point due to the load only in a specific point, summed over all modes. The deflection only has to be considered in the i^{th} mode, but due to loading in all points.

From Eqs.(3.42) and (3.43) the amplitude of vibration in point q, due to loads over all points for the i^{th} mode can be expressed as:

$$\hat{u}_{part,i,q} = \sum_{p=1}^N \phi_{i,q} \frac{1}{\sqrt{\left(1 - \frac{\Omega^2}{\omega_{n,i}^2}\right)^2 + 4\zeta_i^2 \frac{\Omega^2}{\omega_{n,i}^2}}} \frac{1}{m_{ii}^* \omega_{n,i}^2} \phi_{i,p} \hat{F}_p \quad (3.48)$$

From this an expression for the modal force (also called effective force) can be derived:

$$\hat{F}_{e,i} = \sum_{p=1}^N \phi_{i,p} \hat{F}_p = \underline{\phi}_i^T \hat{\underline{F}} \quad (3.49)$$

Thus, for the i^{th} mode, there is a linear relation between the modal force and the displacement at point q.

$$\hat{u}_{part,i,q} = H_{u_q F_{e,i}}(\Omega) \cdot \hat{F}_{e,i} = \phi_{i,q} \frac{1}{\sqrt{\left(1 - \frac{\Omega^2}{\omega_{n,i}^2}\right)^2 + 4\zeta_i^2 \frac{\Omega^2}{\omega_{n,i}^2}}} \frac{1}{m_{ii}^* \omega_{n,i}^2} \cdot \hat{F}_{e,i} \quad (3.50)$$

Also a modal mass, stiffness and damping can be calculated for every mode:

$$m_{ii}^* = m_{e,i} = \underline{\phi}_i^T \mathbf{M} \underline{\phi}_i \quad (3.51)$$

$$k_{ii}^* = k_{e,i} = \underline{\phi}_i^T \mathbf{K} \underline{\phi}_i \quad (3.52)$$

$$c_{ii}^* = c_{e,i} = \underline{\phi}_i^T \mathbf{C} \underline{\phi}_i \quad (3.53)$$

The natural frequency and the modal damping can be calculated from these modal properties:

$$\omega_{n,i} = \sqrt{\frac{k_{e,i}}{m_{e,i}}} \quad (3.54)$$

$$\zeta_i = \frac{c_{e,i}}{2\sqrt{k_{e,i} m_{e,i}}} \quad (3.55)$$

The same kind of expressions can be found for the continuous system (see appendix F.3.5)

Thus for every mode, the displacement at a certain point can be calculated as the deflection of a single degree of freedom system (with modal properties) to a modal force.

The maximum deflection occurs at the top and can be studied as the deflection of a SDOF system with modal properties and a modal force according to the first mode.

It has to be noted that according to this approach, the loads at different points have their maximum at the same moment of time (or the load on each node has the same frequency). Therefore, the response according to the modal approach has to be decreased by the aerodynamic admittance function. (which basically has been derived from the correlation between the wind velocity at different heights, for an explanation, see [Vrouwenvelder, 2004, §6.4])

3.4. Spectral analysis of the response

In section 3.2 a linear relation between the fluctuating wind speed and the fluctuating wind load has been derived (Eq. (3.13)) and a wind loading spectrum (Eq. (3.14)) has been obtained.

In section 3.3 a linear relation between the load and the response has been derived with a transfer function. The total transfer function can be obtained in two ways:

- In Eq. (3.46) a linear relation between the response at a specific point q due to a load at only a specific point p , has been derived. This response includes the response of all modes. The total transfer function has to be obtained by a summation of the spectra for all points.
- In Eq. (3.50) a linear relation between the response at a specific point q due to a load at all points, has been derived. This response, only includes one mode. The total transfer function has to be obtained by a summation of the spectra for all modes.

In this analysis, the last linear relation will be used. The response to the wind load can be obtained by multiplication of the square root of the transfer function of the structure with the wind loading spectrum. [Vrouwenvelder & Geurts, 2006]

$$S_{u_{top}}(\omega) = \left| H_{u_{top}F}(\omega) \right|^2 \chi^2 S_{FF}(\omega) \quad (3.56)$$

In which the transfer function is a summation over all modes and all points:

$$\begin{aligned} \left| H_{u_{top}F}(\omega) \right|^2 &= \sum_{i=1}^N \left| H_{u_{top,i}F}(\omega) \right|^2 \left[\frac{m}{N} \right]^2 \\ \left| H_{u_{top,i}F}(\omega) \right| &= \sum_{p=1}^N \frac{\phi_{i,top} \phi_{i,p}}{k_{e,i} \sqrt{\left(1 - \frac{\omega^2}{\omega_{n,i}^2} \right)^2 + 4 \zeta_i^2 \frac{\omega^2}{\omega_{n,i}^2}}} \left[\frac{m}{N} \right] \end{aligned} \quad (3.57)$$

The first natural frequency and modal damping of the New EMC in x-direction have been measured ($f_{n,1}=0,536$ Hz and $\zeta_1=1.63\%$, see Table 10). The New EMC has been schematized as a clamped beam with distributed dampers along the height. Equivalent modal parameters for the deflection at the top have been derived (see appendix F.3.6) from which the transfer function has been derived.

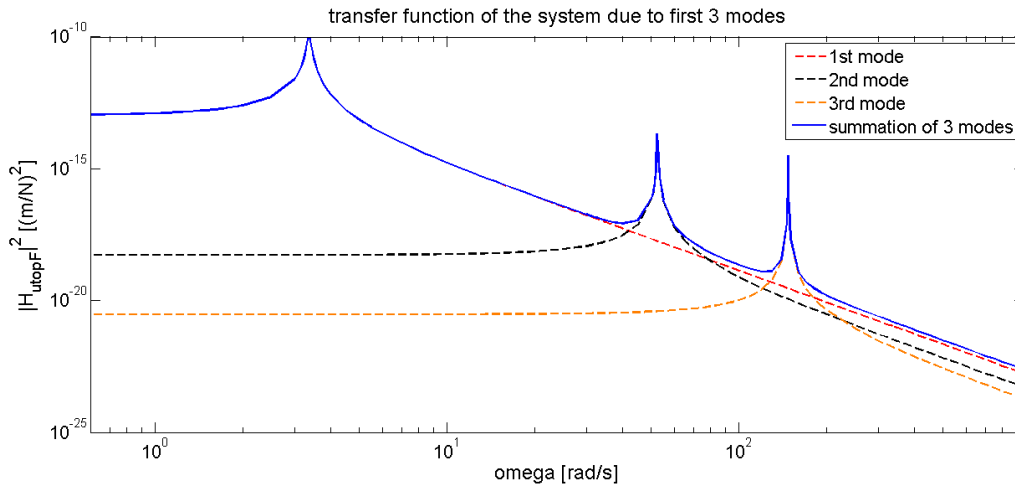


Figure 36 – transfer function for the deflection at the top, for the NEMC ($\omega_{n,1}=0,536 \cdot 2\pi=3,37$ rad/s, $\zeta_1=0,0163$, $\rho A=430 \cdot 10^3$ kg/m)

The peaks at the first three natural frequencies can be observed in Figure 36. It can be considered that the peaks in the 2nd and 3rd mode are significant smaller (log-scale on vertical axis) and are out of frequency range of the wind loads. This makes clear that for this direction only the response due to the first mode has to be considered.

3.4.1. Response spectrum

Multiplication of the transfer function with the load and aerodynamic function gives the following response spectrum:

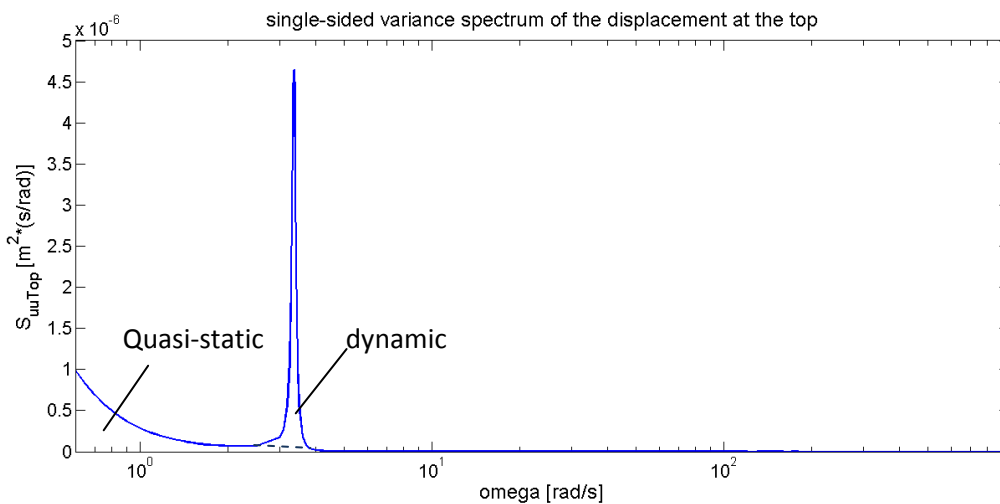


Figure 37 – single sided variance spectrum of the displacement at the top of the NEW EMC ($\omega_{n,1}=0,536 \cdot 2\pi=3,37$ rad/s, $\zeta_1=0,0163$, $\rho A=430 \cdot 10^3$ kg/m, $\sigma_v=6.3$ m/s, spectrum taken at $z=0,6h$, $h=121,5$ m and $b=44,3$)

The total variance (=the standard deviation to the power 2) of the response is equal to the area under the response spectrum and can be split up into a quasi-static response and a dynamic response. [Vrouwenvelder, 2004, §3.1]:

$$\sigma_u^2 = \int_0^{\infty} S_{uu}(\omega) d\omega \quad (3.58)$$

$$\sigma_u^2 = \sigma_{uQS}^2 + \sigma_{uD}^2 = \int_0^{\infty} S_{uuQS}(\omega) d\omega + \int_0^{\infty} S_{uuD}(\omega) d\omega \quad (3.59)$$

$$\sigma_u^2 = \int_0^{\infty} |H_{uF}(0)|^2 \chi^2(\omega) S_{FF}(\omega) d\omega + \int_0^{\infty} |H_{uF}(\omega)|^2 \chi^2(\omega_{n,1}) S_{FF}(\omega_{n,1}) d\omega$$

The quasi static part is the response for a structure that only reacts statically (the transfer function at $\omega=0$). The quasi static peak is the result of the peak in the wind spectrum. The transfer function at $\omega=0$ depends mainly on the stiffness of the first mode because this is most dominant. The quasi static variance is equal to:

$$\sigma_{uQS}^2 = |H_{uF}(0)|^2 \int_0^{\infty} \chi^2(\omega) S_{FF}(\omega) d\omega = \frac{1}{k_{e,1}^2} \int_0^{\infty} S_{FeFe}(\omega) d\omega = \frac{\sigma_{Fe}^2}{k_{e,1}^2} \quad (3.60)$$

The dynamic part is the difference between the total response and the static response. This peak is caused by the peak in the transfer function at the first natural frequency. The white noise approach is a convenient method to approximate the dynamic response. In this approach, the wind loading spectrum is replaced by a spectrum with constant spectral density S_0 equal to $S_{FeFe} = \chi^2 S_{FF}$ at the natural frequency.

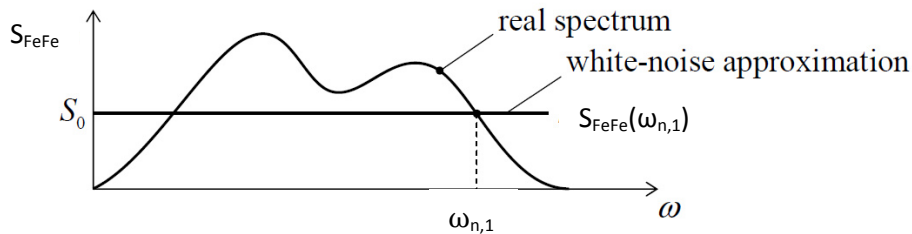


Figure 38 – approximation of the load spectrum by a white noise approach, ω_e is the first natural frequency [Vrouwenvelder, 2004]

Solution of the integral gives:

$$\sigma_{uD}^2 = \chi^2(\omega_{n,1}) S_{FF}(\omega_{n,1}) \int_0^{\infty} |H_{uF}(\omega)|^2 d\omega \quad (3.61)$$

$$\sigma_{uD}^2 = \chi^2(\omega_{n,1}) S_{FF}(\omega_{n,1}) \cdot \frac{\pi \omega_{n,1}}{4 \zeta k_{e,1}^2}$$

The total variance is equal to:

$$\sigma_u^2 = \sigma_{uQS}^2 + \sigma_{uD}^2 = \frac{\sigma_{Fe}^2}{k^2} + \chi^2(\omega_{n,1}) S_{FF}(\omega_{n,1}) \cdot \frac{\pi\omega_{n,1}}{4\zeta k_{e,1}^2} \quad (3.62)$$

$$\sigma_u^2 \approx \chi^2(\omega_{n,1}) S_{FF}(\omega_{n,1}) \cdot \frac{\pi\omega_{n,1}}{4\zeta k_{e,1}^2}$$

For lightly damped structures (as for high-rise buildings) the peak in the transfer function at resonance is so strong, that the dynamic response part is dominant and the quasi static response can be neglected. [Vrouwenvelder, 2004, §3.3]

From this theory, the maximum peak displacement at the top has been calculated for the NEW EMC (see appendix F.3.6):

$$u_{top,max} = \bar{u} + 3,5\sigma_u = u_{Static} + 3,5[\sigma_{uQS} + \sigma_{uD}] \quad (3.63)$$

$$u_{top,max} = 0,0235 + 3,5[0,0102 + 0,0032] = 0,0704m$$

3.4.2. The resonant acceleration response

The variance in terms of acceleration can be estimated by multiplication of the variance of the dynamic displacement with $\omega_{n,1}^2$:

$$\sigma_a = \omega_{n,1}^2 \sigma_u = \omega_{n,1}^2 \sqrt{\chi^2(\omega_{n,1}) S_{FF}(\omega_{n,1}) \cdot \frac{\pi\omega_{n,1}}{4\zeta k_{e,1}^2}} \quad (3.64)$$

The peak acceleration has been calculated for the NEW EMC (see appendix F.3.6):

$$a_{top,max} = 3,5\sigma_a = 3,5\omega_{n,1}^2 \sigma_{uD} = 3,5 \cdot 3,37^2 \cdot 0,0032 = 0,127m/s^2 \quad (3.65)$$

3.5. The influence of structural properties on the dynamic response

The dynamic behaviour under wind-loading is influenced by multiple factors. First there are multiple environmental factors that influence the dynamic wind load on the building. The “wind loading chain” of prof. A.G. Davenport clearly shows the parameters that influence the dynamic load of wind on a building. Secondly the response depends on the building properties: building shape, mass, stiffness and damping.

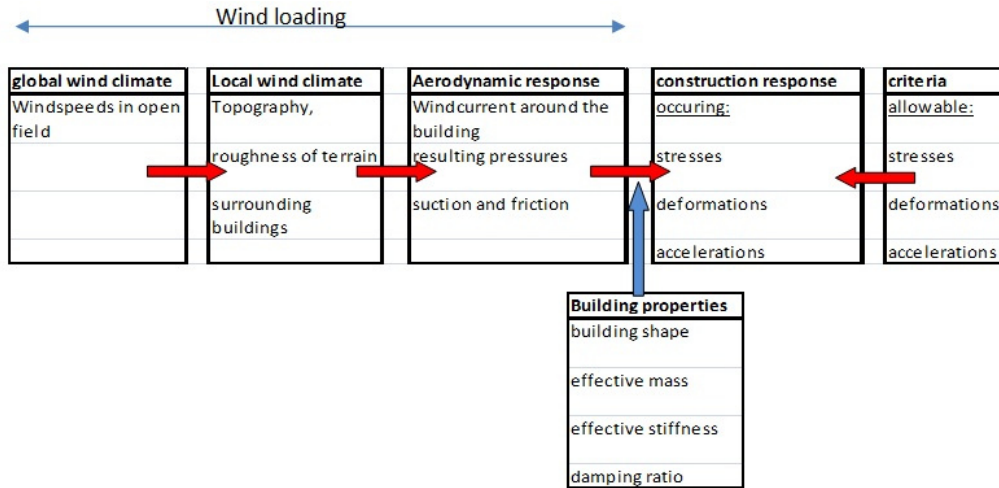


Figure 39 – “wind loading chain” according to prof. A.G. davenport [Woudenberg & Vambersky, 2003]

In this research only the influence of the mass, stiffness and damping will be investigated because it is assumed that the shape and height of the building have been determined by the architect. By this assumption, changing of the shape of the building to improve the dynamic behaviour isn’t an option.

3.5.1. The theoretical effect on the maximum displacement

The maximum displacement is equal to the mean displacement plus 3,5 times the standard deviation of the displacement. In the last section the standard deviation of the response due to the fluctuating wind velocity has been derived and the static displacement at the top due to the mean wind load is equal to the modal force of the mean wind velocity divided by the modal stiffness of the first mode:

$$u_{top,max} = \bar{u} + 3,5\sigma_u = u_{Static} + 3,5[\sigma_{uQS} + \sigma_{uD}]$$

$$u_{top,max} = \frac{F_{e,mean}}{k_{e,1}} + 3,5 \left[\frac{\sigma_{Fe}}{k_{e,1}} + \sqrt{\chi^2(\omega_{n,1}) S_{FF}(\omega_{n,1}) \cdot \frac{\pi\omega_{n,1}}{4\zeta k_{e,1}^2}} \right] \tag{3.66}$$

The relation between the frequency and the aerodynamic admittance and the force spectrum has been estimated from a fit on the curves between 0,1 and 1,0 Hz. (see Figure 27 and Figure 28). By making use of this relation and because $\omega_{n,1} = k_{e,1}^{0,5} m_{e,1}^{-0,5}$, the influence of the modal parameters can be approximated by:

$$u_{top,max} \sim k_{e,1}^{-1} + \left[k_{e,1}^{-1} + \sqrt{\omega_{n,1}^{-1,15} \omega_{n,1}^{-1,40} \cdot \omega_{n,1}^1 \zeta^{-1} k_{e,1}^{-2}} \right]$$

$$u_{top,max} \sim k_{e,1}^{-1} + k_{e,1}^{-1} + m_{e,1}^{0,39} \zeta^{-0,5} k_{e,1}^{-1,39} \tag{3.67}$$

As already could be expected, the maximum deflection mostly depends on the stiffness.

Dynamic amplification factor

The dynamic effect causes an increase of the mean deflection. The dynamic amplification factor as is used in NEN6702 (ϕ_1) (comparable with $c_s c_d$ in EN 1991-1-4) is defined as the ratio between the maximum response including the quasi static and dynamic response and the response due to the mean wind velocity and the quasi static response [Vrouwenvelder & Geurts, 2006]:

$$\phi_1 = \frac{\bar{u} + 3,5 \left[\sigma_{uQS} + \sigma_{uD} \right]}{\bar{u} + 3,5 \sigma_{uQS}} \quad (3.68)$$

Because the deflection also influence the stresses, this magnification factor is used on the mean load for the strength and stiffness calculations.

3.5.2. The theoretical effect on the maximum acceleration

From the estimation of the maximum acceleration and from the relation derived in the former subsection, the influence of the structural parameters on the maximum acceleration can be estimated:

$$a_{top,max} = 3,5 \sigma_a = 3,5 \omega_{n,1}^2 \sigma_u = 3,5 \omega_{n,1}^2 \sqrt{\chi^2(\omega_{n,1}) S_{FF}(\omega_{n,1}) \cdot \frac{\pi \omega_{n,1}}{4 \zeta k_{e,1}^2}} \quad (3.69)$$

$$a_{top,max} \sim m_{e,1}^{-0,61} \zeta^{-0,5} k_{e,1}^{-0,39}$$

From this it can be concluded that concerning the acceleration, an increase of the mass most effective to reduce the acceleration. An increase of the stiffness decreases the acceleration the least effective.

The effect on the admissible acceleration

The parameters not only influence the maximum occurring acceleration, but also the admissible acceleration (see appendix D). The admissible acceleration depends on the natural frequency and is higher at low natural frequencies.

If the stiffness increases, the natural frequency increases. At higher natural frequencies, the admissible acceleration is lower.

An increase of mass has the opposite effect because it leads to a decrease of the own frequency. Increase of mass reduces the accelerations and brings the building to an area where higher accelerations are admissible.

Increase of damping reduces the accelerations and doesn't influence the natural frequency (the frequency can be influenced by the damping, but this effect is negligible for the low damped high-rise buildings).

Most effective parameter to decrease acceleration

It can be concluded that the mass most effectively influences the comfort criterion, the stiffness is least effective and the effect of damping is moderate. A more extended sensitivity analysis has been performed by also considering the effect of the slenderness. [Oosterhout & Geurts, 2001]. The figure below shows the result. The arrows indicate how the parameters influence the maximum acceleration. This figure also shows that increase of mass is most effective to reduce accelerations

for a slender building. Damping is also an effective way to keep the accelerations in the admissible area.

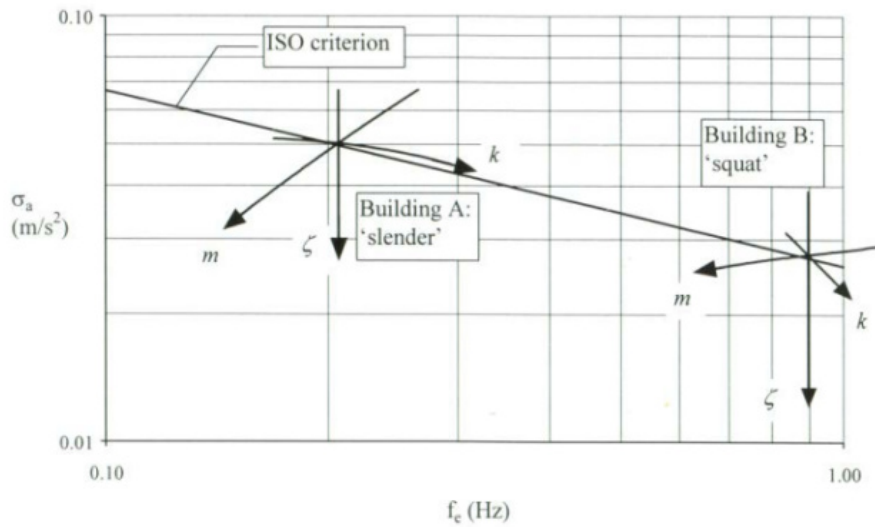


Figure 40 – effects of the main structural parameters on the acceleration in respect to the ISO criterion [Oosterhout, 1996]

In practice, an increase of mass isn't a good option. In the design phase of a building, its outer shape has already been determined. It is not very practical to increase the mass, since it results in more costs for material, less usable space and more vertical loads on the foundation (higher costs!). Therefore it can be concluded:

Increase of damping is the most practical measure to keep the accelerations in the admissible area.

3.5.3. The effect according to the Eurocode

The effect of the structural properties on the deflection and acceleration has been investigated by making use of the procedure described in the EN 1991-1-4 to obtain the structural amplification factor c_{s,c_d} .

The effect of the effective mass, stiffness and the modal damping ratio on this factor and the peak displacement has been investigated. The Eurocode also provides a method to calculate the peak acceleration. From this method the influence on the acceleration has also been investigated.

A sensitivity analysis has been performed by variation of the stiffness, mass and damping around a reference value. The reference value is based on the measured natural frequency, the modal damping ratio and the assumed mass density for the NEMC in x-direction. (see appendix F.3.6)

Table 2 – reference input and output values based on the structural properties of the NEMC

input	m_e	12,96	$\cdot 10^6$ kg
ref. Val.	k_e	147,10	$\cdot 10^6$ N/m
	$\delta = \zeta 2\pi$	0,1	-
output	c_{s,c_d}	1,15	-
ref. Val.	u_{max}	0,083	m
	$a_{top,max}$	0,190	m/s^2

Influence on $c_s c_d$

The $c_s c_d$ factor is the ratio between the maximum dynamic displacement and the static displacement. It depends on mass, stiffness and damping.

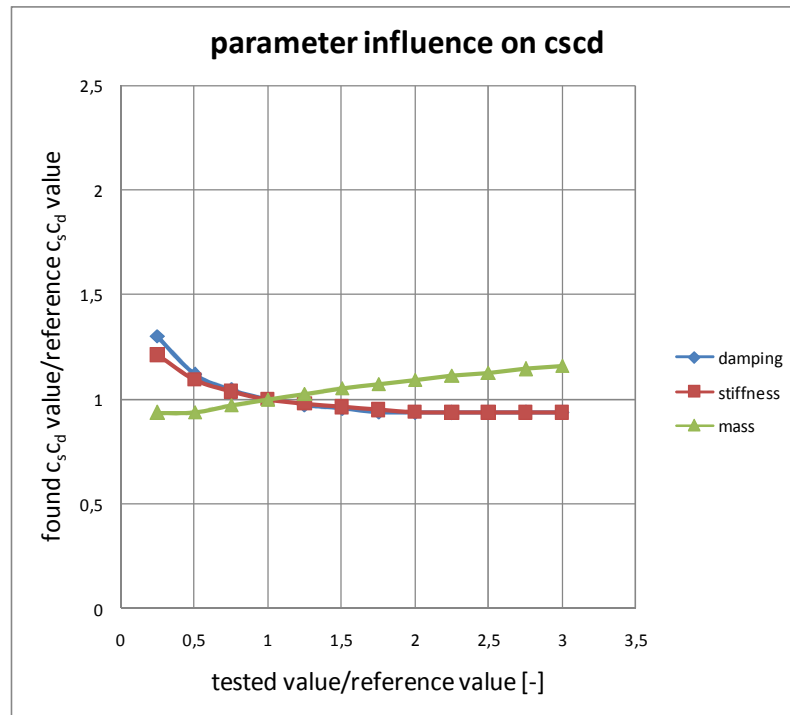


Figure 41 – the structural factor $c_s c_d$ as a function of mass, stiffness and damping

The stiffness and mass influence the natural frequency of the building. When the stiffness increases, the frequency also increases. When the mass increases, the frequency decreases. The frequency influences the resonance response factor, R^2 and the peak factor k_p . These two factors influence $c_s c_d$. At higher frequencies, R^2 decreases much more than the increase of k_p . (see appendix C.1) As a result $c_s c_d$ decreases as the natural frequency increases. This result is in line with the theory because the structure is less vulnerable for wind gusts at higher natural frequencies. (This can be concluded from the wind spectra, see Figure 28).

The resonance response factor, R^2 , is inversely proportional to the logarithmic damping decrement. Thus as the damping increases, the structural factor decreases. This is also in line with the theory because damping decreases the maximum deflection at resonance. (see Figure 31)

Influence on displacement

The displacement has been related to the representative force and the stiffness: $u_{\max} = F_{w,rep}/k_e$. The representative force is proportional to the structural factor. Thus the influence of the damping and mass on the deflection is the same as the influence on the structural factor $c_s c_d$. An increase of the stiffness not only indirectly affects the displacement via $c_s c_d$ but also directly. As a consequence, the displacement is most strongly dependent on the stiffness. This is also in line with the conclusions from the theoretical approach.

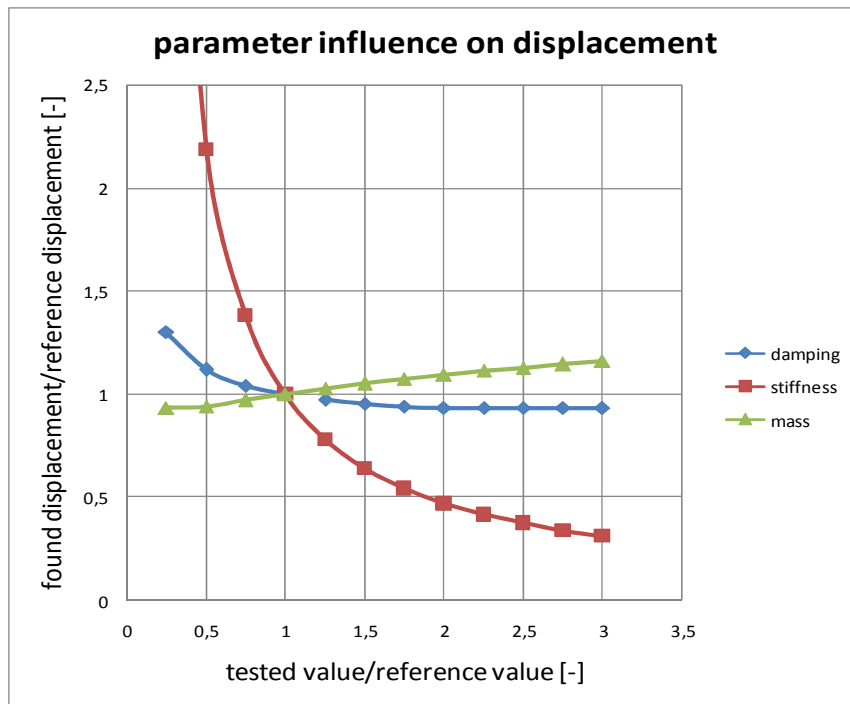


Figure 42 – the displacement due to wind load as a function of the mass, stiffness and damping

Influence of the acceleration

According to figure 43, the peak acceleration depends to the same degree on damping, stiffness and mass. This can be explained by study of the method in the Eurocode.

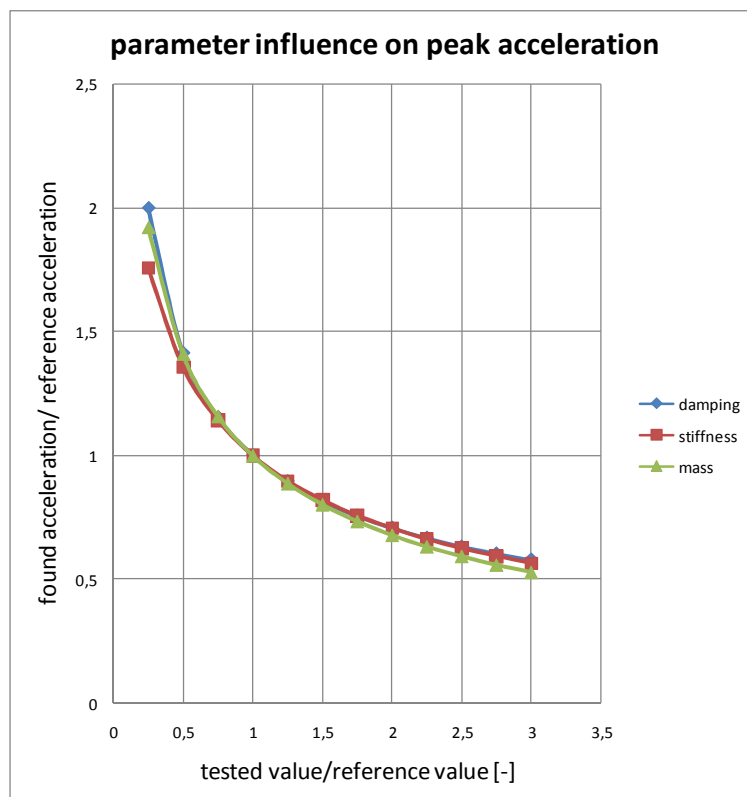


figure 43 – the characteristic peak-acceleration due to wind load as a function of mass, stiffness and damping

According to Eq. (B.26) and (B.28) the acceleration is proportional to k_{p_nat} , R and $1/\mu_e$. (μ_e is the reference mass [kg/m²]). It has been investigated how R^2 and k_{p_nat} depend on the natural frequency ($n_{1,x}$). It has been found that R^2 is about proportional to $n_{1,x}^{-2}$. k_{p_nat} is insensitive to variations of $n_{1,x}$. (see appendix C.1)

$$R^2(n_{1,x}) \sim \frac{1}{n_{1,x}^2} \quad (3.70)$$

R^2 is also proportional with $1/\delta$. With these relations it can be concluded that, the peak acceleration is equally sensitive to all the three parameters:

$$a_{top,max} = \sigma_{a,peak}(h) = k_{p,nat} \cdot c_f \cdot \rho \cdot I_v(z_s) \cdot v_m^2(z_s) \cdot R \cdot \frac{K_y \cdot K_z \cdot \phi(h)}{\mu_e \cdot \phi_{max}} \quad (3.71)$$

$$a_{top,max} = \sigma_{a,peak}(h) \sim R(n_{1,x}) \frac{1}{\mu_e} \sim \sqrt{\frac{1}{\delta}} \sqrt{\frac{1}{n_{1,x}^2}} \frac{1}{m_e} = \sqrt{\frac{1}{\delta}} \frac{1}{\sqrt{\frac{k_e}{m_e}}} \frac{1}{m_e} \quad (3.72)$$

$$a_{top,max} \sim \delta^{-0,5} m_e^{-0,5} k_e^{-0,5}$$

The found influence of the structural parameters on the peak acceleration is about equal to the found dependencies from the theory. By also considering the effect on the admissible acceleration (see §3.5.2) and because it is not practical to increase the mass, it can be concluded that damping is the most effective parameter to decrease the accelerations.

4. Damping in high-rise buildings

This chapter describes damping in high-rise buildings. First a definition of damping will be given. Secondly results of damping measurements in high-rise buildings will be presented. Next, the theoretical model proposed by Jeary will be presented to give a physical explanation for the observed behaviour. Based on the theoretical background and the measurements, available predictors of damping will be presented and their usability will be discussed.

In the first four sections the total damping in a building will be considered. However, different sources of damping will be distinguished in a structure. The fifth section will give a summation, description and explanation of different sources of damping in a high-rise building

4.1. General

When a guitar string is given an initial displacement, the string starts to vibrate, producing a tone with a certain sound intensity. After the first moment, the loudness of the tone decreases until it can't be heard anymore. At this point the string stopped vibrating. The faster the vibration reduces, the stronger the damping is.

Since the sound intensity of the tone is proportional to the amplitude of the vibration, the decrease of loudness indicates a decreasing amplitude which implies a loss of energy. This example illustrates the general applicable definition of damping:

"Damping is best defined as the dissipation of mechanical vibration energy from the system"
[Spijkers, et al., 2005, p. 163]

Results of vibration tests of beams of different materials also show a decrease of amplitude in displacement-time diagrams [Koten, 1977].

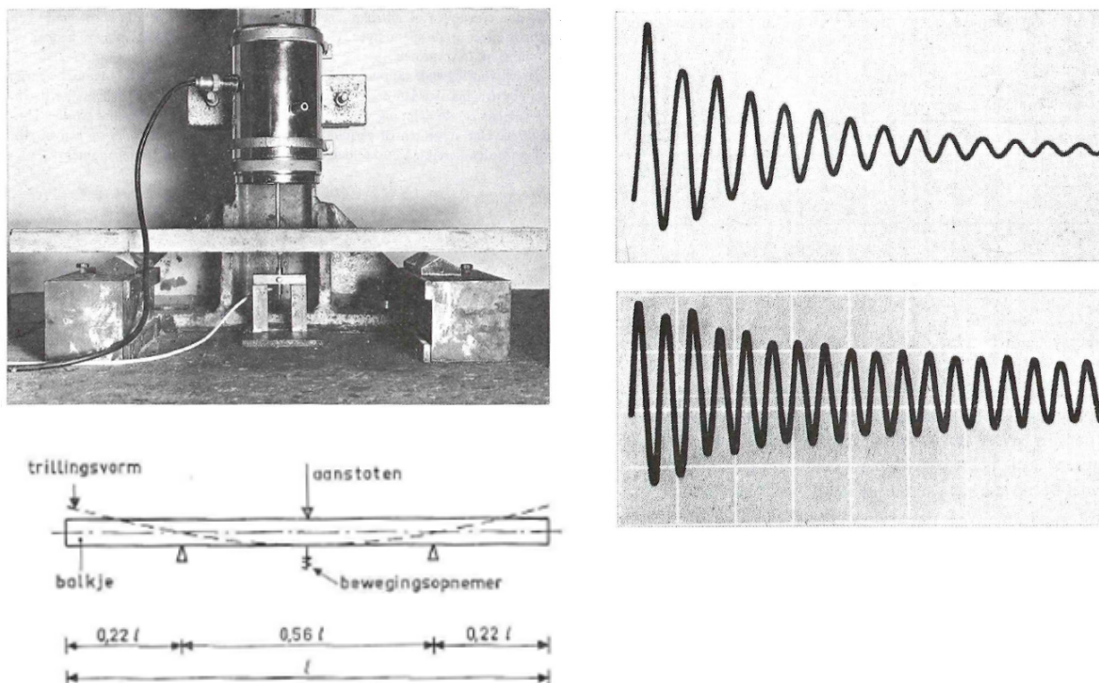


Figure 44 – left: test set up, right: displacement time diagrams of a steel and concrete beam [Koten, 1977]

4.1.1. Mathematical representation of viscous damping

The damped free vibration of a single degree of freedom system with viscous damping shows very good resemblances with the test results in Figure 44. In this model, the amplitude decreases exponentially and quantification of the amount of damping is based on this model.

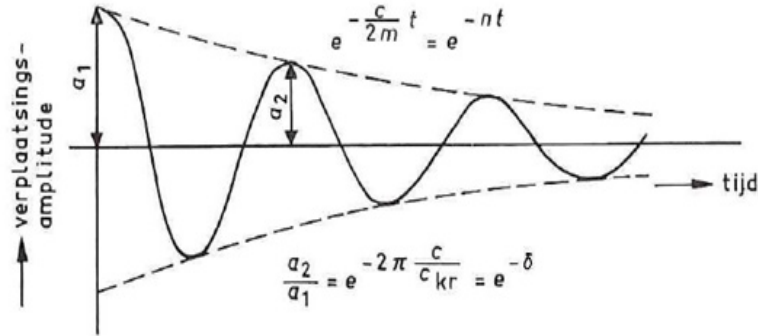


Figure 45 – damping of a vibration, decreasing displacement in time and damping representations [Koten, 1977]

In this thesis the following definitions of damping (related to viscous damping) will be used:

- The damping factor (c [N/ms^{-1}]) used in the equation of motion in a SDOF.
- The critical damping (c_{kr}) is the quantity of the damping factor that causes a system to fail to oscillate. In a one-degree of freedom system the critical damping is:

$$c_{kr} = 2\sqrt{km} \quad (4.1)$$

If $c < c_{kr}$ the vibration is periodic, if $c > c_{kr}$ the system fails to vibrate, see figure below. For slender buildings structures, it may be assumed that $c \ll c_{kr}$.

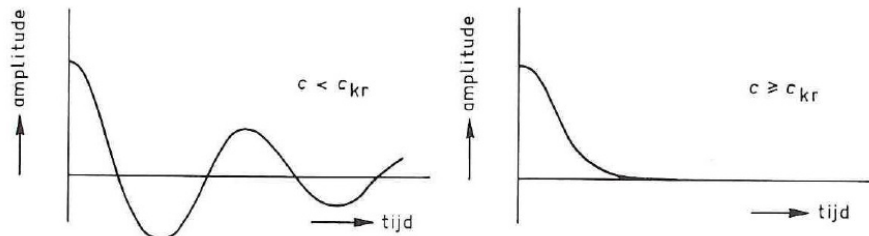


Figure 46 - left periodic vibration, right a-periodic vibration [Koten, 1977]

- The damping ratio (ζ [-]) is the actual quantity of damping in a mode of vibration divided by the critical value for that mode. For slender buildings $\zeta \ll 1$.

$$\zeta = \frac{c}{c_{kr}} \quad (4.2)$$

- Damping coefficient (n) is based on the damping ratio and the natural frequency of the vibration.

$$n = \zeta \omega_n = \frac{c}{2m} \quad (4.3)$$

- The logarithmic decrement (δ), is the natural logarithm of the decrement per cycle of oscillation when a system is vibrating in a mode of vibration; In the Eurocode the total damping of the building is represented by δ and can be related to ζ by the following expression:

$$\delta = \ln \frac{a_1}{a_2} = \frac{2\pi\zeta}{\sqrt{1-\zeta^2}} \rightarrow \delta = 2\pi\zeta \quad \text{for } \zeta \ll 1 \quad (4.4)$$

4.1.2. Other mathematical representations damping

It is convenient to use viscous damping in the dynamic modeling. However there are other mathematical models to describe damping. A hysteresis loop can be observed in the force-displacement diagram. By a comparison between the hysteresis loops of viscous damping and other types of damping, an equivalent viscous damping value can be found useable in the convenient dynamic modeling.

Hysteresis loop

A hysteresis loop can be observed in a force-displacement diagram (or equivalent, in a stress-strain diagram) when a material is (quickly) loaded and unloaded. It is harder to stretch a material during loading, than during unloading.

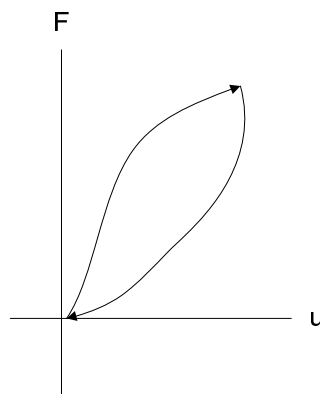


figure 47 – example of a hysteresis loop

The amount of energy/work needed to stretch a material is the area under the force-displacement line. So more energy is needed during loading than during unloading. The difference is the loss of energy during loading and unloading. When a material is harmonically loaded, the obtained loop in the force displacement diagram, is the hysteresis loop and the area of the loop is the energy being dissipated during one cycle. [Spijkers, et al., 2005, §5.2]

Hysteresis loop for viscous damping

If a viscous damping is assumed, the damper force is proportional to the velocity. If a harmonic force is applied on a system with a spring and a damper, the damper force reaches its maximum half a period later than the spring force. The total force on the mass is:

$$F = F_c + F_s$$

$$F = c\omega\hat{u} \cos(\omega t) + k\hat{u} \sin(\omega t) \quad (4.5)$$

This represents an ellipse in the force-displacement diagram.

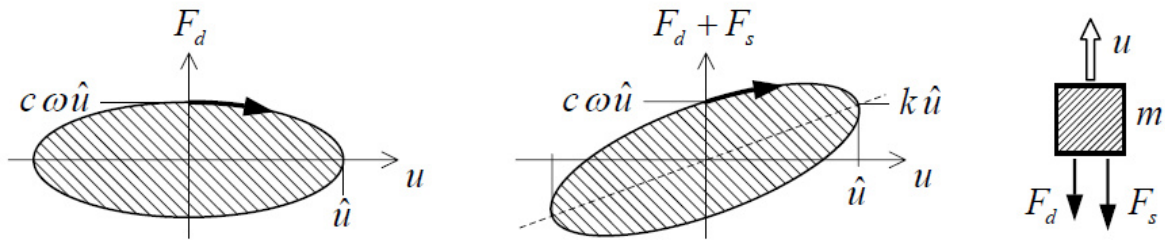


Figure 48 – development of the forces in spring and damper per oscillation for viscous damping [Spijkers, et al., 2005, §5.2]

in which the area of the right ellipse is equal to:

$$E_{diss} = \int_0^T F du = \int_0^T F \dot{u} dt = c\pi\omega\hat{u}^2 \tag{4.6}$$

Equivalent viscous damping

If the force-displacement diagram isn't shaped like an ellipse as in Figure 48, an equivalent viscous damper can be determined that gives the same amount of energy dissipation per cycle.

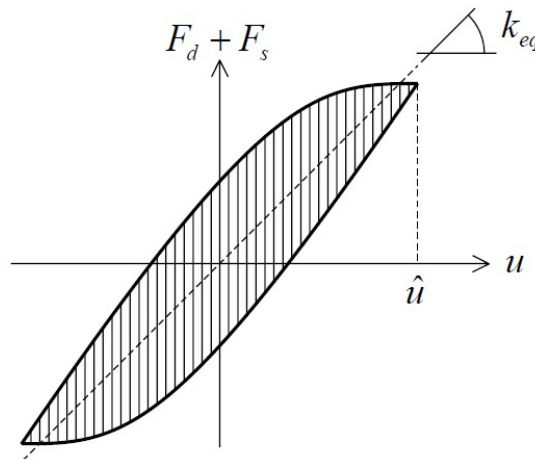


Figure 49 - Irregular shaped force-displacement diagram [Spijkers, et al., 2005, §5.2]

The equivalent viscous damper can be calculated assuming that the energy dissipated by the non-viscous damping must be equal to the energy dissipated by the equivalent viscous damper.

$$E_{viscous, equ} = E_{diss} \tag{4.7}$$

$$c_{equ} \pi\omega\hat{u}^2 = E_{diss} \rightarrow c_{equ} = \frac{E_{diss}}{\pi\omega\hat{u}^2}$$

In appendix H, a description and formula for the equivalent viscous damping for other mathematical representations of damping can be found.

4.2. Measured values of damping in high-rise buildings

There are multiple methods to determine damping from time-response measurements of high-rise buildings. An explanation about different methods can be found in appendix I. In the past, damping values have been determined from the response due to random wind loading with the half-power bandwidth method or the autocorrelation method. These results are most likely to be invalid because the length of the datasets is too short to be stationary. As a consequence, the derived statistical properties from the measurements are not invariant of time. The random decrement technique gives the best results for measurement in practice because under random loading it provides accurate results on short datasets. It also enables to obtain damping values at different amplitude values.

Because it is not always clear what method has been used, results from the past have been used with care. The used damping values in this section are selected on their reliability. Damping values obtain from articles that also mention the amplitude dependency of damping are considered to be reliable because they have most likely been obtained by the random decrement technique.

Important results and conclusions from diverse damping databases and full scale measurements will be summarized in this section. The amplitude dependency of damping will be discussed in the last subsection.

4.2.1. The world wide damping database

The most recent collection of measured damping around the world [R.J. Smith, et al., 2010] can be found in Figure 50. The primary source is the Japanese Damping Database [Satake, et al., 2003]. Damping values of buildings around the world from diverse published articles have been added. For buildings with different damping values per mode of vibration, an average has been taken.

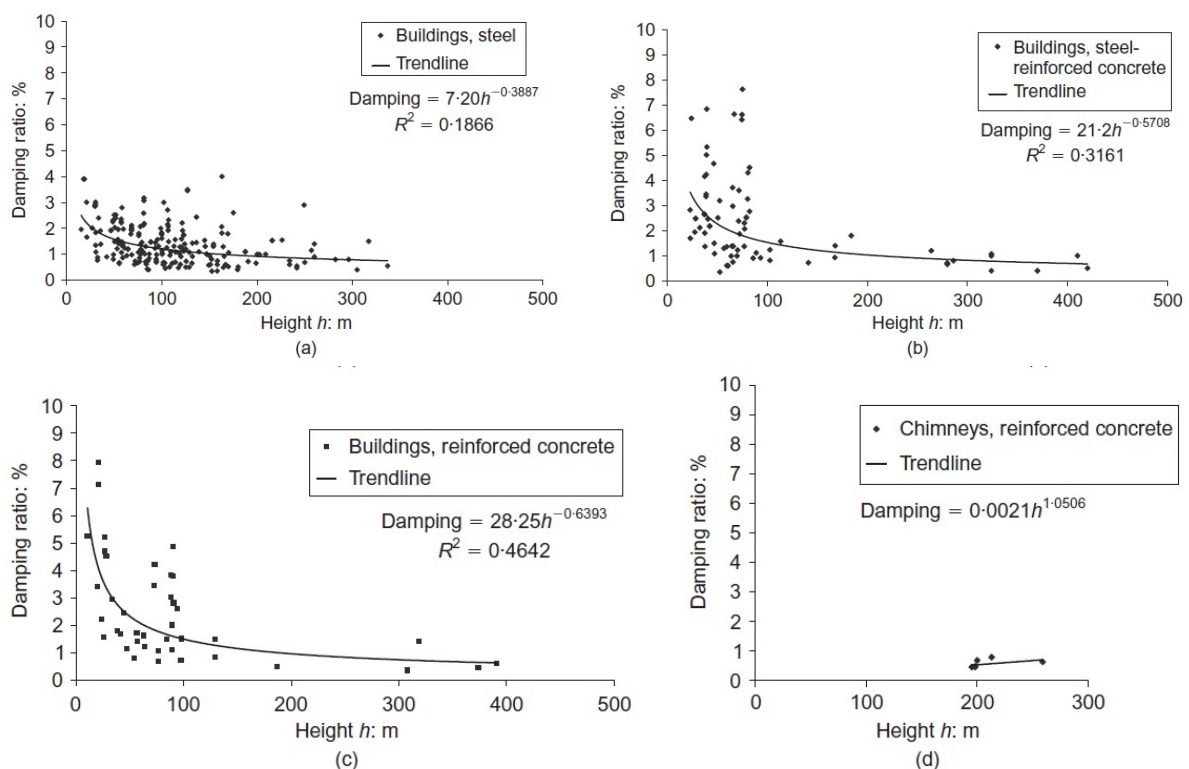


Figure 50 – most recent damping database. (A) steel buildings, (B) steel-reinforced concrete buildings, (C) reinforced concrete buildings and (D) reinforced concrete chimneys. [R.J. Smith, et al., 2010]

The following conclusions have been based on this database.

- 1) The trend lines seem to have a lower bound value. This damping ratio of 0.3% might be interpreted as the intrinsic damping of the structural material itself (irrespective of the material)
- 2) A lot of scatter can be observed in the results. This can be caused by variability in type and age of the buildings, type of non-structural fit-out, foundation type and amplitude of measurement.
- 3) A downward trend of damping ratio can be observed in the fitted curves as building height increases. For buildings higher than 250 meter, no damping ratio higher than 1% has been measured.

According to the author, this effect can be explained by the relative small contribution of non-structural components since the primary load-bearing structure is relatively large in tall buildings. Façades of tall buildings are also less activated for damping since they tend to have little resistance against in-plane deformation (otherwise they would be damaged because of the larger movement in a tall building).

- 4) Based on the results, no clear relation between the material and magnitude of damping ratio has been observed. This is in contradiction with the common practice where higher damping ratios are assumed for concrete structures, than for steel structures. However this relation can be disturbed by the influence factors that have been mentioned at point 2.

4.2.2. The Japanese Damping Database

Although the Japanese damping database has been used as the main source for the former mentioned collection and conclusions, the measured damping values also have been studied more into detail [Satake, et al., 2003].

In total the database contains 205 carefully selected buildings. 137 steel-framed buildings, 25 reinforced concrete buildings (RC) and 43 steel-framed reinforced concrete buildings (SRC). The damping ratios for translational vibration modes in two orthogonal directions and torsional vibration modes, have been determined, together with amplitudes. Every record holds information about features that may influence dynamic properties: building height, number of stories, building plan, building use, structural type, cladding type, foundation type, depth of foundation and length of piles. From this database, effects of several building factors have been investigated.

Natural period and building height

The relation between natural period and building height has been studied. A well correlated regression line can be fitted in graphs. There is a linear relation between building height H , and the natural period T_1 . From this it can be concluded that the natural period is proportional to the height.

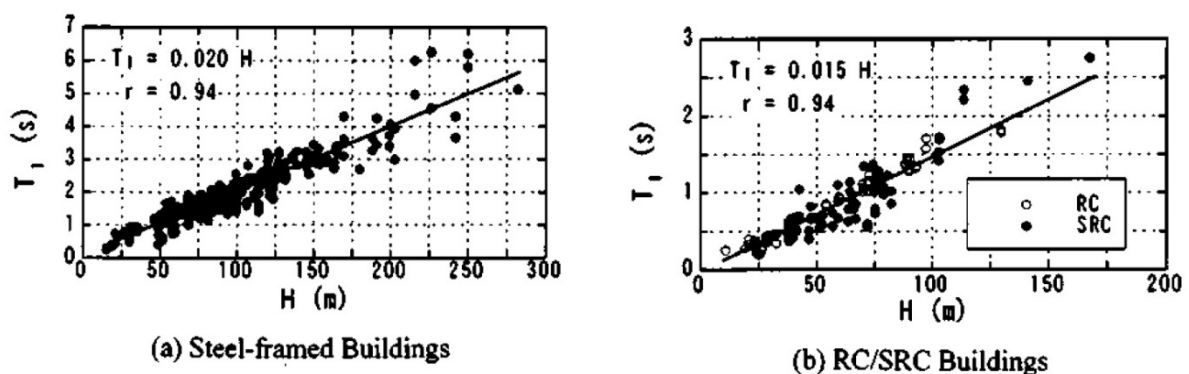


Figure 51 – linear relation between building height and translation first-mode natural period T_1 [Satake, et al., 2003]

Damping ratio and building height

The relation between building height and damping ratio has been investigated. A fitted line was drawn through the results, but the scatter is much larger than for the natural period and building height. Prediction of damping with the fitted line is very inaccurate. The author suggests that the scatter is caused by amplitude dependency of the damping ratio. Despite this, it can be observed that the damping ratio decreases as building height increases. It can also be observed that the damping ratio of concrete buildings is higher than for steel buildings.

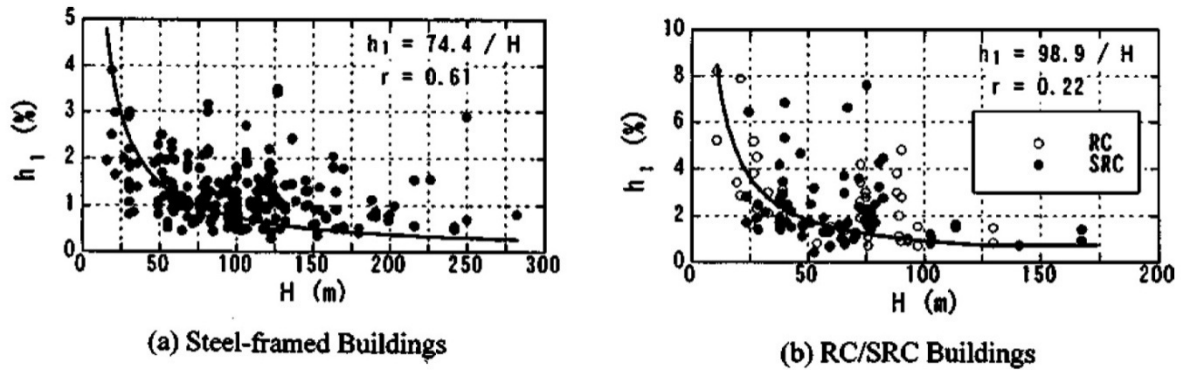


Figure 52 – (fitted) relation between damping ratio (h_1) and building height (H) [Satake, et al., 2003]

Damping ratio and natural period

Because a linear relation between building height and natural period has been observed, the same shaped relation between damping ratio and height can be observed as for the relation between damping ratio and building height.

Foundation Type

The influence of the foundation type has been investigated. A spread and a pile foundation have been distinguished, but no clear trend has been found.

D_f is the depth from ground level to the basement level for both the spread and the pile foundations. D_p is the length of piles. Although it is not very clear from the graphs, the author has indicated that the damping ratio decreases with increasing D_f . But the decrease could also correspond to the lower damping for larger heights, because D_f is mostly designed deeper for higher buildings

No clear correlation between D_p and the damping ratio has been found. The influence of soil conditions haven't been researched because insufficient data was available.

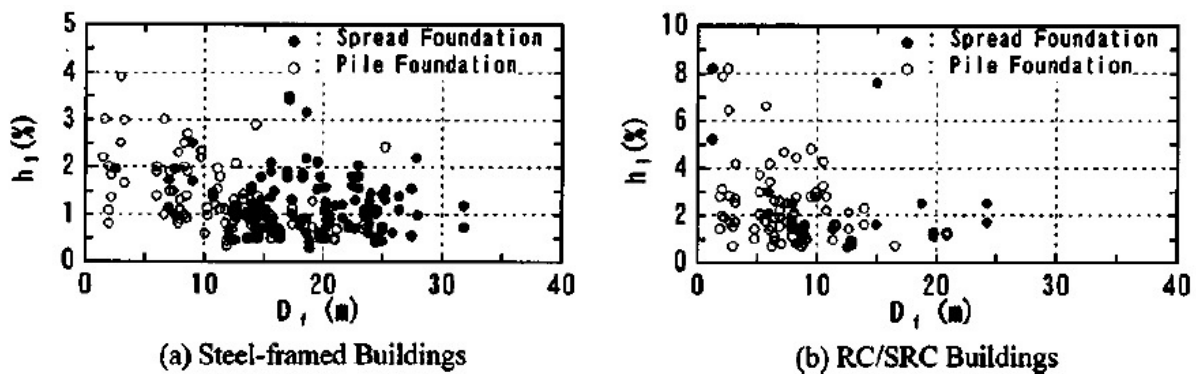


Figure 53 – relation between the foundation depth D_f and translational first-mode damping ratio [Satake, et al., 2003]

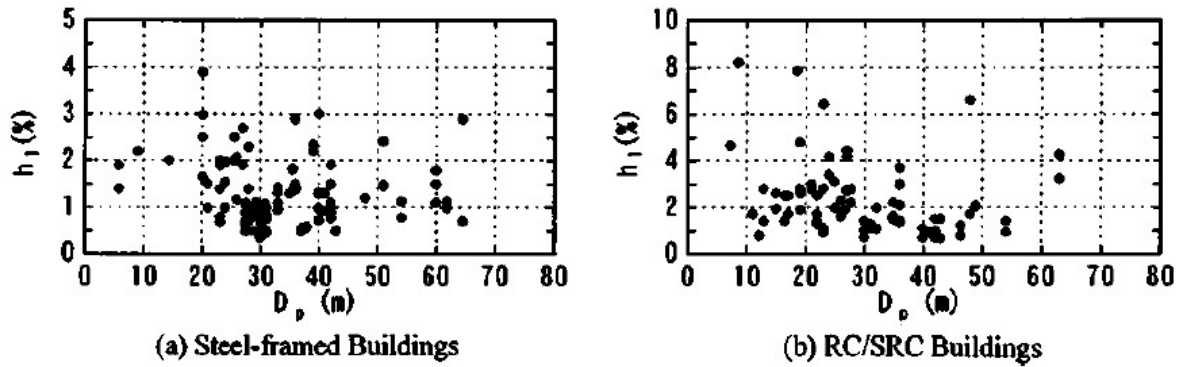


Figure 54 – relation between the pile length D_p and translational first-mode damping ratio [Satake, et al., 2003]

Building use

To investigate the effect of non-structural elements on the damping ratio, a distinction has been made between apartments and offices. It has been assumed that apartments have more and more rigid partition walls than offices. The result can be found in the figure below. For steel-framed buildings the mean value for apartments are slightly larger. This effect is not as clear as in concrete buildings. It has been concluded by the author that despite even more in depth investigations of the results, no accurate correlation has been obtained for the effect of non-structural members.

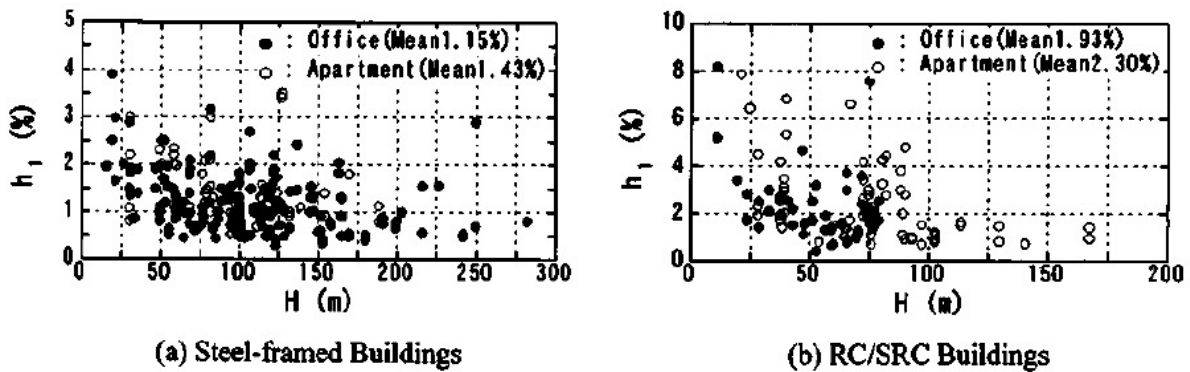


Figure 55 - relation between building use and translational first-mode damping ratio [Satake, et al., 2003]

4.2.3. Chicago full-scale monitoring program

In [Kijewski-Correa & Pirnia, 2007] the effect of the structural type on the dynamic properties has been observed based on full scale monitoring of 5 buildings: B1, S1, C1, C2 and C3. The properties of these buildings can be found in the table below.

Table 3 - Results of the measurements presented in the paper [Kijewski-Correa & Pirnia, 2007]

Building	material	constructive system	Height	Damping ratio (%) design			Damping ratio (%) in situ		
				X	Y	T	X	Y	T
B1	Steel	Framed	245,7	n.a.	n.a.	n.a.	n.a.	n.a.	n.a.
S1	High strength RC	Core wall system	264	1,5	1,5	1,5	1,45	1,3	1,7
				X	Y	T	X	Y	T
C1	Steel	tube of exterior columns	n.a.	1	1	n.a.	0,8	0,7	n.a.
C2	RC	shear walls+outrigger	n.a.	1	1	n.a.	1,2	2,1	n.a.
C3	Steel	moment-connected, framed tubular system	n.a.	1	1	n.a.	1	1	n.a.

From observation of the measured damping ratios at different levels of amplitude, it has been concluded that a larger damping ratios can be observed in modes of vibration with significant ‘frame action’ in comparison with ‘cantilever/axial shortening action’.

Frame action is observed as un-braced frames with stiff connections between beams and columns resist the lateral load. The deformation is shaped like the shear deformation of a panel. Deformations are due to a combination of shearing and flexure of the frame members and flexibility of the connections.

Cantilever/axial shortening action is observed as braced frames or cantilevered beams resist the lateral load. The deformation is shaped like bending of a beam. Deformations are due to axial shortening of the material.

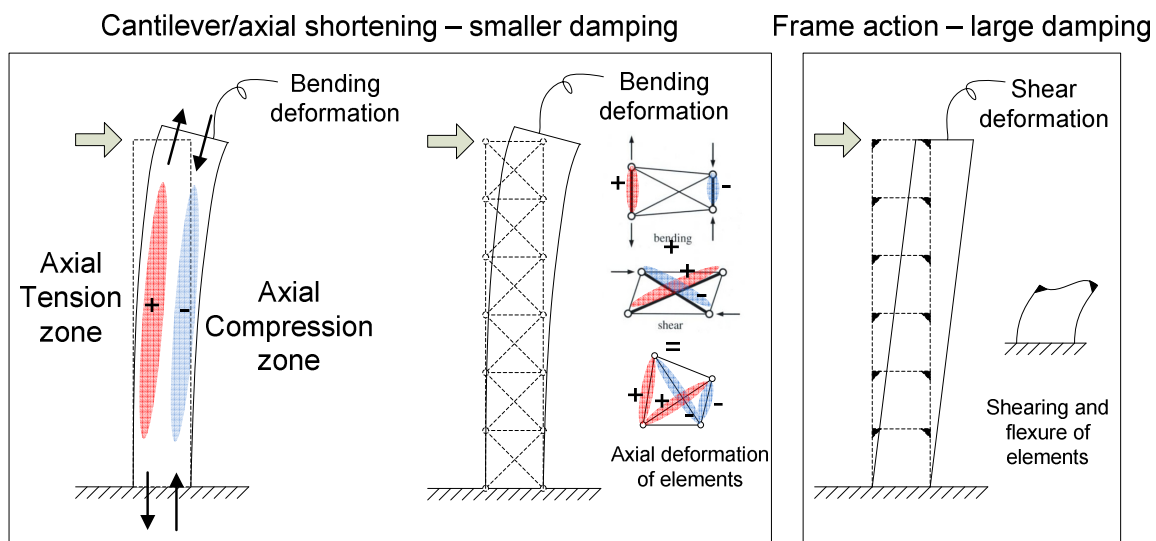


Figure 56 – more damping observed under frame action (right) than under cantilever/axial shortening (left)

4.2.4. The UK-damping database

The natural frequency and damping ratio of 16 buildings in the UK can be found in appendix J.2. On the basis of these results, the author suggests that safe estimations of damping are 1.0% for normal buildings and 0.5% for very tall buildings. The soil structure interaction has also been investigated and it has been concluded that: *“base motion of a building will generate ground waves and provide an extra mechanism of dissipation of energy. But this soil structure interaction is usually insignificant for the fundamental modes of tall buildings, although it can be significant for shorter or very stiff structures.”* [Ellis, 1996] The damping values have been obtained in the low amplitude region.

According to the author, it would be unwise to extrapolate these to the higher amplitude region because at higher amplitude regions, close to damaging, other mechanism of energy dissipation can occur that have not yet been investigated.

It can be concluded that the amplitude plays an important role on the damping value and the significance of damping in the foundation is still unclear and needs to be investigated.

4.2.5. Other damping measurements

The results from full scale monitoring of three individual buildings have been gathered because the results of the amplitude dependency has been determined as well. The results can be found in appendix J.3 and J.4. The properties of these buildings can be found in the table below:

Table 4 – properties of three buildings in China [Fu, et al., 2008; Li, et al., 2004]

Building	Location	material	Main load bearing structure	height [m]	Damping ratios [%] (range, first mode)
CITIC Plaza Tower	Guangzhou	concrete	tube in tube + outriggers at three levels	391	0,2-0,5
Di Wang Tower Guangdong	Shenzen	concrete+steel	core + steel tube coupled with outriggers at 4 levels	384	0,2-0,7
International building	Guangzhou	concrete	core	200	0,12-0,3

Although the first two buildings have different types of structural systems, it has been observed that both buildings have comparable damping ratios. The measured damping ratios of the third building are very low compared to damping ratios of other buildings with a concrete main load bearing structure although it has to be noted that the damping has been determined in the low amplitude region.

4.2.6. The influence of the amplitude on damping

An increase of the amplitude causes an increase of the damping and a small decrease of the natural frequency. This has been concluded from the Japanese damping database [Satake, et al., 2003], The Chicago full-scale monitoring program [Kijewski-Correa & Pirnia, 2007] and the other measurements.

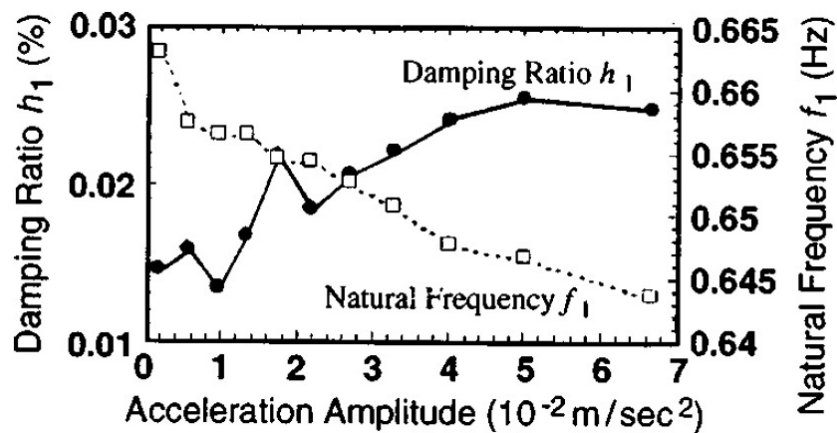


Figure 57 – variation of damping ratio and natural frequency in a 99 m high steel-framed building [Satake, et al., 2003]

The increase of damping at higher amplitudes can be explained by the activation of energy dissipation in more and smaller cracks at higher amplitudes, this is in accordance with Jeary's theoretical model that will be explained in the next section (see §4.3). The decrease of natural frequency can be explained by the same mechanism as stiffness decreases with more cracks.

Tamura, Kijeski-Correa and Pirnia have shown that damping sometimes decreases with amplitude [R.J. Smith, et al., 2010]. Tamura has proposed a '*critical tip deflection*', the deflection at which the damping is maximum. According to Tamura this happens already at relative small amplitude (10^{-5} to 10^{-4} of the building's height). This '*critical tip deflection*' can be observed in Figure 58.

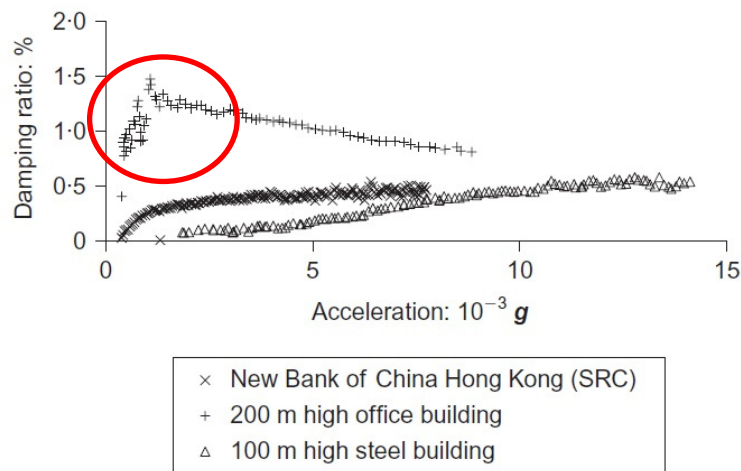


Figure 58 – relation between damping and amplitude (transformed in acceleration) [R.J. Smith, et al., 2010]

This “critical tip deflection” at relative small amplitudes contradicts with the Jeary’s theoretical relation between amplitude and damping. According to his theory, a drop of damping will only be expected in the high amplitude region. In this thesis Jeary’s theoretical damping model will be adopted because it is adopted more general.

4.2.7. Conclusion

From the damping values that have been obtained from measurements, it can be concluded that multiple aspects can influence the damping. The dimensions of the building are of importance. In general a downward trend is visible as damping is plotted as a function of height. At larger heights (>250 m), there seems to be a lower bound of 1% of damping. Structural aspects such as type and material of the main load bearing structure (MLBS), type of foundation and non structural fit-out are also aspects that will probably influence the amount of damping. Measurements have shown that higher damping ratios can be expected especially at buildings that are stabilized by systems with considerable frame-action.

In practice, higher damping ratios are assumed for concrete MLBS, than for steel MLBS. This relation between material and magnitude of damping ratio has not always been observed, but this relation will probably be disturbed by the already mentioned factors and because of the amplitude dependency of damping.

The amplitude dependency has to be taken into account to be able to give a good comparison between obtained damping values, this relation will be discussed in the next two sections. The structural aspects will be dealt with in §4.5.

4.3. Theoretical mechanism behind damping

Based on measurements a theory behind the mechanisms of damping has been proposed. [Jeary, 1986] Two plateaus and a non-linear region have been distinguished. Later measurements in the low amplitude region also show good resemblances with this model [Li, et al., 1998]. In this section, the mechanism behind this model will be explained.

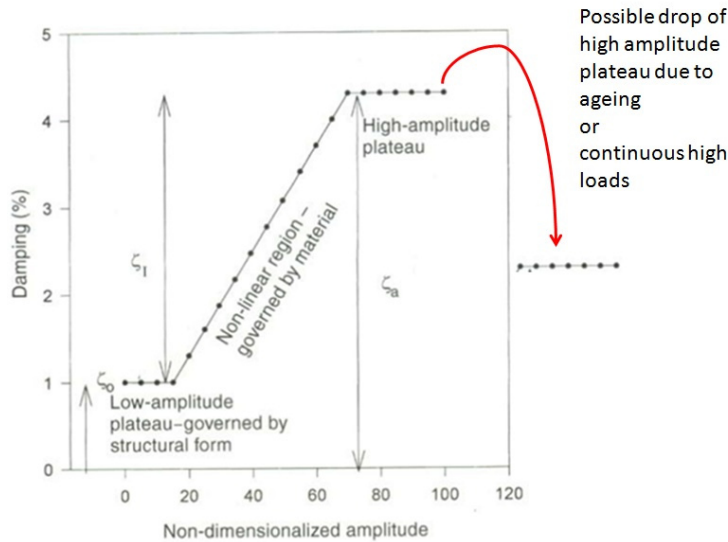


Figure 59 – Jeary’s theoretical damping model [Jeary, 1986], which is supported by measurements

4.3.1. Energy dissipation in a structure

Based on the early works of T.A. Wyatt, the dominant energy losses are assumed to be caused by friction. This friction is associated with a stick-slip model and occurs at two different scales in a structure: between structural elements (in joints, at interfaces between structural elements, interface between wall and doors or windows) and at micro scale in the material. [Jeary, 1997b, pp. 164-173]

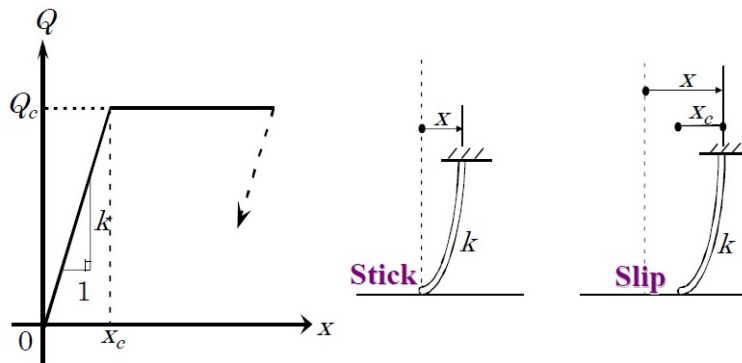


Figure 60 – Stick-slip model for damping mechanisms in material [Tamura, 2005]

4.3.2. Explanation of the observed plateaus

Micro cracks of different lengths exist through the material. The critical shear stress at which lengthening of the micro cracks occurs is given by [Jeary, 1986]:

$$S_{cr} = \frac{4ET}{l} \tag{4.8}$$

T is the surface energy of the crack, and l is the length of the crack. This equation and model give the physical explanation of the observed amplitude dependency.

- The low amplitude plateau is caused by the friction between structural elements. The length of the interface can be considered as the largest available crack lengths. At low amplitude these cracks shall first be mobilized. *“Since the amount of energy dissipated in this way will be relatively large, this mechanism seems to represent, for practical purpose, a relatively constant damping value for a range of low amplitudes”* [Jeary, 1986, p. 740]
- Increase of damping with amplitude is caused by the presence of cracks with different lengths. As amplitudes increases, more cracks, with smaller lengths will participate in the energy dissipation
- The high amplitude plateau is reached as all joint are mobilized and all cracks have been lengthened.

Lengths associated with the low amplitude region extend from 0,5 m down to 20 mm. The non-linear region has been associated with cracks of length from 20 mm up to 100 μm . [Jeary, 1997b, §7.1]

4.3.3. Conversion

More recent work [Jeary, 1996] also provides a further explanation of the damping at micro scale. At micro scale of a concrete building a change of needle-shape crystals to plate-like crystals have been observed at locations where higher dynamic stress have occurred. This process occurring in time is called *conversion*. The conversion process creates smoother surfaces and the potential for energy dissipation in material will decrease in time. As a consequence:

Older buildings will have lower damping.

Jeary has also indicated this as an additional mechanism that occurs at very high loading. The high amplitude plateau falls if this high loading continues for some time. In practice this is not very likely to occur since earthquake loads will only act during short periods.

4.3.4. Equivalent viscous damping

The theory of Jeary makes clear that the mechanism behind structural damping is dominated by friction damping. According to [Jeary, 1997b, p. 166] it is allowed to describe damping in high-rise structures by viscous damping because:

“Luckily work by Wyatt (1977) has shown that a multitude of friction mechanisms, which are clearly present in structures, when summed over a range of amplitudes, actually produce a result that looks like a viscous-type response.”

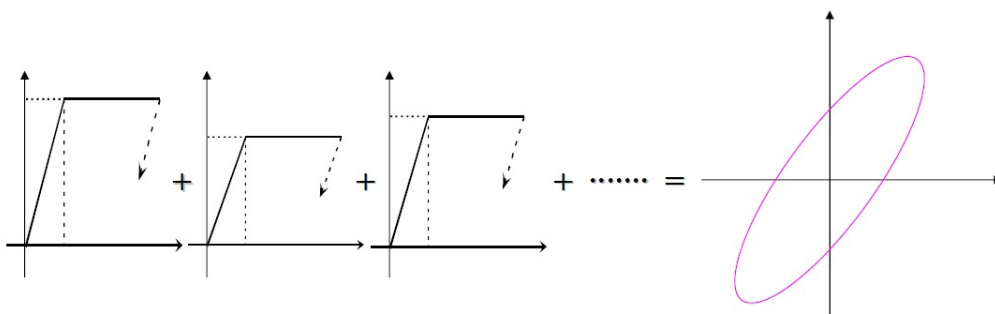


Figure 61 – friction damping over a large range of amplitudes, gives a viscous damping model. [Tamura, 2005]

4.4. Prediction of damping

Based on measurements and the theory behind damping, predictors of damping have been formulated. Three different predictors are presented and compared. The usability of the predictors is discussed in the fifth subsection.

4.4.1. Jeary's damping predictor

A formula to estimate the damping for buildings in the first two areas of Jeary's damping model (low amplitude plateau and non-linear region, see Figure 59) has been proposed [Jeary, 1986]:

$$\zeta = \zeta_0 + \frac{x}{h} \cdot \zeta_I \quad (4.9)$$

$$\zeta = f_n + \frac{x}{h} \cdot 10^{0.5\sqrt{d}}$$

In this formula, ζ_0 is the low amplitude damping. It has been indicated that this factor can be related to the natural frequency f_n , x is the amplitude, h is the height of the building and d is the depth of the building at its base. Since the largest stresses occur at the base of a tall building, the dimension is of influence on the damping.

Drawback of this predictor is that it doesn't take the following cases into account:

- Significant Soil Structure interaction can't be taken into account
- The formula doesn't take effects into account when amplitude exceeds the yield point.
- No distinction has been made between a cladded and un-cladded building
- Artificial damping can't be taken into account.
- The formula is based on a small database of 8 buildings measured in the U.K.

4.4.2. Damping predictor from the Japanese Database (AIJ2000)

Based on measurements on a large amount of buildings [Satake, et al., 2003] a damping predictor for reinforced concrete buildings has been derived

$$\zeta = 0.014 \cdot f_n + 470 \left(\frac{x}{h} \right) - 0.0018 \quad (4.10)$$

This formula can be used in the low amplitude range ($x/h < 2 \cdot 10^{-5}$) and for building heights 10 m < h < 130 m. A predictor for steel-framed buildings has also been derived

$$\zeta = 0.013 \cdot f_n + 400 \left(\frac{x}{h} \right) + 0.0029 \quad (4.11)$$

This formula can be used in the low amplitude range ($x/H < 2 \cdot 10^{-5}$) and for building heights 30 m < H < 200 m.

4.4.3. Lagomarsino's damping predictor

Lagomarsino's predictor describes Rayleigh-type damping and doesn't depend on the amplitude [Satake, et al., 2003]:

$$\zeta = \alpha T_n + \frac{\beta}{T_n} \tag{4.12}$$

T_n is the natural period ($T_n=1/f_n$). For reinforced concrete buildings $\alpha=0.0072$ and $\beta=0.0070$. For Steel-framed buildings $\alpha=0.0032$ and $\beta=0.0078$.

4.4.4. Comparison of different predictors

AIJ2000 and Lagomarsino’s predictor have been compared to each other.

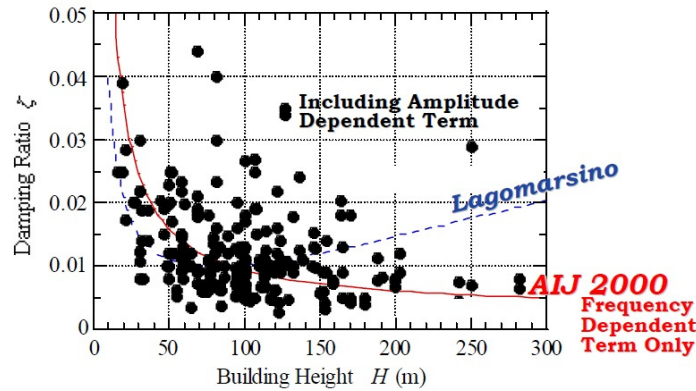


Figure 62 – comparison between two damping predictors for steel buildings [Tamura, 2005]

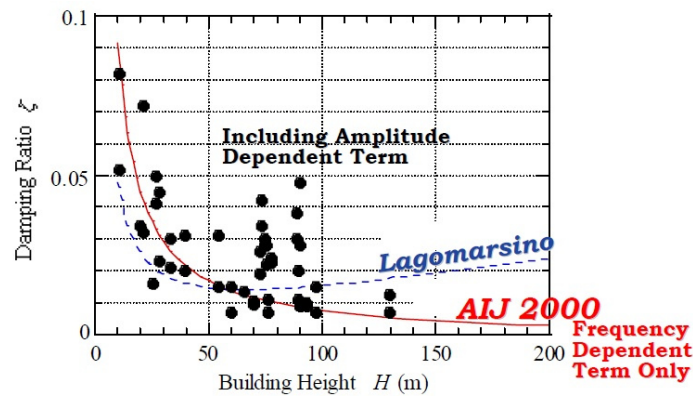


Figure 63 – comparison between two damping predictors for reinforced concrete buildings [Tamura, 2005]

The relation between damping ratio and building height has been plotted for the predictors by making use of the relation between the fundamental natural frequency and the building height based on the Japanese Database. [Tamura, 2005]

$$f_n = \frac{67}{H} \text{ for reinforced concrete buildings} \tag{4.13}$$

$$f_n = \frac{50}{H} \text{ for steel buildings} \tag{4.14}$$

Jeary’s predictor will show the same behaviour as AIJ2000 since the relation between damping and frequency is of the same form. From the comparison it can be concluded that Lagomarsino’s predictor underestimates the damping ratio for buildings lower than 60 m and overestimates the damping for buildings higher than 60 m.

Despite the fact that amplitude dependency of damping has been taken into account, many data points still deviate a lot from the predicted line. Assuming that the proposed amplitude dependency is valid, it can be concluded that the influence of different structural aspects is also of importance.

4.4.5. Usability of damping predictors

Buildings must be designed to withstand a maximum hourly mean wind speed with a return period of 50 year. This characteristic wind speed in the Netherlands is about 25-30 m/s. [NNI, 2005] The chance of actually determine the damping during these extreme wind conditions is very small. In theory a building should be monitored during 50 year to actual measure during this extreme condition. Formulae for prediction of damping have been based on damping values that have been determined under moderate wind conditions up to wind speeds of 18 m/s (wind force 9 on Beaufort's scale). [Galanti & Oostvogels, 2006]

For the design of most high-rise buildings in the Netherlands, the maximum deflection has been taken as the governing criterion for the design. With increasing slenderness and application of lighter building materials, human comfort will become more governing. This criterion has to be checked in the SLS, so use of damping predictors based on measurements under moderate wind conditions is a valid method, mainly because deformations in the SLS are reversible and damping mechanisms as described by Jeary in the non-linear region (§4.4.1) will occur.

Structural engineers are still interested in damping ratios at higher wind speeds (=higher amplitude) since design can be based on strength requirements during higher wind speeds. Also in other countries, the design of high-rise buildings is more governed by stresses in the ULS caused by typhoons and severe earthquakes. Measurement of damping at this amplitude level is scarce and the presented predictors are not usable for this.

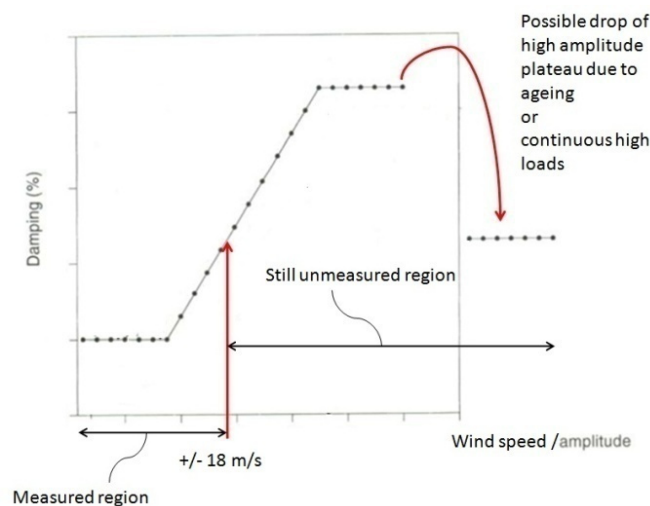


Figure 64 – indication of measured area and still uncertain prediction of damping in the unmeasured region

The damping predictors based on damping values obtained from measurements are most usable for design criteria concerning the deflection and the acceleration in the SLS.

4.5. Sources of damping in high-rise building

In the former sections a definition of damping has been given and damping values obtained from measurements of buildings around the world have been gathered. Also the mechanism behind the amplitude dependency of damping has been elucidated with the theory of Jeary. Based on this theory, damping predictors have been proposed that take into account the used building material of the main load bearing structure and the dimensions of the building (height and depth). Still the data points deviate from the predicted line. The influence of the type of foundation, non-structural fit out and type of main load bearing system can be the cause of this scatter. To get a better estimation of the damping, the influence of these structural characteristics should be taken into account.

Damping is the dissipation of energy. Different sources of energy dissipation can be found in the table below. Four different sources have been distinguished in a high-rise building. The damping that has been discussed so far is the total damping due to energy dissipation from all these sources.

The total damping in the Eurocode (see appendix B.2.3) has been split into the structural damping (δ_s), the aerodynamic damping (δ_a) and the damping from additional devices (δ_d). The first part represents the loss of energy through the main load bearing structure deformation, non structural elements interaction and the soil structure interaction.

$$\delta = \delta_s + \delta_a + \delta_d \tag{4.15}$$

Characteristic values and/or calculation methods, influence factors and the mechanisms behind these sources will be explained in the following subsections.

Table 5 – overview of different sources of energy dissipation and type of damping [Tamura, 2005]

	Energy Dissipation Inside			Energy Dissipation Outside		
	Solid	Liquid	Gas	S-S	S-L	S-G
Friction	Internal Friction Damping	-	-	External Friction Damping	-	-
Viscosity	-	Internal Viscous Damping	-	-	External Viscous Damping	-
Radiation	-	-	-	Radiation Damping	-	-
Interaction	-	-	-	-	Hydro-dynamic Damping	Aero-dynamic Damping
Plasticity	Hysteretic Damping	-	-	-	-	-

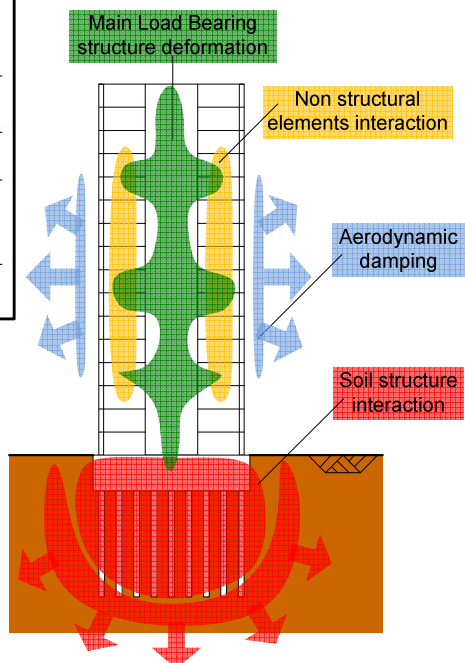


Figure 65 – four different areas of energy dissipation

4.5.1. Main load bearing structure deformation

There are three main types of mechanisms behind the loss of energy in the main load bearing structure:

- The internal material damping of the construction material. *“The energy dissipation occurs in the material itself at an atomic or molecular level. Thermo-elastic, thermodynamic, magneto-dynamic, etc. are terms, which indicate the different damping mechanisms. The (damping) energy finally disappears as heat from the structure. In the case of material damping the energy dissipation occurs all over, and especially there were stresses are large.”* [Spijkers, et al., 2005, p. 164]
- Damping that develops when the structure is subjected to load reversals that cause plastic deformation. Due to this non linear relation between load and deformation, a hysteresis loop will develop. [Spijkers, et al., 2005, p. 164]
- Loss of energy through friction damping in the joints between structural elements or simply supports. *Steel buildings with bolted connections have more friction damping as compared to a fully welded construction. A prestressed concrete building has less damping as compared to a mild steel-reinforced construction because in prestressed concrete cracking of concrete is relatively less.* [Taranath, 1998, p. 279]

Internal material damping

Dynamic tests of different beams [Koten, 1977] have shown that the internal material damping shows a good fit with viscous damping, so the internal material damping is proportional to the velocity of loading and unloading and damping ratios have been derived (see Table 6)

Table 6 –damping ratio's for different materials [Spijkers, et al., 2005]

Material	Material damping $\zeta=c/c_{kr}$ (%)	remark
steel	0,4	
reinforced concrete	0,9	before and after cracking
prestressed concrete	0,9	
wood (Picea)	2,1	
wood (Fagus sylvatica)	2,5	
Rubber	3	frequency above 10 Hz
Rubber with canvas	8	frequency above 1 Hz
Aluminium	1,8	
Glass	6	
masonry	4	
Dry Sand	1-3	
Sand-gravel	3-7	
Clay	2-5	

Non-linear influence

For many construction materials, the strains increase more than linear at increasing stress beyond the yielding point. Therefore the stress-strain diagram of many construction materials has been schematized as a bi-linear diagram. A hysteresis loop as described for Elastic-Plastic damping will occur (see appendix H.3). Because of the more than linear increase of strain, the area of the hysteresis loop will increase. The damping increases and this has been observed in testing of damping in materials. [Koten, 1977]

Dynamic loading beyond yielding normally doesn't occur in buildings because the material will be weaker because of fatigue. The design would be bad if this occurs. However small loads, at resonance frequencies can cause stresses close to the yielding point. But because the increase of damping when the material yields is so strong, the maximum displacements will occur just before yielding.

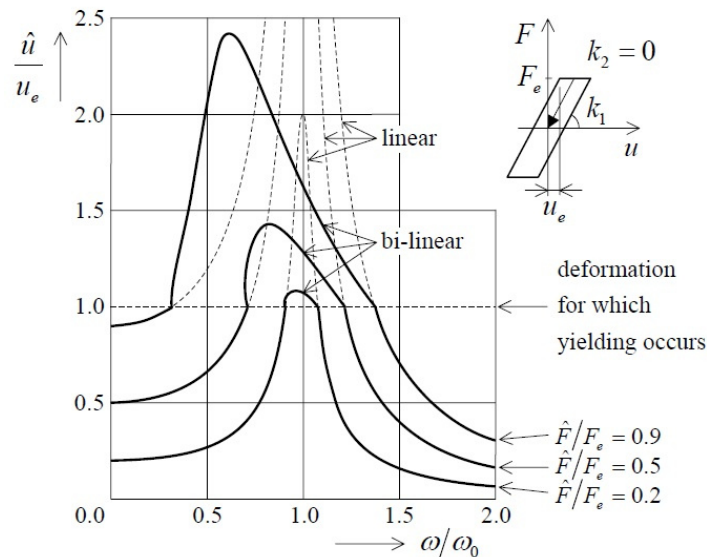


Figure 66 – comparison of the frequency response function of a linear and a bi-linear stress-strain relationship. [Spijkers, et al., 2005]

When the bi-linear stress-strain relationship is taken into account, the frequency response function is adapted. A negative skew appears and the maximum response occurs at a lower frequency, this behaviour is denoted as softening. The opposite behaviour is called hardening. This behaviour has also been observed at high-rise buildings [Ellis, 1996].

4.5.2. Non structural elements interaction

Two types of energy dissipation can occur for non structural elements:

- Energy dissipation can be lost through friction forces at contact surfaces in joints between non structural elements or between non structural elements and the main load bearing structure. [Spijkers, et al., 2005, p. 164; Taranath, 1998, pp. 279-280]
- Internal material damping of the non structural elements (see internal material damping §4.5.1)

Results of measurements have been reported that cladding of buildings will lead to higher damping ratios [Oosterhout, 1996, p. 103]. In the next two subsections the damping mechanisms that most likely will occur at the separation walls and the façade will be explained.

Separation walls

When a separation wall has been connected to the MLBS, it will deform when two floors move relative because of dynamic wind loading. Energy can be lost because of internal material damping.

However, it is conveniently to vertically support a separation wall only at the bottom or top side in order to prevent internal stresses in the separation wall. At one side, a sliding connection (U-profile in Figure 67) allows the wall to move relative to the main load bearing structure. Energy can be lost

because friction forces can developed at this surface when two floors move relative to each other because of dynamic wind loading.

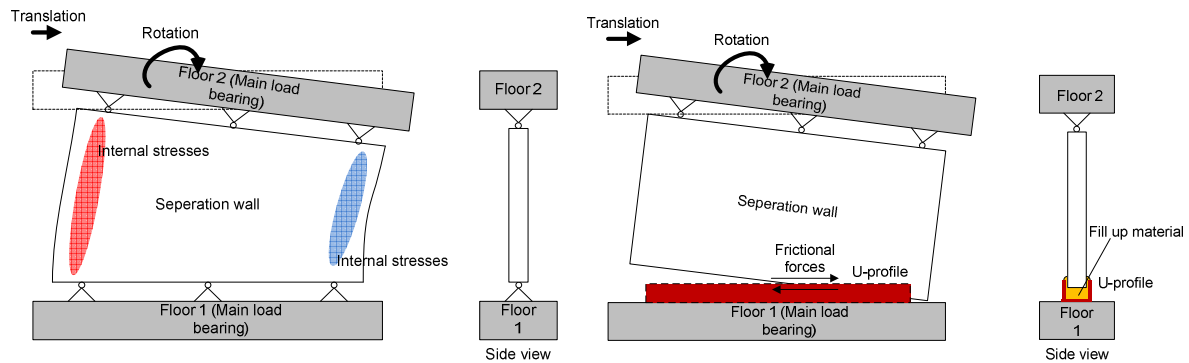


Figure 67 – Two types of connection and two damping mechanisms

More separation walls will cause more damping. The amount of internal material damping depends on the used material. The magnitude of the developed friction force, depends on the type of connection.

Façade

Façades have the function of protecting the interior against the exterior environment. Façades are attached to the main load bearing structure and can be made in different ways. The type of energy dissipation can be related to the construction of the façade and three types of facades will be distinguished in this thesis: separate façade elements, traditional cavity wall and framed façades. The difference between the façade types and the different energy mechanisms are indicated in Table 7.

In a façade of type 1, the frictional force develops at the interface between the façade elements and at the loose connection between façade element and floor. The magnitude of the friction force will depend on the weight of the elements.

Façades of type 2 will deform under dynamic wind load. The inner layer will act like a shear wall and will stiffen the frame. The material will deform and energy will be lost because of internal material damping. Depending on the type of connection, the outer layer may also stiffen the frame and may contribute via internal material damping. The amount of damping depends on the material of the façade.

Traditional façades with a concrete parapet and a window frame have also been categorized as this type of façade, because the façade is more or less clamped between the floors and will stiffen the frame also leading to internal material damping.

The damping mechanism in façades of type 3 depends on the type of connection, some relative movement can occur in these connections. A very stiff connection will also make the framework contribute to stabilization of the building. If this happens, the framework and the infill panels might deform, causing energy dissipation through internal material damping. Both mechanisms can occur thus type of connection, weight and used material is of importance.

Table 7 – three different types of façades

<p>Front view</p> <p>Side view</p>	<p>Type 1</p> <p>Separate elements</p> <p>Attached to MLBS</p> <p>Elements move relative to each other</p> <p>Energy dissipation by frictional forces at interfaces between façade elements and between façade elements and MLBS</p>
<p>Front view</p> <p>Side view</p>	<p>Type 2</p> <p>Traditionally cavity wall</p> <p>Inner layer on floor</p> <p>Outer layer attached to inner layer</p> <p>Internal deformation of inner and outer layer</p> <p>Energy dissipation by internal material damping of the inner and outer layer.</p>
<p>Front view</p> <p>Side view</p>	<p>Type 3</p> <p>Façade with beams and posts</p> <p>Attached to MLBS</p> <p>Relative movement between frame and MLBS and internal deformation of infill panels in frame</p> <p>Energy dissipation by internal material damping of the infill panels or frictional forces between frame and MLBS.</p>

4.5.3. Aerodynamic damping

When an object moves in air, energy can be dissipated because of the viscosity of air. The amount of energy dissipated is related to the speed of the object with respect to the air flow, the mass of the air, the frontal area and the shape of the object.

Theoretical formula

The aerodynamic damping in a laminar/uniform wind flow has can be calculated with [Koten, 1977]:

$$\zeta_{aero} = \frac{c}{c_{kr}} = \frac{\frac{1}{2} \rho_{air} v_r A C_f}{2m_e \omega_{n,1}} \quad (4.16)$$

In which v_r [m/s] is the speed of the construction with respect to the air speed and C_f is the air pressure coefficient. In turbulent flows, the damping can be different.

Significance of the aerodynamic damping

Aerodynamic damping is likely to be very small for tall buildings because it is especially important for objects with small mass density and large movements, like cables. Indeed an example calculation shows that aerodynamic damping for a building (mass density 200 kg/m^3 , $\zeta_{aero}=0.21 \%$) is much smaller than for a electric cable (diameter is $0,03 \text{ m}$, $\zeta_{aero}=16 \%$). [Koten, 1977, Ch 7]

Under turbulent wind conditions larger aerodynamic damping values have also been observed. Aerodynamic damping ratio's from 0-1% have been observed in relation with a structural damping of 1%. [Marukawa, et al., 1996] Also an empirical aerodynamic damping function for tall buildings and prisms has been derived, the highest observed aerodynamic damping for a square building based on this function is [Watanabe, et al., 1997]:

$$\eta = \frac{\rho_{air}}{\rho_{building}} = \frac{1.25}{200} \quad (\text{equal conditions as used in the example}) \quad (4.17)$$

$$\frac{\zeta_{aero}}{\eta} = 2 \rightarrow \zeta_{aero} = 2 \cdot \frac{1.25}{200} = 1.25\%$$

Unfortunately the article doesn't present the total damping value of the measured buildings, so it is hard to judge the significance of the aerodynamic damping. A formula to calculate the aerodynamic damping has also been given in the Eurocode (see appendix B.2.3) and $\zeta_{aero}=0,08\%$ (derived from the logarithmic decrement, see appendix C) has been calculated for the New EMC.

4.5.4. Soil structure Interaction

Because of the soil structure interaction energy is dissipated because of two main mechanisms:

- Internal damping in the foundation and the activated ground volume (comparable with the damping in the MLBS, §4.5.1)
- Rocking: radiation of energy waves to the soil below the foundation, caused by rotation of the foundation.

Theoretical formula for rocking

With the following formula, it is possible to calculate the rotation stiffness (k_r) and rotation damping ratio (ζ_r) of a rotating structure on a homogeneous half-space [Koten, 1977 §4.2]:

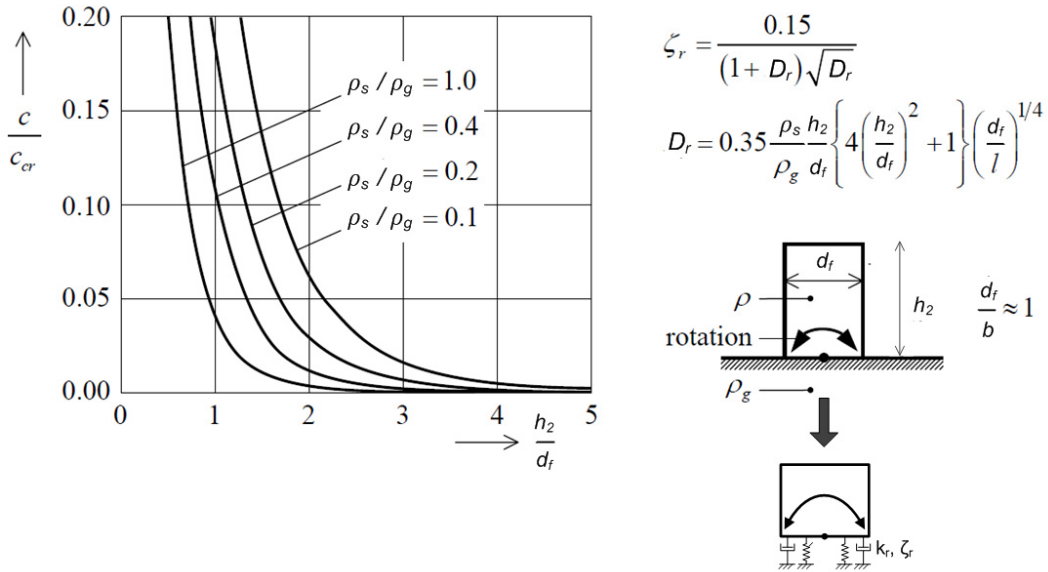


Figure 68 – damping of a building in horizontal direction (rocking) [Koten, 1977, §4.2]

$$k_r = \frac{8G_g r_0^3}{3(1-\nu_g)} \text{ in which } G_g = \frac{E_g}{2(1-\nu_g)} \text{ \& } r_0 = \left(\frac{bd_f(b^2 + d_f^2)}{6\pi} \right)^{1/4} \quad (4.18)$$

It can be concluded that the radiation damping depends on the ratio between height and depth of the structure on the half-space (h_2/d_f) and the ratio between the mass density of the structure and the underground (ρ_s/ρ_g). If h_2/d_f increases, the damping ratio decreases, if ρ_s/ρ_g decreases, the damping ratio increases. The ratio h_2/d_f will be called the Rocking Ratio. The rotation stiffness depends on the base dimensions and the stiffness of the ground (E_g) and Poisson’s ratio (ν_g).

Modeling of the structure

It is assumed that the horizontal load could be transferred in two ways from the foundation to the underground. When the building will move due to wind load, a large ground volume can be activated that wants to slide over a certain plane, this movement will be resisted by shear resistance of the soil.

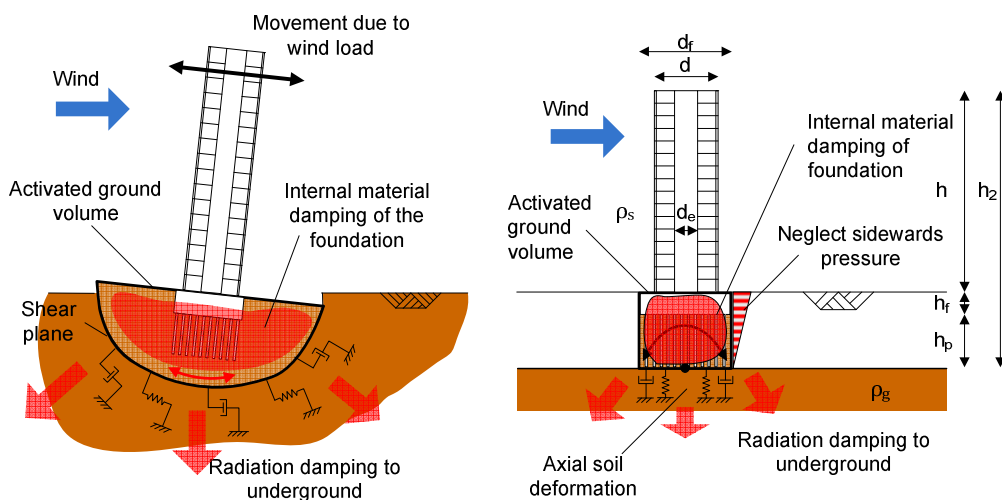


Figure 69 – two case of horizontal wind load transfer from foundation to underground

In the second case, a smaller ground volume is activated and the horizontal load is resisted by axial deformation of the soil under the foundation piles. No large sideward support can be expected of the ground volume in the top layers because these layers are probably badly compacted. Therefore, it will be assumed that no large ground volume as depicted in case one can develop. The sideways pressure will be neglected. The schematization in case 2 will be adopted in which it will be assumed that the radiation of damping to the underground can be estimated by using the theoretical formula for rocking (the dimensions needed for the formula are indicated in the figure). Internal damping occurs because of deformation in the foundation and the ground in the activated ground volume.

Observed soil structure interaction (introduction of IR)

The soil structure interaction has been investigated. Four buildings have been subjected to harmonic loading and the energy input per cycle has been calculated. Based on the movement at the base, the energy dissipation in the foundation per cycle has been calculated as well. By comparison with the total damping in the structure, the contribution of the soil structure interaction in the total damping has been determined. [Ellis, 1996] the results are visible in the following table.

Table 8 - Effects of soil structure interaction on the fundamental modes of four buildings in the UK [Ellis, 1996]

Building	Location	H (m)	b (m)	d (m)	mode	f_n (Hz)	ζ (%)	IR*	% fn reduction	% energy loss in foundation
Dustan Flour Mill	Newcastle	49	24,4	12,2	Trans	1,49	2,3	0,027	8,6	17
					Trans	2,22	2,9	0,1	21,5	31,3
					Tor	3,9	3,1	0,081	4,03	11,9
South Stoneham	Southampton	44,6	17	15	Trans	1,33	2,5	0,025	35,6	60,2
					Trans	1,35	2,4	0,032	48,1	59,5
					Tor	1,83	1,7	-	-	-
Ronan Point	London	64	23,7	17,9	Trans	0,83	1,1	0,021	11	22,1
					Trans	1	1,3	-	-	-
					Tor	1,08	2	-	-	-
Hume Point	London	64	23,7	17,9	Trans	0,9	1	0,029	21	39,3
					Trans	1,1	1,2	0,034	23,3	42,8
					Tor	1,26	1,6	0,019	0,64	2,9

The interaction ratio has been introduced, which is the ratio between the translational deflection at the base divided by the translational deflection at the top of the building. It can be assumed that if IR is zero, SSI is negligible.

Significance of the SSI

After investigation of the IR for buildings of different heights, it has been concluded that: "Generally, SSI is negligible in the fundamental mode of tall buildings, however it can be important in some buildings." [Ellis, 1996, p. 372] More recent articles concerning the world wide database [Satake, et al., 2003; R.J. Smith, et al., 2010] suggest that the type of foundation can be of significance.

4.5.5. Artificial damping

Artificial damping is damping added to the system by extra provisions in the structure. Because artificial damping needs to be engineered, the amount of energy dissipation in these systems are known. Therefore these systems diminish the uncertainty around the naturally present damping (the uncertainty becomes relative smaller when the damping artificially is increased). There're many ways to generate extra damping. Passive and active systems are two main methods to add extra damping to a building. [Oosterhout & Geurts, 2001]

Passive damping

Passive dampers have a predefined working. Tuned mass dampers (TMD) can be added to a building. Properties are chosen such their vibrations are in anti-phase with the movement of the building. In this way they absorb kinetic energy and decrease deflections.

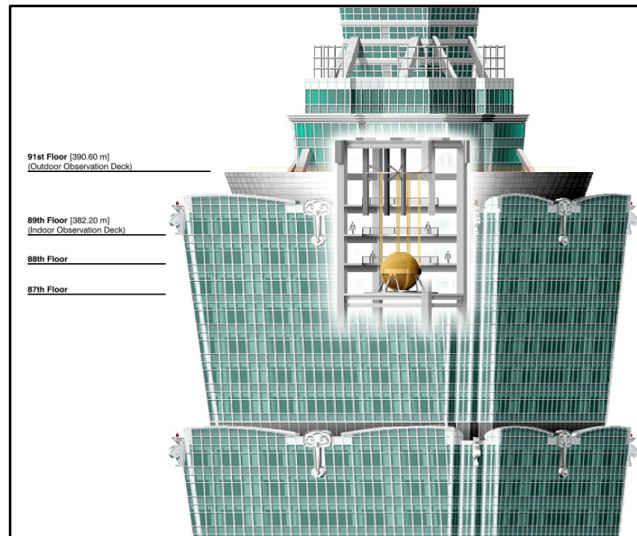


Figure 70 – example of a tuned Mass Damper (TMD) in Taipei 101

(http://upload.wikimedia.org/wikipedia/commons/1/15/Taipei_101_Tuned_Mass_Damper.png, accessed 07-08-2011)

When subjected to deformation, visco-elastic dampers convert kinetic energy into warmth. They must be placed where relative large displacement occurs. At an interface between structural elements, a small layer of visco-elastic material is already sufficient. Arup has used viscous dampers in the outriggers of a building design and visco-elastic materials have been first used in the WTC in 1969. Another example of passive damping is friction damping based on friction and slip. This damping can be enlarged by putting suitable materials on contact surfaces between elements.

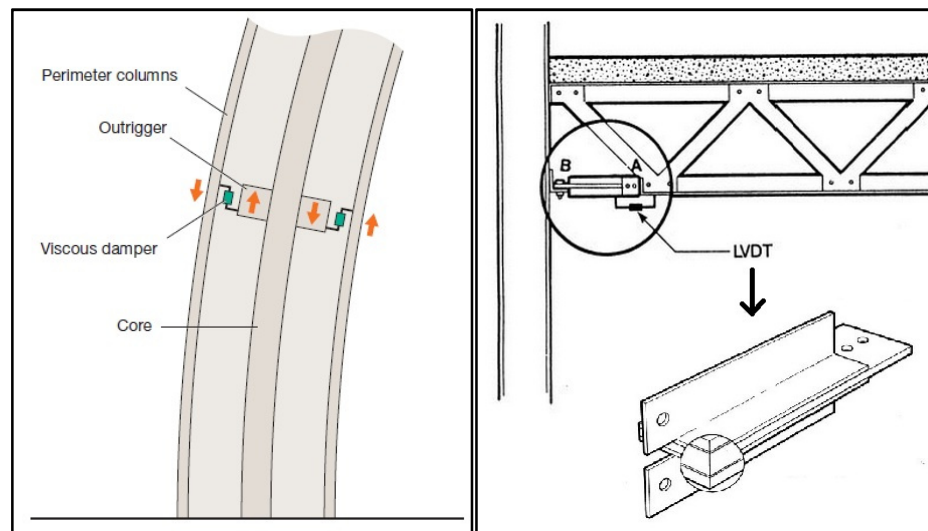


Figure 71 – left: damped outrigger concept [R.J. Smith & Willford, 2008] right: visco-elastic damper in world trade center (<http://www.designcommunity.com/discussion/7551.html> accessed at 07-08-2011)

Active damping

The energy dissipation in active systems is coupled to the response of a building. Active damping has not yet been applied on large scale, but elegant systems might be possible in analogy with the human muscle-system. A system of cables can be made in a high-rise building. The cables can be tensioned as a response to the movement of the building to compensate the vibrations.

4.5.6. Conclusion

Four different sources of damping have been distinguished. In the main load bearing structure (MLBS) energy can be lost by internal material damping and by friction damping in the joints between structural elements. The amount of energy that will be lost depends on the material, the type of main load bearing structure and the type of connections between the structural elements. Secondly, energy can be dissipated in non structural elements (NSE) such as the façade and the separation walls. The amount of damping will probably depend on the amount of non structural elements, the used material and weight of the elements and the type of connection between the NSE and MLBS.

Energy can also be dissipated through aerodynamic damping because of the viscosity of air. However the aerodynamic damping is small in comparison with the total damping and therefore will be neglected for high-rise buildings.

Because of soil structure interaction, energy will be lost through internal deformation of the construction material in the foundation and the soil in the activated ground volume. Energy will also be lost because of radiation of waves to the underground (rocking). The type of foundation and the material of the foundation and ground volume will influence the amount of energy lost through internal deformation. The amount of energy lost because of rocking depends on the rocking ratio of the and the ratio between the mass density of the structure and the underground. The significance of this source of damping is not clear, therefore, this aspect needs further investigation.

With active and passive damping systems, additional damping can be achieved. Because artificial damping needs to be engineered, it can be assumed that the amount of extra energy dissipation is known. Therefore these systems diminish the uncertainty around the naturally present damping (the uncertainty becomes relative smaller when the damping is artificially increased). Because artificial damping systems haven't been observed in the buildings that will be discussed in the next section and because this type of damping isn't a source of uncertainty, this doesn't need to be taken into account.

5. Case studies

The former four sections contain the results of the literature study. It can be expected that the new generation for high-rise buildings will become higher and lighter. The comfort criterion concerning acceleration, will become more governing for these buildings. Damping has the most influence on the maximum acceleration while it is the most uncertain factor in comparison with the mass and stiffness of the building.

Estimations of damping according to the Eurocode are based on used building material and lead to large uncertainty around damping. Predictors based on the Japanese damping database are available. These predictors take into account the used material and also the influence of height (or equivalent the influence of natural frequency) and the amplitude dependency, but still these predictors show a lot of scatter in comparison with the actual values of damping.

The scatter around the predicted damping values is probably caused by the influence of the structural characteristics of the structure. This influence has not yet been taken into account in a method or formula to predict the damping.

Therefore, the influence of the structural characteristics will be investigated. This will be done based on, what shall be called, the Dutch damping database. This database contains the damping ratios of 11 Dutch buildings (obtained from TNO). Information about structural characteristics concerning the main load bearing structure, the foundation and the non structural elements have been gathered from drawings, design calculations, building visit and by interviews of the structural engineers. An extensive description of the studied buildings can be found in appendix N.

The first section will explain which structural characteristics have been taken into account, Table 10 and Table 11 will give an overview of these characteristics. In the second section the influence of the structural characteristics will be investigated on the basis of the information in the overview table.

The last section contains conclusions based on this investigation. The obtained results will be discussed.

5.1. Structural characteristics

In the next subsections it will be explained what characteristics have been taken into account for the main load bearing structure, the non-structural elements and the foundation and why they have been taken into account. The results can be viewed in Table 10 and Table 11.

5.1.1. Main load bearing structure (MLBS)

In §4.5.1 it has been explained that the damping in the MLBS depends on the used material of the MLBS, the structural system of the MLBS and the connections between the different structural elements. The different materials of the MLBS have been described and the types of structural system have been classified according to the different systems: rigid frames, shear walls/core, braced frames or tube (see §2.3).

The classification for connections has been based on the possibility of relative movement of elements, since it is likely that more energy will be lost due to friction as more relative movement occurs.

For steel; welded and bolted connections have been distinguished. Bolted connections allow some relative movement of elements and will likely cause more damping. In all studied steel buildings it has been found that the connections have been bolted.

Concrete main load bearing structures have either been cast in-situ or have been built with prefabricated elements. Prefabricated elements can be connected with dry or wet connections. Dry connections will allow some relative movement of the elements and will allow more energy to be lost due to friction damping. In a structure made out of prefabricated elements that have been connected with wet connections and in a cast in-situ structure, it is assumed that no relative movement is possible between elements of the main load bearing structure. The connection in a cast in-situ MLBS and a MLBS made out of prefabricated elements with wet connections have both been classified to have monolithic connections.

Some MLBS of the studied buildings have been made out of prefabricated elements. In all buildings, the prefabricated elements have been jointed with anchors and sleeves that have been grouted, thus have been classified as monolithic. Even the CD20 system (see appendix N about 's-Graventower) that has dry pin and hole connections between the prefabricated elements, has been classified as monolithic since concrete has been poured in the connections.

5.1.2. Non-structural elements (NSE)

It has been concluded that two types of non-structural elements might influence the damping: separation walls and the façade. The mechanisms behind damping from these sources of damping have been explained in §4.5.2. Energy can be lost because of internal material damping and because of friction forces between different elements.

Separation walls

The amount of separation walls is indicated in the table because more separation walls will probably cause more damping. The amount of internal material damping depends on the used material which has been indicated in the table. The magnitude of the developed friction force, depends on the type of connection. Because of the lack of information on the type of connection and the material of the walls, this has not been presented in the table.

Façade

The type of energy dissipation is related to the construction of the façade. Three types of facades have been distinguished: separate façade elements, traditional cavity wall and framed façade. The damping mechanism per type can be different and have been explained. (see Table 7, §4.5.2).

Because the internal damping depends on the material of the facade, the material has been indicated in the table. Frictional forces can develop at the interface between the façade elements and at the loose connection between façade element and MLBS. Because the magnitude of the friction force depends on the weight of the elements, this has been indicated in the table as well. What damping mechanisms are active, depends on the type of the connection between the elements (as has been explained in §4.5.2). Exact information about the connection has not been obtained, this hasn't been taken into account.

5.1.3. Foundation

It has been explained (see §4.5.4) that energy will be lost because of internal material damping in the subsoil structure and the ground volume and because of radiation of energy to the soil below.

Internal damping in the foundation

As for the internal material damping of the MLBS, the internal damping of the foundation will depend on the applied material, the type of structure and the type of connection.

In every foundation, concrete has been applied in the subsoil structure and the connections are monolithic. Because there is no difference between the buildings, it wasn't relevant to investigate the influence of the material and the connections in the foundation.

Three major types of foundation can be distinguished at the buildings and have been indicated in the table: a basement, a plate foundation or beam foundation. The type of foundation influences the way forces are transferred to the subsoil and it is interesting to investigate if there is a clear influence of the foundation type on the amount of damping.

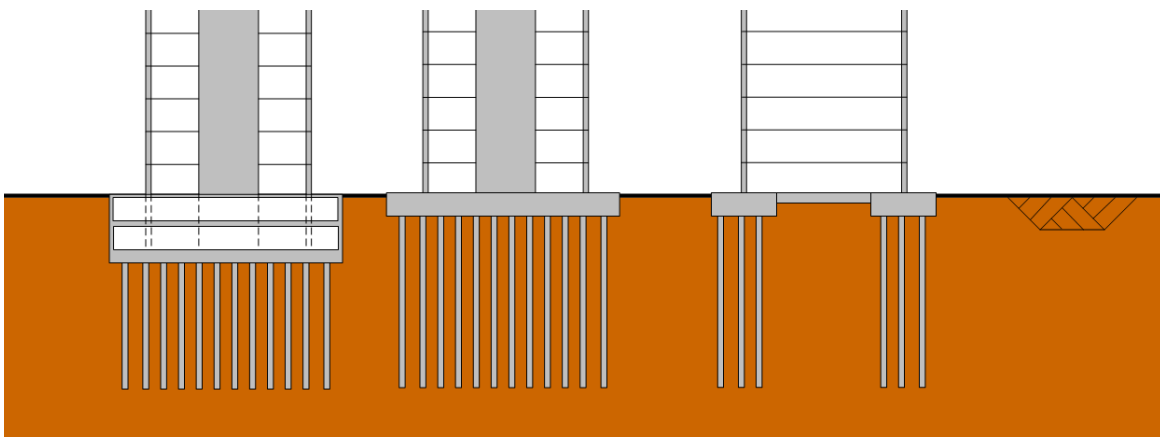


Figure 72 – types of foundation from left to right: basement, plate foundation and beam foundation

The activated ground volume of the buildings can contain different types of ground, which can influence the damping. There are indications of the internal material damping of different types of ground, but only a range for the damping ratio (see Table 9) is given because of the uncertainty around the ground properties. Because next to this, the exact build up of the ground layers for a lot of buildings is unknown, the influence of this property can't be investigated and hasn't been mentioned in the table.

Table 9 - damping ratio of three types of ground [Spijkers, et al., 2005, p. 180]

Material	Material damping $\zeta=c/ckr$ (%)
Dry Sand	1-3
Sand-gravel	3-7
Clay	2-5

If more ground is activated under a wind load, the total damping from ground will also be larger. One can easily imagine that a larger ground volume is activated at larger pile lengths and larger width of the foundation. These dimensions have been indicated in the table.

Rocking

By neglecting the ground next to the foundation, the energy dissipated to the soil below can be considered with the equations (Figure 68) given for rocking. The amount of damping depends on the Rocking Ratio and the ratio between the mass of the structure and the underground.

The total height of the structure on the half space is a summation of the building height, the depth of foundation below surface level and the length of the piles: $h_2=h+h_f+h_p$. The depth of the foundation is d_f . The ratio h_2/d_f is called the Rocking Ratio and has been presented in the overview table. Again because of the lack of information about the soil characteristics, only the density of the structure has been indicated in the table.

5.1.4. Other

The height of the building, the width of the building at its base and the slenderness in the considered direction, have been described in the table. The effective depth has also been described, from this the effective slenderness has been calculated (see also §2.1).

If possible, the mass and stiffness of the building have been derived from drawings, calculations or reports of measurements. The values of the parameters can be used as input for the dynamic model in chapter 6.

The first natural frequency and the corresponding damping ratio that have been measured for the considered direction have also been gathered in the table.

5.1.5. Overview table with structural characteristics

Table 10 shows the results for the x-direction (the weak direction) and Table 11 for the y-direction (the strong direction). The top part of the table contains characteristics that have been described qualitatively and the bottom part contains characteristics that have been described quantitatively. Because Montevideo and La Fenêtre both have changing structural systems and façades over height, different parts of the building have been described. The characteristics of Mexx, HBG and CIG haven't been described for the y-direction, because the natural frequency and damping ratio haven't been measured for this direction.

Table 10 – structural characteristics derived from case studies, for x-direction

	X-direction	Montevideo		N EMC	O EMC	EWI	Kennedy	Winston Churchill	La Fenêtre			Mexx	's-Graventower	HBG building	CIG
		part	top						bottom	top	middle				
qualitative structural characteristics	main load bearing structure														
	material	steel	concrete	concrete (prefab)	concrete (in-situ)	concrete (in-situ)	steel	concrete (in-situ)	steel	concrete (in-situ)+steel	concrete (in-situ)	steel	concrete (prefab)	concrete (in-situ+ prefab)	steel
	structural system	tube with mega brace welded	core/coupled shear walls monolithic	tube (prefab) monolithic	shear walls monolithic	shear walls monolithic	braced frames bolted	core monolithic	braced frames bolted	core-diagonal monolithic	stiff box, shear walls monolithic	rigid frames bolted	core monolithic	shear walls monolithic	braced & rigid frames bolted
	non-structural elements														
	function of the building	residential	residential	office	office/laboratoria	office	office	office	residential	transport	storage	office	office	office	office
	amount of non load bearing separation walls	many	none	none	many	many	few	few	many	none	none	few	many	many	?
	type of facade	1	2	-	1	-	1	3	1	-	3	1	2 and 3	2	2
	facade weight	moderate	heavy	moderate	light	-	heavy	light	light	-	light	heavy	heavy/lightweight	heavy	heavy
	facade material	masonry/concrete	lime stone, masonry	stony	sandwich / aluminum	-	aluminum + glass	aluminum + glass	wood + glass	-	aluminum + glass	concrete	heavy/lightweight concrete and emalit/aluminum on and attached to columns/attached to MLBS	concrete and aluminum	lime stone + masonry/steel
	connection of facade	attached to frame	on floors, between walls	attached to tube	attached to frame	-	attached to frame	attached to floor	attached to frame	-	attached to walls	attached to frame	on and attached to columns/attached to MLBS	on the floor	on floors, between columns
contribution to stiffness	low	moderate	low	low	-	low	low	low	-	low	low	high/low	high	high	
quantitative description of structural characteristics	Foundation														
	underground structure	dilatated basement	plate foundation	plate foundation	dilatated basement	dilatated basement	basement + thick beam foundation	basement	basement	beam foundation	beam foundation	basement/plate foundation	?	?	
	depth below surface level, h _f (m)	11	3,5	3	6	9	4	3	3	2	0,6	3	?	?	
	length of foundation piles, h _p (m)	17,5	18,5	15,5	12	17,5	16	15	18	24	24	17,5	?	?	
	depth of foundation, d _f (m)	34	24	38	19	23	22	25	28	22	22	16	?	?	
	rocking ratio, h ₂ /d _f (-)	5,3	5,9	3,4	5,9	4,8	4,5	3,5	2,6	2,8	2,8	3,4	?	?	
	structural mass density, ρ _s (kg/m ³)	368	373	262	350	147	227	215	156	236	?	?	?	?	
	Dimensions														
	h (m)	150	120	112	90	83	80	70	52	37	34	23	12,6	1,8	
	depth, d (m)	27,6	20	32	17,7	14,4	22	12	15	22	14	4	5,8	2,1	
slenderness h/d (-)	5,4	6,0	3,5	5,1	5,8	3,6	5,8	3,5	1,7	2,4	1,8	7,2	5,8		
effective depth, d _{eff} (m)	27,6	20	9	17,7	14,4	7,2	12	15	7,2	7	4	5,1	2,1		
effective slenderness h/d _{eff} (-)	5,4	6,0	12,4	5,1	5,8	11,1	5,8	3,5	5,1	4,9	5,8	2,1	2,8		
Model input Parameters															
ρA (-10 ³ kg/m)	413	430	795	467	176	250	290	349	114						
EI (-10 ¹² Nm ²)	27,9	25	45	13	4,9	2	0,12	0,11							
k _x (-10 ¹² Nm/rad)	1,8	1,5	3,9	2,1	0,8	1,3	0,07	0,02							
k _r (-10 ¹⁰ N/m)		1,0	1	1	1										
Measurements															
f ₁ (Hz)	0,42	0,54	0,48	0,44	0,45	0,55	0,62	0,6	1,6	1,3	2,1	2,8			
ζ ₁ (%)	1	1,6	2,1	1,5	1,8	1,7	1,5	3,1	2,2	2,6	2,8				

Table 11 – structural characteristics derived from case studies, for y-direction

	Y-direction	Montevideo		N EMC	O EMC	EWI	Kennedy	Winston Churchill	La Fenêtre			Mexx	's-Graventower	HBG building	CIG
		part	top						bottom	top	middle				
qualitative structural characteristics	main load bearing structure														
	material	steel	concrete	concrete	concrete	concrete	steel	concrete	steel	concrete+steel	concrete	concrete	concrete	concrete	
	structural system	tube with mega brace welded	core/coupled shear walls monolithic	tube (prefab) monolithic	rigid frames monolithic	core (I-shaped) monolithic	braced frames + outrigger bolted	core monolithic	braced frames bolted	core-diagonal monolithic	stiff box, shear walls monolithic	core (prefab) monolithic	core (prefab) monolithic	core (prefab) monolithic	
	non-structural elements														
	function of the building	residential	residential	office	office/laboratoria	office	office	office	residential	transport	storage	office	office	office	
	amount of non load bearing separation walls	many	none	none	many	many	few	few	many	none	none	many	many	many	
	type of facade	1	2	-	1	2 and 3	1	3	1	-	3	2 and 3	2 and 3	2 and 3	
	facade weight	moderate	heavy	moderate	light	moderate / lightweight	heavy	light	light	-	light	heavy/lightweight	heavy/lightweight	heavy/lightweight	
	facade material	stony	masonry	stony	sandwich / aluminum	wood / steel + glass	aluminum + glass	aluminum + glass	wood + glass	-	aluminum + glass	concrete and emalit/aluminum	concrete and emalit/aluminum	concrete and emalit/aluminum	
	connection of facade	attached to frame	attached to walls	attached to tube	attached to frame	build on floor between columns / attached to floors	attached to frame	attached to floor	attached to frame	-	attached to walls	on and attached to columns/attached to MLBS	on and attached to columns/attached to MLBS	on and attached to columns/attached to MLBS	
contribution to stiffness	low	?	none	low	moderate	low	low	low	-	low	high/low	high/low	high/low		
quantitative description of structural characteristics	Foundation														
	underground structure	dilatated basement	plate foundation	plate foundation	dilatated basement	dilatated basement	basement + thick beam foundation	basement	basement	beam foundation	beam foundation	basement/plate foundation	?	?	
	depth below surface level, h _f (m)	11	3,5	3	6	9	4	3	3	0,6	0,6	3	?	?	
	length of foundation piles, h _p (m)	17,5	18,5	15,5	12	17,5	16	15	18	24	24	17,5	?	?	
	depth of foundation, d _f (m)	33	48	80	80	52	50	54	80	22	22	16	?	?	
	rocking ratio, h ₂ /d _f (-)	5,4	3,0	1,6	1,4	2,1	2,0	1,6	2,6	2,8	2,8	3,4	?	?	
	structural mass density, ρ _s (kg/m ³)	368	373	262	350	147	227	215	156	236	?	?	?	?	
	Dimensions														
	h (m)	150	120	112	90	83	80	70	52	37	34	23	12,6	1,8	
	depth, d (m)	24	44	80	82,6	36	51	60	60	22	14	4	5,8	2,1	
slenderness h/d (-)	6,3	2,7	1,4	1,1	2,3	1,6	1,2	1,2	1,7	2,4	1,8	7,2	5,8		
effective depth, d _{eff} (m)	24	44	80	16	21,6	21,6	60	60	7,2	7	4	5,1	2,1		
effective slenderness h/d _{eff} (-)	6,3	2,7	1,4	5,6	3,8	3,7	1,2	1,2	5,1	4,9	5,8	2,1	2,8		
Model input Parameters															
ρA (-10 ³ kg/m)	413	430	795	267	176	250	290	349	114						
EI (-10 ¹² Nm ²)	39	68	170	27	4,5	2	no information available	0,12	0,11						
k _x (-10 ¹² Nm/rad)	2,6	5,8	3,9	3,2	0,8	1,3	0,07	0,02							
k _r (-10 ¹⁰ N/m)		0,5	0,5	0,5	0,5										
Measurements															
f ₁ (Hz)	0,5	0,68	0,5	0,68	0,72	0,79	0,7	0,6	1,6	1,3	2,1	2,8			
ζ ₁ (%)	1,1	2	3,6	2,2	2	1,4	2,4	3,1	2,2	2,6	2,8				

Table 12 – structural characteristics of the buildings and their classification

direction	building	Facade			Separation walls	Foundation			MLBS			h [m]	slenderness, h/d [-]	actual damping [%]	damping trend line (2.689*(h/d)^-0.32) [%]	classification based on ratio2: (actual damping)/(damping trend line)
		type of facade	weight	material of the facade		amount of separation walls	type of foundation	Rocking Ratio, h2/b [-]	ps (kg/m³)	structural system	connection					
x	Montevideo	2 heavy	masonry	few	basement	5,3	368	shear walls (coupled)	monolithic	concrete (in-situ)/steel	150	5,4	1,0	1,6	0,64	
x	La Fenetre	1 light	wood+glass	few	basement	3,5	215	braced frames	monolithic	steel/concrete(in-situ)	70	5,8	1,5	1,5	0,98	
y	Montevideo	2 heavy	masonry	few	basement	5,4	368	shear walls (coupled)	monolithic	concrete (in-situ)/steel	150	6,3	1,1	1,5	0,74	
y	La Fenetre	1 light	wood+glass	few	basement	1,6	215	braced frames	monolithic	steel/concrete(in-situ)	70	1,2	2,4	2,6	0,94	
x	O EMC	1 light	sandwich	many	plate	3,4	262	shear walls	monolithic	concrete (in-situ+prefab)	112	3,5	2,1	1,8	1,17	
x	EWI	-	-	many	basement	5,7	350	shear walls	monolithic	concrete (in-situ)	90	5,1	1,5	1,6	0,94	
x	Winston Churchill	3 light	aluminum+glass	few	basement	4,5	227	shear walls (core)	monolithic	concrete (in-situ)	80	3,6	1,7	1,8	0,96	
x	's-graventower	2 heavy	concrete	many	beam	2,8	236	shear walls	monolithic	concrete (prefab)	37	1,7	2,2	2,3	0,97	
x	HBG building	2 heavy	concrete	many	basement/plate	3,4		shear walls (coupled)	monolithic	concrete (in-situ+prefab)	34	2,4	2,6	2,0	1,28	
y	O EMC	1 light	sandwich	many	plate	1,6	262	rigid frames	monolithic	concrete (in-situ+prefab)	112	1,4	3,6	2,4	1,49	
y	EWI	2 light	wood+glass	many	basement	1,4	350	shear walls	monolithic	concrete (in-situ)	90	1,1	2,2	2,6	0,84	
y	Winston Churchill	3 light	aluminum+glass	few	basement/beam	2	227	shear walls (core)	monolithic	concrete (in-situ)	80	1,6	1,4	2,3	0,60	
y	's-graventower	2 heavy	concrete	many	beam	2,8	236	shear walls	monolithic	concrete (prefab)	37	1,7	1,8	2,3	0,79	
x	NEMC	- light	stony	normal	plate	5,9	373	tube	monolithic	concrete (prefab)	120	6,0	1,6	1,5	1,06	
y	NEMC	- light	stony	normal	plate	3	373	tube	monolithic	concrete (prefab)	120	2,7	2,0	2,0	1,03	
x	Kennedy	1 heavy	aluminum+glass	few	basement	5,8	147	braced frames	bolted	steel	83	5,8	1,8	1,5	1,17	
x	Mexx	1 heavy	concrete	few	beam	2,6	156	rigid frames	bolted	steel	52	3,5	3,1	1,8	1,72	
x	CIG	2 heavy	masonry	few	beam	2,6	156	rigid and braced frame	bolted	steel	23	1,8	2,8	2,2	1,26	
y	Kennedy	1 heavy	aluminum and glass	few	basement	2,1	147	braced frame + outrigger	bolted	steel	83	2,3	2,0	2,1	0,97	
															μ=	1,03
															σ=	0,27
															min	0,6
															max	1,7
															low class	ratio2<0,8
															normal class	0,8<=ratio2<=1,25
															high class	ratio2>1,25

Table 13 – left: method with points to classify buildings based on their structural characteristics. Right: predicted damping on the basis of Lagomarsino's and AIJ2000's formula

direction	Building	Classification based on ratio2	type of facade	weight of facade	material of the facade	amount of separation walls	type of foundation	Rocking Ratio, h2/b [-]	structural mass density ps (kg/m3)	MLBS: structural system	MLBS: connection	MLBS: material	Total points (predicted classification)	predicted damping based on low, normal and high classes. (%)	predicted damping/ actual damping (-)	AIJ2000's predictor without amplitude component $\zeta = \alpha f_n$						
																natural frequency (=1/7) [Hz]	damping LAG (%) steel building (α=0,0032 β=0,0078)	damping LAG (%) concrete building (α=0,0072 β=0,0070)	damping LAG/actual damping (-)	damping AIJ (%) steel building (α=0,013)	damping AIJ (%) concrete building (α=0,014)	damping AIJ/actual damping (-)
x	Montevideo	0,64	0	0	0	-7	0	-7	-12	-7	-10	-10	-53	1,04	1,0	0,42	1,0	2,0	2,0	0,6	0,6	
x	La Fenetre	0,98	0	0	0	-7	0	0	15	-7	30	30	61	1,58	1,1	0,62	1,0	2,0	0,7	0,8	0,5	0,5
y	Montevideo	0,74	0	0	0	-7	0	-7	-12	-7	-10	-10	-53	1,00	0,9	0,50	1,0	1,8	1,6	0,7	0,7	0,6
y	La Fenetre	0,94	0	0	0	-7	0	0	15	-7	30	30	61	2,25	0,9	0,70	1,0	1,8	1,6	0,9	0,7	0,6
x	O EMC	1,17	0	0	0	7	0	0	-12	-7	30	30	48	1,77	0,8	0,48	1,0	1,8	1,6	0,9	0,7	0,4
x	EWI	0,94	0	0	0	7	0	-7	-12	-7	-10	-10	-39	1,63	1,1	0,44	1,0	1,8	1,6	0,9	0,7	0,3
x	Winston Churchill	0,96	0	0	0	-7	0	-7	-12	-7	-10	-10	-53	1,18	0,7	0,55	1,0	1,8	1,6	0,9	0,7	0,4
x	's-graventower	0,97	0	0	0	7	0	0	-12	-7	-10	-10	-32	2,08	0,9	0,68	1,0	1,8	1,6	0,9	0,7	0,4
x	HBG building	1,28	0	0	0	7	0	0	15	-7	30	30	75	2,84	1,1	0,48	1,0	1,8	1,6	0,9	0,7	0,3
y	O EMC	1,49	0	0	0	7	0	0	-12	40	30	30	95	3,08	0,9	0,50	1,0	1,8	1,6	0,9	0,7	0,2
y	EWI	0,84	0	0	0	7	0	0	-12	-7	-10	-10	-32	2,29	1,0	0,68	1,0	1,8	1,6	0,9	0,7	0,2
y	Winston Churchill	0,60	0	0	0	-7	0	0	-12	-7	-10	-10	-46	1,53	1,1	0,79	1,0	1,8	1,6	0,9	0,7	0,2
y	's-graventower	0,79	0	0	0	7	0	0	-12	-7	-10	-10	-32	2,08	1,2	1,60	1,0	1,8	1,6	0,9	0,7	0,2
x	NEMC	1,06	0	0	0	0	0	-7	-12	-7	-10	-10	-46	1,01	0,6	0,53	1,0	1,8	1,6	0,9	0,7	0,5
y	NEMC	1,03	0	0	0	0	0	-7	-12	-7	-10	-10	-39	1,87	0,9	0,66	1,0	1,8	1,6	0,9	0,7	0,5
x	Kennedy	1,17	0	0	0	-7	0	-7	15	40	30	30	101	2,49	1,4	0,45	1,1	1,6	1,6	0,8	0,9	0,5
x	Mexx	1,72	0	0	0	-7	0	0	15	40	30	30	108	2,69	0,9	0,60	1,0	1,8	1,6	0,8	0,9	0,5
x	CIG	1,26	0	0	0	0	0	0	15	40	30	30	100	2,96	1,1	2,10	1,8	1,6	0,8	0,9	0,7	0,5
y	Kennedy	0,97	0	0	0	-7	0	0	15	40	30	30	108	2,86	1,4	0,72	1,0	1,8	1,6	0,8	0,9	0,5
															μ=	1,00						
															min	0,6						
															max	1,4						
															low class	points<-40						
															normal class	-40<=points<=70						
															high class	points>70						

5.2. Influence of structural characteristics on damping

In this section, the influence of the structural characteristics that have been described in the former section and are visible in the overview table will be investigated. First the trend line will be derived to make a fair comparison between the measured damping ratios. It will be explained why the damping ratio has been plotted as function of the slenderness to find this trend line. In the following subsections, the influence of different structural characteristics on the damping ratio will be investigated by definition of different categories and comparing the damping values with the trend line. If a category shows significant higher damping ratios in comparison with the trend line, it will be assumed that the structural characteristics will have a positive effect on the damping ratio. A larger difference between the damping of a category and the trend line, indicates a stronger relation between the structural characteristic and the damping.

5.2.1. Trend line

When looking at large database with damping ratios, the damping ratio has been plotted as a function of the height. This has also been done for the case studies. In the figure below, the results can be found, together with a fitted power function. A clear downward trend is visible. This trend has also been observed at other measurements [Satake, et al., 2003].

An explanation for this trend can be given based on amount of non-structural elements in the structure. *“In taller buildings, the primary structure is relatively large, it dominates the elastic stiffness and the contribution of non-structural components is relatively small.”*[R.J. Smith, et al., 2010] Because non structural components increase the damping of the building, the total damping will be lower if their relative contribution is smaller.

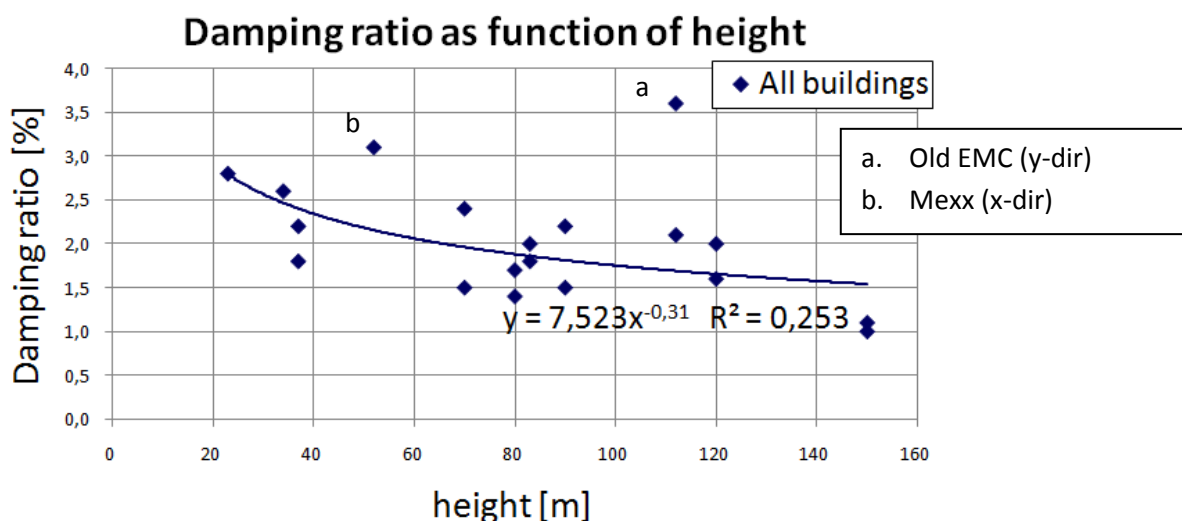


Figure 73 – plot of the damping as function of the height

If available, both x- and y-direction have been plotted for a building. As a result, different damping ratios are present at the same height for the same building. Change of building characteristics in x and y direction can be an explanation for this difference.

The major difference between the weak and strong direction is the slenderness of the building. The depth of a building at its base is an important influence parameter for the damping ratio [Jeary, 1997b, p. 173]. The maximum stresses caused by horizontal wind loads occur at the base. At larger

displacements caused by increased wind loading, the increase of stresses at the bottom is the largest. If the base dimensions are larger, more material will be activated in resisting the increased stresses. When more material is activated, it can also be expected that the increase of energy dissipation through internal material damping increases more, leading to higher damping ratios. Because the base dimension can have influence on the damping ratio, the damping ratio is studied as a function of the slenderness (see figure below).

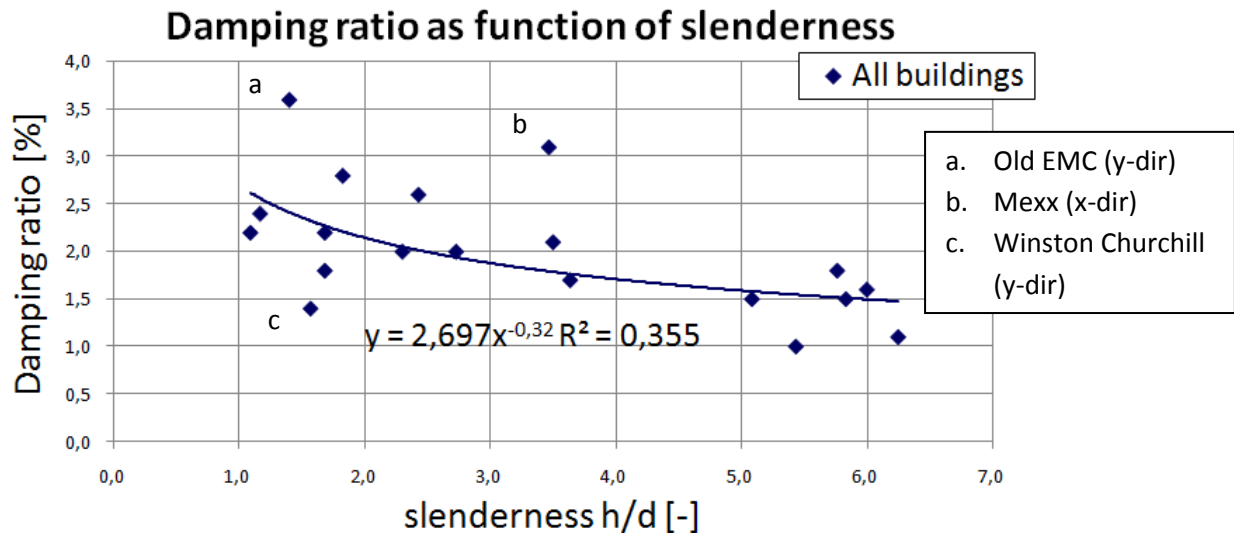


Figure 74 – plot of the damping as function of slenderness

Again a clear downward trend is visible at increasing aspect ratios, which is in line with the expectation that damping is larger at larger base dimensions and smaller at increasing heights.

The fitted trend line as function of the slenderness shows less scatter (a larger value of R^2 means less scatter, which is a better fit). This does however not necessarily mean that the trend line is better, because when the points that deviate the most in both graphs are neglected, the fitted lines will show about equal scatter.

But because the damping ratio for a building is different for the weak and strong direction with different slenderness values and because the depth of a building at its base is an important influence parameter for the damping ratio, it has been decided that the trend line as function of the slenderness will be used.

The trend line makes it possible to give a fair comparison between the different buildings, because the general downward trend at increasing slenderness has been taken into account. Deviations to the trend line will probably be caused by a combination of different structural characteristics. The influence of structural characteristics on the damping ratio and how large the influence is, will be investigated by distinguish different categories and comparing the results with the trend line.

5.2.2. Material

The buildings have been divided into steel and concrete buildings. Montevideo and La Fenêtre both have concrete and steel in their main load bearing structure. Because the largest deformation in Montevideo occurs in the concrete part, this building has been categorized as concrete, for the same reason la Fenêtre has been categorized as a steel building. The result can be found in the figure below.

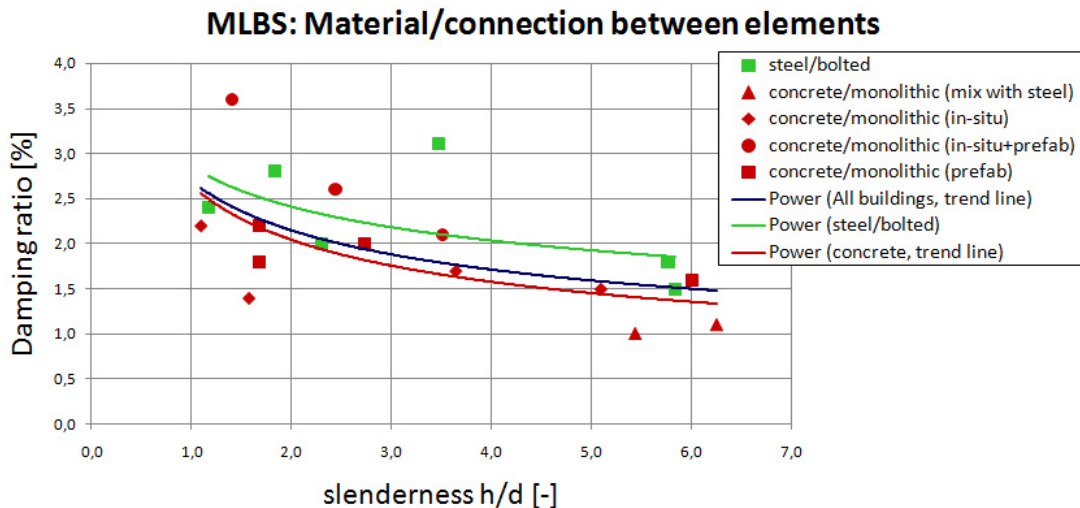


Figure 75- plot of the damping ratio against the slenderness for different materials/connections of the MLBS

From the plot it can be observed that (in comparison with the trend) the damping in steel buildings is higher than for concrete buildings. On average, the damping ratio for steel buildings is about 30% higher than the trend and for concrete buildings about 10% lower. Because the internal material damping of concrete is higher than steel, this results shows that the structural damping can't only be based on the internal material damping. It is clear that also other factors influence the structural damping.

5.2.3. Connection

Two major types of connections in the main load bearing structure have been distinguished:

- monolithic/welded connections: very few relative movement of elements is possible
- dry/bolted connections: allow some relative movement because of slip in the connection

Because all steel buildings have bolted connections, and the concrete buildings have monolithic/welded connections, the same pattern as for material can be found (Figure 75). The higher damping ratio of the steel buildings is probably caused by the bolted connections. It can also be observed that in general concrete structures where prefab elements have been used show higher damping than structures made out of in-situ concrete.

5.2.4. Structural system

At the considered direction of vibration, four systems with different structural behaviour, have been distinguished: rigid frame system, core/shear wall systems, braced frame system and tube systems.

The results have been plotted in Figure 76. It can be observed the three buildings with the highest damping ratios are buildings with rigid frames. From this it can be concluded that that rigid frames will probably lead to higher damping ratios. This is also in line with conclusions from literature study

[Kijewski-Correa & Pirnia, 2007] in which it has been concluded that a larger damping ratios can be observed in modes of vibration with significant ‘frame action’ in comparison with ‘cantilever/axial shortening action’. It can also be observed that structural systems with ‘cantilever/axial shortening action’ show lower damping values.

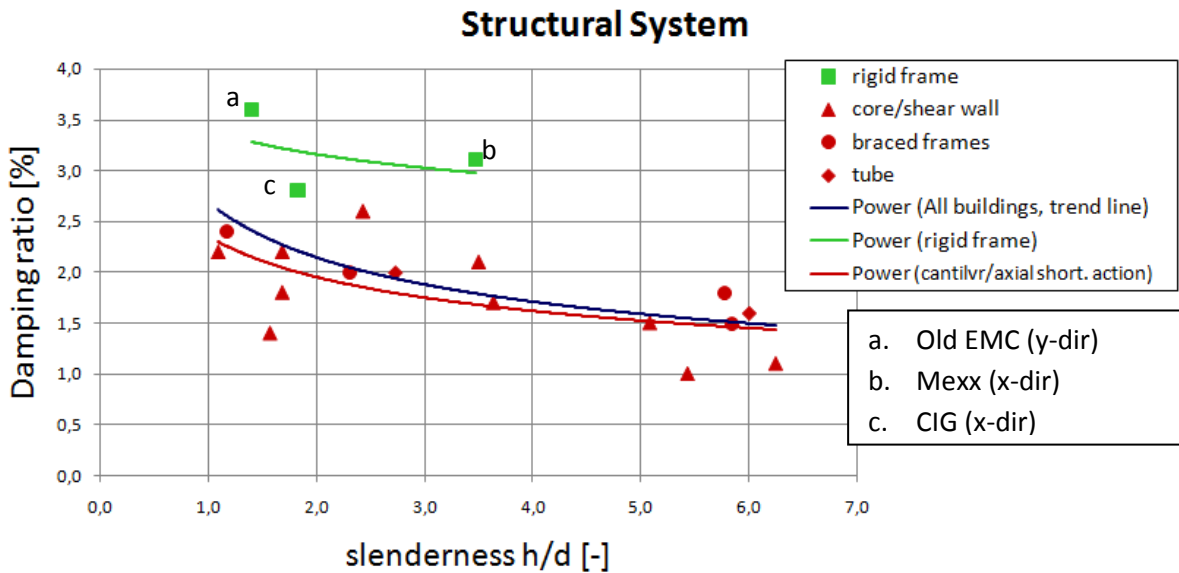


Figure 76 - plot of the damping ratio against the slenderness for different structural systems

On average, the damping ratio for buildings with rigid frames is about 40% higher than the trend and for buildings with cantilever/axial shortening action the damping ratios are about 7% lower.

5.2.5. Amount of separation walls

The influence of the amount of separation walls have been analyzed by assuming three categories. CIG has been left out of this analysis, because no information about the separation walls has been obtained. The NEW EMC has an own category because very few separation walls were present at the time of measurement. But because prefab floors have been simply supported by the tube and the central core inside, some relative movement between these elements can occur. It can be expected that this mechanism will generate some loss of energy because of friction forces.

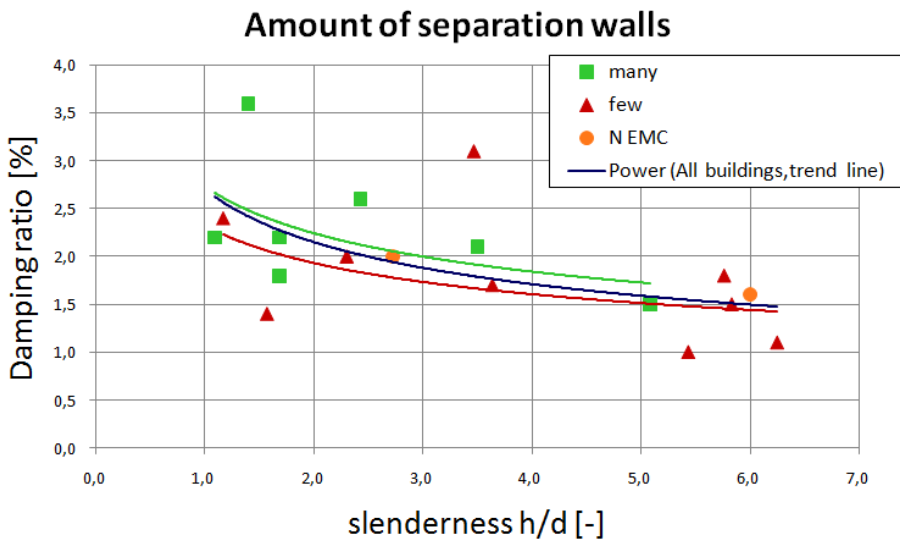


Figure 77 – plot of the damping ratio against the slenderness for different amounts of separation walls

From the figure it can be observed that the buildings with many separation walls have some more damping than buildings with few separation walls. The damping of the New EMC corresponds with the trend line.

On average, the damping ratio for buildings with many separation walls is about 7% higher than the trend and for buildings with few separation walls about 7% lower.

5.2.6. Façade

Three types of façades have been distinguished:

- Type 1: separate façade elements.
- Type 2: traditional cavity wall.
- Type 3: frames façade.

The façade of the New Erasmus Medical Centre and EWI in x-direction have been categorized as load bearing, because part of the façade is part of the MLBS. For these two cases the façade leads to less extra energy dissipation because the internal material damping of these parts have already been taken into account by considering the material of the MLBS.

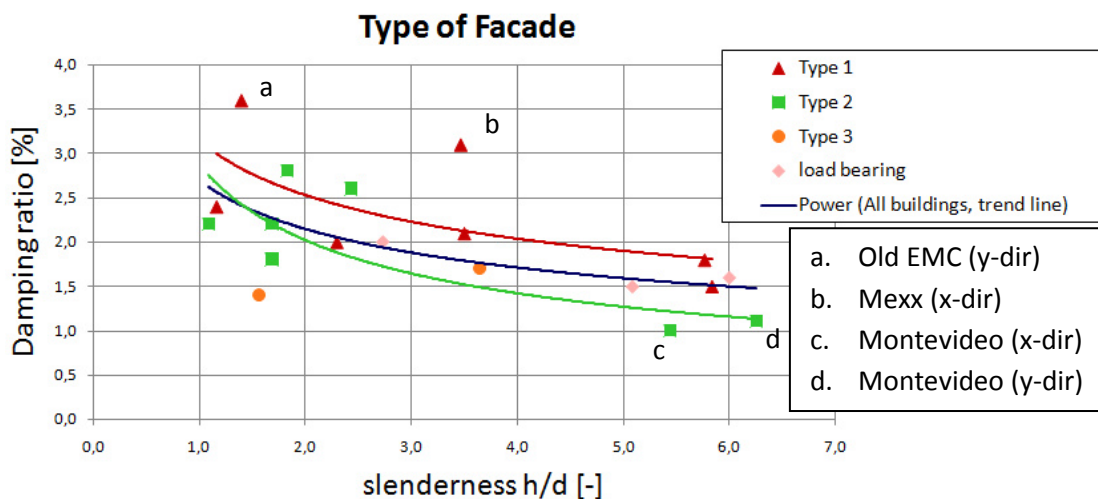


Figure 78 – plot of the damping ratio against the slenderness for different types of facades

The observed trend lines are doubtful. In general it seems that buildings with façades of type 1 show higher damping ratios, buildings with type 2 show lower damping values. However, the positive influence of type 1 on the damping is doubtful because the higher line is mainly caused by building a and b. It has been analyzed that the higher damping ratio of building a and b is most probably influenced by the ‘frame action’ of the MLBS. If these points are neglected, no clear positive effect of type 1 will be observed.

The negative influence of type 2 is also doubtful, because it mainly depends on the low damping values of building c and d. Actually there are too few data points at larger slenderness too really speak about a trend line.

Buildings with façades of type 3 seems to show lower damping ratios, but this conclusion isn’t well founded because it is only based on two results. Buildings categorized as load bearing show damping values corresponding to the trend line.

The weight and material of the façade can also be of importance. The results have also been plotted in graphs in order to investigate if there is a clear relation between the damping ratio and these two characteristics.

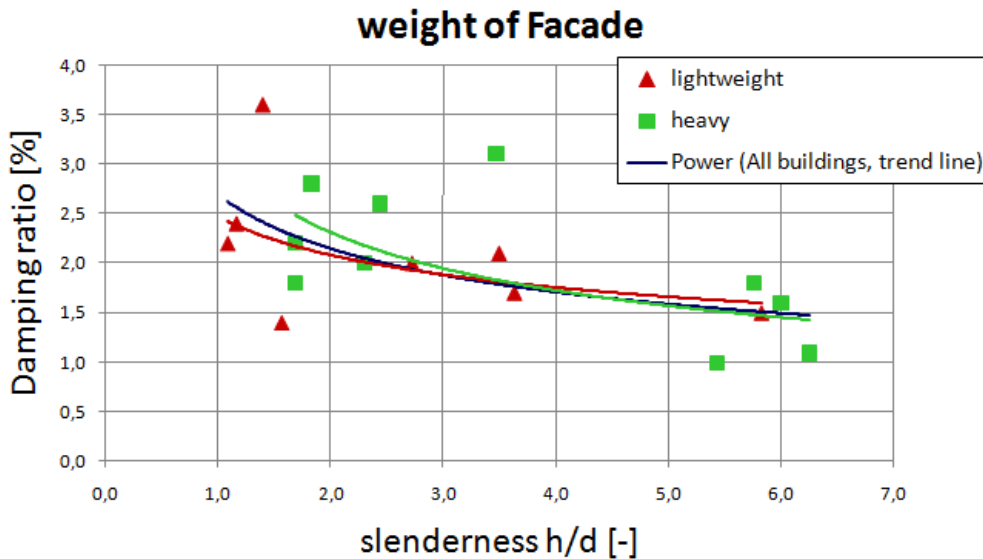


Figure 79 – plot of the damping ratio against the slenderness for different classes of weight of the façade

No clear relation between the weight of the façade and the damping ratio can be observed.

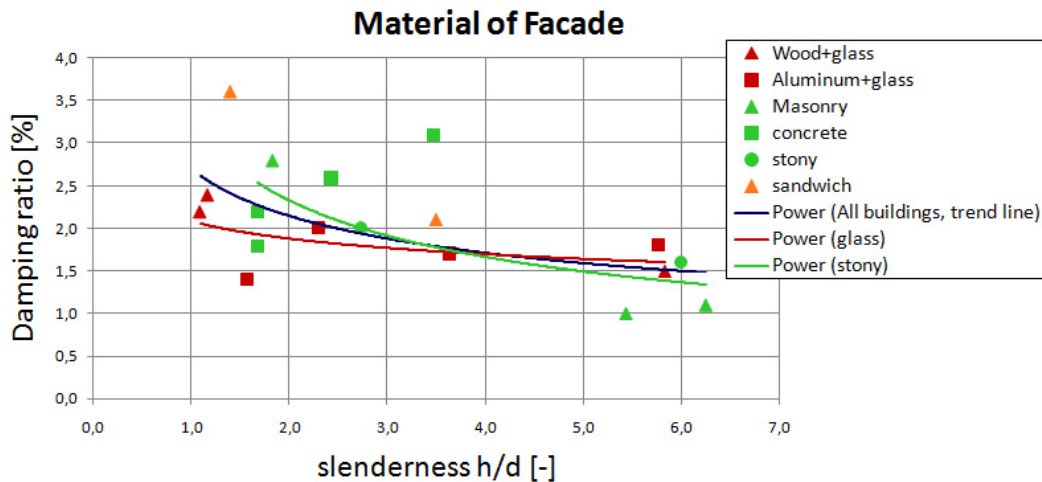


Figure 80 – plot of the damping ratio against the slenderness for different weight of the façade

The influence of the material of the façade has also been analyzed. Many different materials are present, no clear relation can be observed. The façades have also been classified as façades with a lot of glass and façades with a lot of stony material. However, this classification also didn't result in a clear relation.

5.2.7. Foundation

Three major types of foundation have been distinguished and the results for these types have been plotted in Figure 81. No information about the foundation of CIG was available, therefore this building has been left out of this serie.

- Basement: one large box below the building with a field of piles below
- Plate foundation: one large plate below the building with a field of piles below

- Beam foundation: separate foundation blocks below the building, connected by beams.

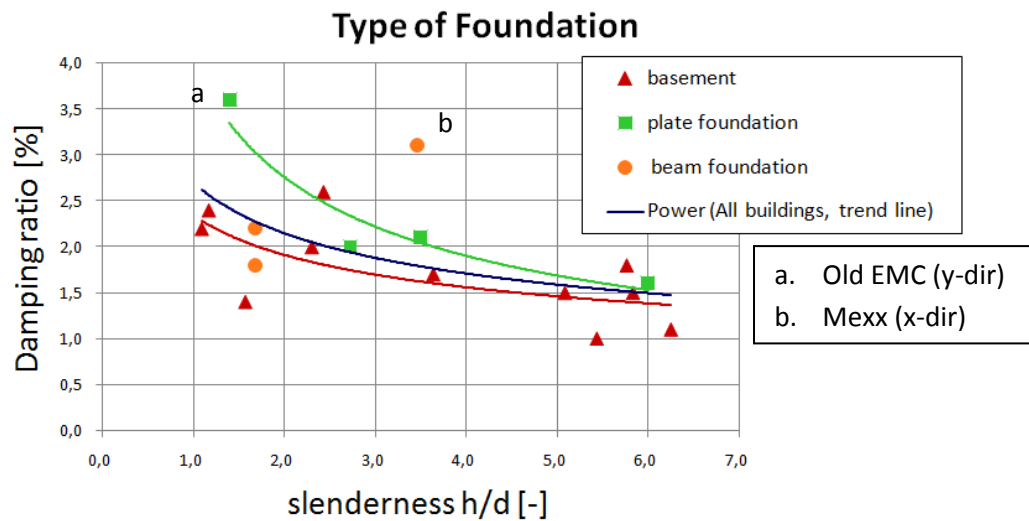


Figure 81 – plot of the damping ratio as a function of the slenderness for different types of foundation

From the graph it can be observed that buildings with basements in general show a bit lower damping. Buildings with plate foundations in general show higher damping. However, the fitted line for plate foundations is influenced to a large extent by building a. Probably the high damping of building a is caused by the considerable 'frame action' in the structural system. If we neglect the result of building a, the green line will come very close to the trend line. In that case there is no strong relation between the type of foundation and the damping ratio.

Because the influence of the type of foundation hasn't also been observed in any former investigation, it will be concluded that no clear relation between the type of foundation and the damping ratio has been found.

The damping ratio's for different values of the rocking ratio have been plotted in the following figure. Because no information about the foundation of CIG was available, the buildings have been left out of this serie.

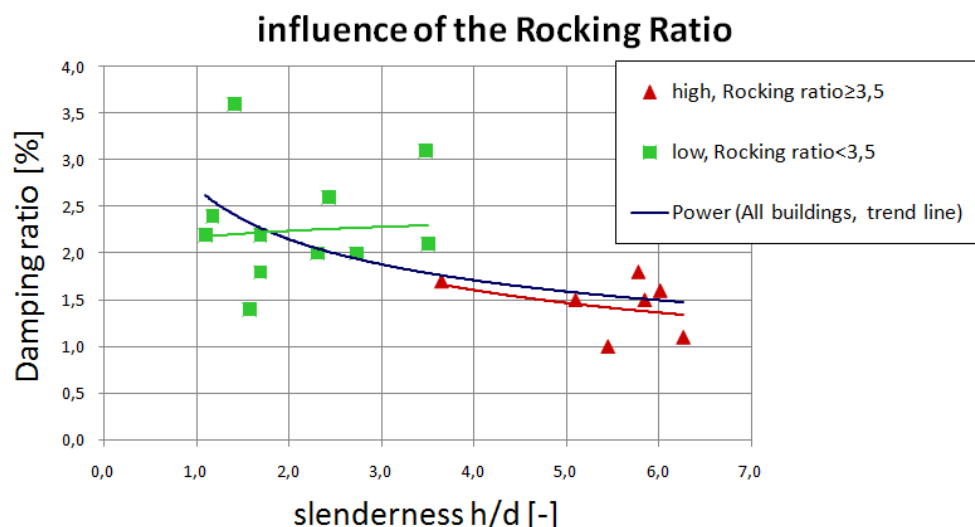


Figure 82 – plot of the damping ratio's as a function of the slenderness for different values of the rocking ratio

In comparison with the trend line it can be observed that buildings with a high rocking ratio show a bit less damping (about 7% less). For low rocking ratios, no useful relation can be observed.

It is striking that the higher rocking ratios can be observed at the highest slenderness. Actually this is very logic, because as the slenderness of the building above surface level is larger, the rocking ratio will be larger as well. On the basis of the formula presented in §5.1.3 smaller damping ratios can be expected. This is clearly visible in the graph.

The influence of rocking ratio is also a good explanation for the downward trend of the damping ratio with increasing slenderness of the building. It does not explain the deviations to this general trendline, because the slenderness of the building above surface level corresponds well with the rocking ratio.

Concerning the mass density of the structures, two categories have been distinguished and the result can be found in the following figure. The mass density of the CIG building and the HBG building hasn't been taken into account because it hasn't been determined.

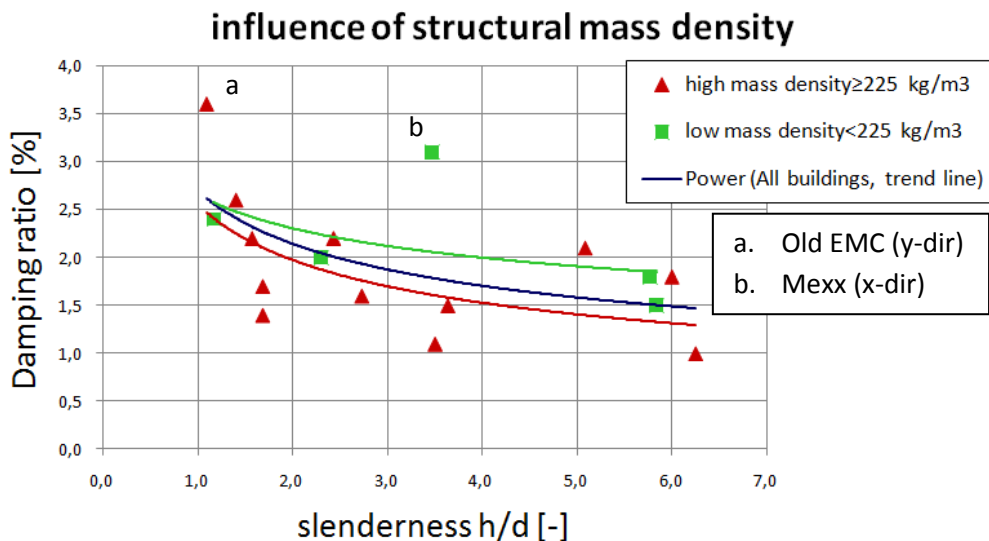


Figure 83 – plot of the damping ratio's as a function of the slenderness for two categories of structural density

It can be observed that higher structural density leads to lower damping and vice versa. This is in line with the formula for rocking presented in §4.5.45.1.3. Even when building a en b will be neglected because their higher damping ratio is probably caused by the influence of considerable 'frame action', the relation will still be clear. From this it will be concluded that the mass density of the structure will influence the damping. On average, the damping ratio for buildings with low mass density is about 15% higher than the trend and for buildings with high mass density this is about 12% lower.

5.3. Conclusions

Based on the actual damping ratio in relation with the trend line, three classes have been defined. The classes represent buildings with a low, normal and high damping ratio. The classes have been illustrated in the following figure.

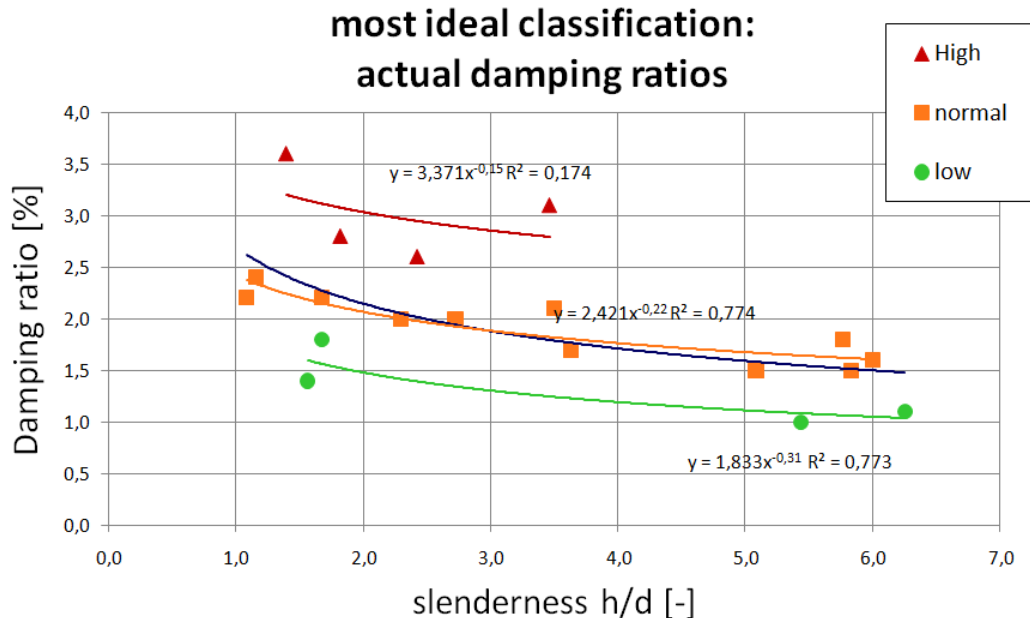


Figure 84 – damping ratio as function of the aspect ratio: low, normal and high classes and their trendlines.

If a building can be classified on the basis of structural characteristics, the damping ratio can be estimated with a formula corresponding with the class. Since the fitted lines for the classes show less scatter than the trend line of all buildings, a more accurate estimate of the damping can be made. In Table 12 the characteristics of buildings, per class can be checked.

High class

The buildings with the relative highest damping ratios (with respect to the trend) are (in order of decreasing damping ratio):

- Mexx building (x-direction)
- Old EMC tower (y-direction)
- HBG building (x-direction)
- CIG building (x-direction)

Structural characteristics corresponding to relative high damping ratios:

- MLBS: Buildings with a steel MLBS with bolted connections and buildings with a concrete MLBS in which cast in-situ stabilizing elements have been combined with prefab elements. Buildings with rigid frames.
- NSE: many separation walls
- Foundation: low rocking ratios ($\leq 3,5$) and low structural mass density

Low class

The buildings with the relative lowest damping ratios (with respect to the trend) are (in order of increasing damping ratio):

- Winston Churchill (y-direction)
- Montevideo (x-direction)
- Montevideo (y-direction)
- 's-Graventower (y-direction)

Structural characteristics corresponding to relative low damping ratios:

- MLBS: cast in-situ, monolithic concrete, core/shear walls (coupled)
- NSE: few separation walls.
- Foundation: high rocking ratio ($\geq 3,5$) and high structural mass density

General

The influence of structural characteristics corresponding to the main load bearing structure, the non-structural elements and the foundation has been investigated.

The influence of the main load bearing structure was very clear. Steel buildings with rigid or braced frames are mostly combined with bolted connections and show significantly more damping. Also in concrete buildings where rigid frames have been applied and in which the connections between (part) of the elements allow some relative movement, more damping is observed (this has been observed in buildings where a stabilizing in-situ core has been combined with prefabricated elements).

The influence of the non-structural elements and the foundation was less clear. No clear influence of the type, the material and the weight of the façade has been discovered.

The rocking ratio does not explain the deviations to the trendline. The influence of rocking ratio is however a good explanation for the downward trend of the damping ratio with increasing slenderness of the building. The mass density of the structure seems to have a significant influence on the damping. Higher damping ratios have been observed at low mass density and lower damping ratios at higher mass density of the structure.

Classification method

Based on the observed influences of diverse structural characteristics, a system with points has been used to classify the diverse buildings. An overview of the classification based on structural characteristics can be found in Table 13 . Depending if a positive/negative effect and a strong/weak influence on the damping ratio has been observed, positive and negative points have been given for the structural characteristics. If no clear influence has been observed or no information was available, zero points have been given.

The points and boundary values have been defined such that the predicted high, normal and low classes corresponds as best as possible with the most ideal classification based on the actual damping. Still 5 out of 19 predictions are not equal to the measurements. The result can be found in the following graph. In this graph the colors indicate the predicted classification based on the structural characteristics and the corresponding fitted line. The shape of the markers indicates what should be the actual classification of the datapoint to get the most ideal classification.

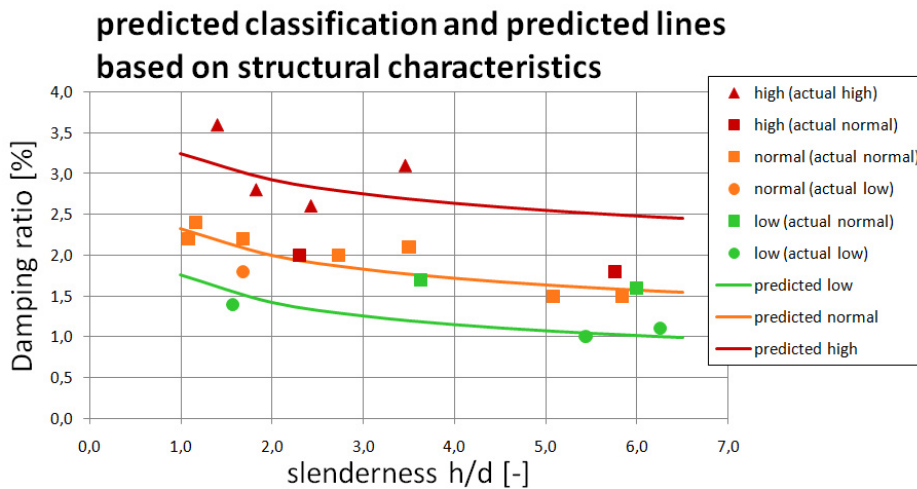


Figure 85 – predicted classification and line based on Table 13 in relation to the actual damping values

Based on the observed structural characteristics of the buildings in the relative high and low class, a simple classification rule has been defined (method called vdBerg). The formula have been based on the fitted lines of Figure 85 and have been multiplied with 0,96 such that on average the difference between the measured and predicted damping values is zero. ($\mu=1,0$ see Table 13)

Table 14 – rule to classify a building

Main Load bearing Structure	Foundation	Non Structural Elements	Class	formula
steel structure with bolted braced/rigid frames	low rocking ratio (< 3,5)	many separation walls	high	$\zeta=3,24 \cdot (h/d)^{-0,31}$
(partly) prefabricated structure with rigid frames	low struct. Mass density (< 225 kg/m ³)			
other combinations			normal	$\zeta=2,32 \cdot (h/d)^{-0,22}$
cast in-situ, monolithic concrete, core/shear walls (coupled)	high rocking ratio ($\geq 3,5$)	few separation walls	low	$\zeta=1,76 \cdot (h/d)^{-0,31}$
	high struct. Mass density (≥ 225 kg/m ³)			

In the following figure, the prediction of Lagomarsino, the prediction based on the Japanese database (AIJ2000, without amplitude dependent term) and vdBerg can be compared with the actual damping ratios. μ in Table 13 and the following figure show that on average Lagmarsino and AIJ2000 underestimate the damping (15% and 44%) while vdBerg on average has $\mu=1,0$

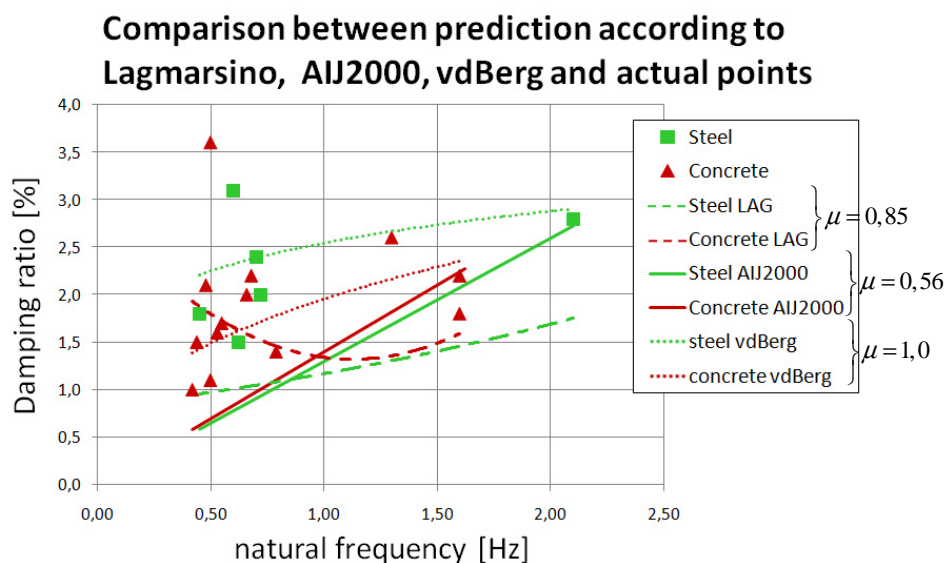


Figure 86 – predicted lines according to Lagmarsino, AIJ2000 (without amplitude dependency) and vdBerg (Table 13)

Discussion

The conclusions from the analysis of the case studies have a suggestive character. Basically the database is too small to really speak about trends. The influence of single characteristics on the damping is also hard to investigate with this method because higher/lower damping ratios are the result of a combination of many multiple structural characteristics, different for every building. A significant higher damping ratio can be caused by one very dominant characteristic or a combination of multiple small positive influences. Therefore, the conclusions have to be used carefully.

There are some combinations that show the variation of only one single characteristic, from which directly the influence of this characteristic could be observed.

The 's-Graventower has more or less equal properties in both x and y direction because the plan of the building is square. There is a difference of 0.4% between the damping ratio for y-direction (1.8%) and the damping ratio for x-direction (2.2%). It would be interesting what has caused this difference. Looking at the building, the transparent façade on both sides could be the explanation.

The structural characteristics for both directions of Montevideo are the same, there is only a slight difference in rocking ratio. A lower damping ratio would be expected in y-direction which has a slightly higher rocking ratio. This is not the case.

The structural characteristics for both directions of NEMC are the same, there is only a difference in rocking ratio. A lower damping ratio would be expected in x-direction which has a slightly higher rocking ratio. Now this is the case!

The x and y-direction of the Old EMC can also be compared. All structural characteristics are the same except for the structural system. It is clear that a higher damping ratio is the consequence of the rigid frames. This effect has also been observed at other buildings.

It can be concluded that the analysis of the cases has given some insight into possible explanations about damping differences but the results have to be used carefully. Because of the small amount of measurements, conclusions are not well based.

The influence of the amplitude has also not been taken into account, because it has not been given at which amplitude the measured damping ratios have been obtained. Actually the amplitude dependency should first be filtered out of the obtained damping ratios before investigating the influence of the structural characteristics.

6. Model

The scatter around the predicted damping values is caused by the influence of the structural characteristics of the structure and the amplitude dependency of damping. The influence of the structural characteristics on the total damping has been investigated in the former chapter. The results are not yet very convincing because they have been based on a small database.

Therefore a model has been developed that contains damping in 4 different parts of the building. The amount of energy dissipation per part can be determined by calibration of the model to the measured response. This can be done for every building. A better investigation of the influence of the structural characteristics can be performed with this information, because the influence on a specific part can be investigated without disturbance of the contribution of damping from other parts. Eventually the damping per part can be linked to the structural characteristics of a building such that the model can be used as a design tool. This model can be used to optimize the design of a building by prediction of damping based on the damping of 4 parts.

In this chapter the developed model of a high-rise building that will be used in the method, will be introduced. In the second section, it will be explained how the natural frequencies of the system can be obtained. The method will be illustrated with the measured time response of the New Erasmus Medical Center. The natural frequency of the New EMC will be predicted on the basis of the structural parameters (bending stiffness, mass and rotation and translational stiffness at the base) that are implemented in the model. The predicted natural frequency turns out to be different than the measured natural frequency. In the third section it will be explained how this has been taken into account.

6.1. Justification of the model

It is wished to develop a model of a high-rise building that contains the most important structural characteristics that can influence the natural frequencies and damping. Therefore, a simplified representation of a building has been developed in which the structural characteristics have been represented by simple parameters. The figure below shows the model and its parameters.

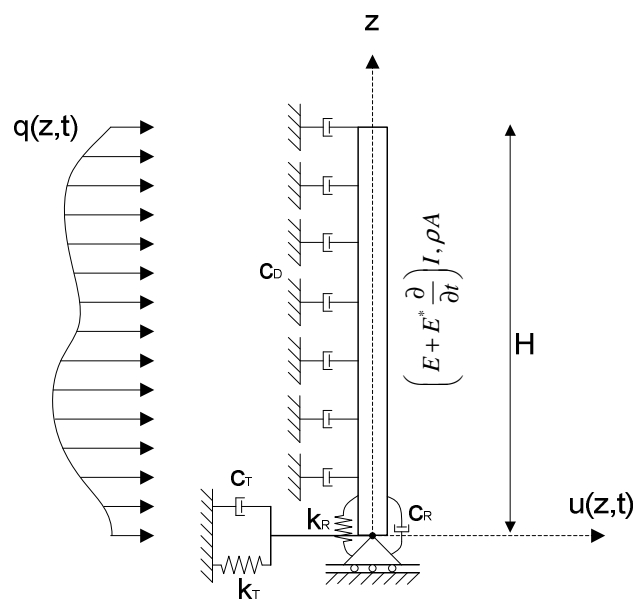


Figure 87 – dynamic model of a high-rise building

6.1.1. Main load bearing structure - Euler Bernoulli beam

A high-rise building has been represented by an Euler Bernoulli beam. In this beam, the deformation is only caused by bending, shear deformation is neglected. In general, both deformations should be taken into account, but for slender beams, the shear deformation is small compared to the bending deformation [Blaauwendraad, 2006, p. 45]. The theory of bending is only valid for small deformations. Since high-rise buildings are slender (larger than 1:5) and the deformations compared to the dimensions of the building are small, an Euler Bernoulli beam is a good approximation for a high-rise building.

According to the theory for an Euler Bernoulli beam, the bending moment and the curvature are related by [Metrikine, , §3.2.5.]:

$$M = -EI \frac{\partial^2 u}{\partial z^2} \tag{6.1}$$

In this relation, the stresses (σ) in the material have been assumed to be linearly dependent on strain (ϵ) according to Hooke’s law. The Elastic Bending Stiffness, EI , only takes into account the stiffness of the main load bearing structure of the building.

6.1.2. Internal material damping – Kelvin Voigt model

Material shows internal damping that can be represented by a viscous damping model (§4.1.1 and §4.1.2). This damping has been modeled by adding an extra term, $E^* \frac{\partial}{\partial t}$, to the Elasticity Modulus, E .

$$M = -\left(E + E^* \frac{\partial}{\partial t}\right) I \frac{\partial^2 u}{\partial z^2} \tag{6.2}$$

By adding this term, the stresses in a material have now been modeled according to the Kelvin Voigt model. In this model the modulus of elasticity depends on the speed of loading and unloading. This property causes a hysteresis loop. The area under the hysteresis loop is a measure for the energy lost during one cycle of loading. [Spijkers, et al., 2005, §5.2]

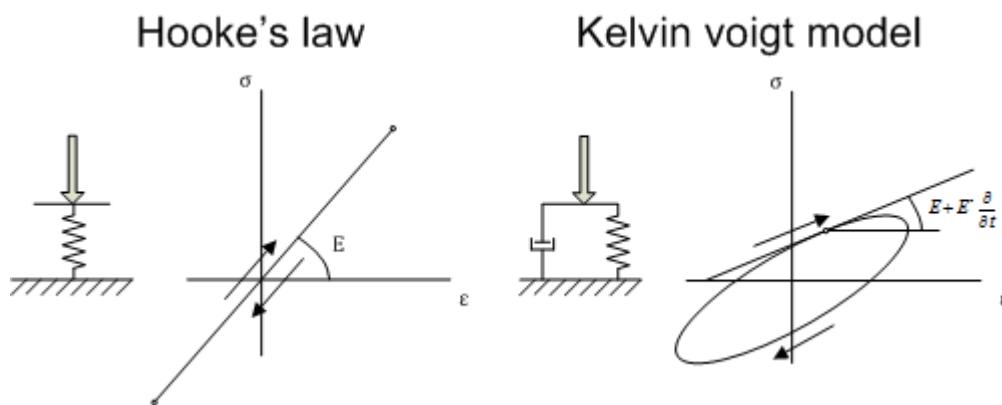


figure 88 – relation between the stress and deformation during loading and unloading. Left: according to Hooke’s law, right: the Kelvin Voigt model.

6.1.3. Foundation – translational and rotational springs and dampers

The foundation of building can rotate and translate under the horizontal load. The elastic rotation stiffness of the piles and sub soil has been modeled with a rotational spring (k_R). The elastic reaction of the subsoil against the underground structure in horizontal direction has been represented by the

translational spring (k_T). Energy will be lost during loading and unloading of the soil. This internal damping of the subsoil has been modeled by a translational (c_T) and rotational (c_R) viscous damper.

6.1.4. Non structural elements – distributed dampers

The non structural elements of a building will move relative to each other or relative to the main load bearing structure. Energy will be lost due to friction at the interfaces. This damping has been modeled by the distributed dampers (c_d) across the whole length of the beam.

6.2. The free vibration

If no load is acting on the beam, the beam will only move if an initial displacement or velocity is given to the beam. When the beam is released, it will vibrate according to its natural frequencies. For low modal damping ratios ($\zeta < 0.10$, valid for high-rise buildings), the natural frequency and mode shapes can be found by setting all damping mechanisms to zero. The most important steps to obtain the natural frequency and mode shapes are described in the following subsections. (An extensive description can be found in F.4.1-F.4.3.)

6.2.1. Procedure to obtain the natural frequencies and mode shapes

By setting the damping mechanisms to zero, the following equation of motion has been derived:

$$\rho A \frac{\partial^2 u}{\partial t^2} + EI \frac{\partial^4 u}{\partial z^4} = 0 \quad (6.3)$$

By setting the damping mechanisms to zero, the boundary conditions become:

At the bottom, $z=0$

$$EI \left. \frac{\partial^2 u}{\partial z^2} \right|_{z=0} = k_R \left. \frac{\partial u}{\partial z} \right|_{z=0} \quad (6.4)$$

$$-EI \left. \frac{\partial^3 u}{\partial z^3} \right|_{z=0} = k_T u(0, t) \quad (6.5)$$

At the top, $z=H$

$$EI \left. \frac{\partial^2 u}{\partial z^2} \right|_{z=H} = 0 \quad (6.6)$$

$$EI \left. \frac{\partial^3 u}{\partial z^3} \right|_{z=H} = 0 \quad (6.7)$$

The solution $u(z,t)$ has been assumed as the multiplication of an unknown coordinate related function, $U(z)$ and an unknown time related function, $\Psi(t)$.

$$u(z, t) = U(z) \Psi(t) \quad (6.8)$$

With the method of separation of variables, a time and coordinate relation differential equation has been obtained. The general solutions for the time and coordinate part have been derived:

$$\Psi(t) = A \sin(\omega t) + B \cos(\omega t) \quad (6.9)$$

$$U(z) = C_1 \cosh(\beta z) + C_2 \sinh(\beta z) + C_3 \cos(\beta z) + C_4 \sin(\beta z) \quad (6.10)$$

With constants A en B depending on the initial conditions and C_1 - C_4 depending on the boundary conditions. By substitution of the general solutions into the boundary conditions a set of 4 algebraic equations has been derived. In matrix notation:

$$\underline{AC} = \underline{0} \quad (6.11)$$

$$EI\beta^2 \begin{bmatrix} 1 & -\frac{k_R}{EI\beta} & -1 & -\frac{k_R}{EI\beta} \\ k_T & \beta & k_T & -\beta \\ \cosh(\beta H) & \sinh(\beta H) & -\cos(\beta H) & -\sin(\beta H) \\ \beta \sinh(\beta H) & \beta \cosh(\beta H) & \beta \sin(\beta H) & -\beta \cos(\beta H) \end{bmatrix} \begin{bmatrix} C_1 \\ C_2 \\ C_3 \\ C_4 \end{bmatrix} = \begin{bmatrix} 0 \\ 0 \\ 0 \\ 0 \end{bmatrix} \quad (6.12)$$

$$\text{in which } \beta^4 = \frac{\rho A \omega^2}{EI}$$

The constants C_1 - C_4 can be found by solving this set of algebraic equations.

To find the non-trivial solution of the set of equations, the determinant of A must be zero. With the help of computer software an expression of the determinant as a function of ω has been defined. By setting this expression equal to zero, the frequency equation has been obtained. The solution of this expression gives the natural frequencies of the system.

By substitution of the found natural frequencies in the set of equations, constants C_1 - C_4 can be found for every natural frequency ω . Because the natural frequencies have been chosen in such manner that the determinant is zero, the system is dependent. This means that the constants C_1 - C_4 that need to be found depend on each other. It is needed to assume that $C_4=1$, in order to find the shapes of the modes.

The total solution of the un-damped free vibration is a summation over all modes. A_i and B_i depend on the initial conditions.

$$\begin{aligned} u(z,t) &= \sum_{i=1}^{\infty} W_i(z) \Psi_i(t) \\ W_i(z) &= C_{1,i} \cosh(\beta_i z) + C_{2,i} \sinh(\beta_i z) + C_{3,i} \cos(\beta_i z) + C_{4,i} \sin(\beta_i z) \\ \Psi_i(t) &= A_i \sin(\omega_{i,t}) + B_i \cos(\omega_{i,t}) \\ \beta_i^4 &= \frac{\rho A \omega_{n,i}^2}{EI} \end{aligned} \quad (6.13)$$

6.2.2. Natural frequencies and mode shapes for the New EMC

The model parameters concerning the mass and stiffness have been derived from the design calculations of the New EMC (see appendix G):

Table 15 – structural parameters of the New EMC derived from design calculations

	ρA [kg/m]	EI [Nm ²]	k_R [Nm/rad]	k_T [N/m]
x	4,30E+05	2,48E+13	1,47E+12	1,00E+10
y	4,30E+05	6,78E+13	5,81E+12	5,00E+09

With these values, the natural frequencies and C_1 - C_4 have been obtained with the procedure described above (see appendix L.1 for the matlab files) for the first four modes in x-direction.

Table 16 – natural frequencies and constants for the New EMC in x-direction

mode	ω_n [rad/s]	C1	C2	C3	C4
1	1,44	0,93	-0,57	-0,20	1
2	9,24	0,49	-0,51	-0,33	1
3	24,68	0,58	-0,58	0,14	1
4	44,63	1,14	-1,14	1,25	1

By substitution of these natural frequencies and the constants in the total solution, the mode shapes can be found. The i^{th} mode shape vibrates with frequency $\omega_{1,i}$. The lowest natural frequency is equal to $f_{n,1}=1,44/2\pi=0,230$ Hz.

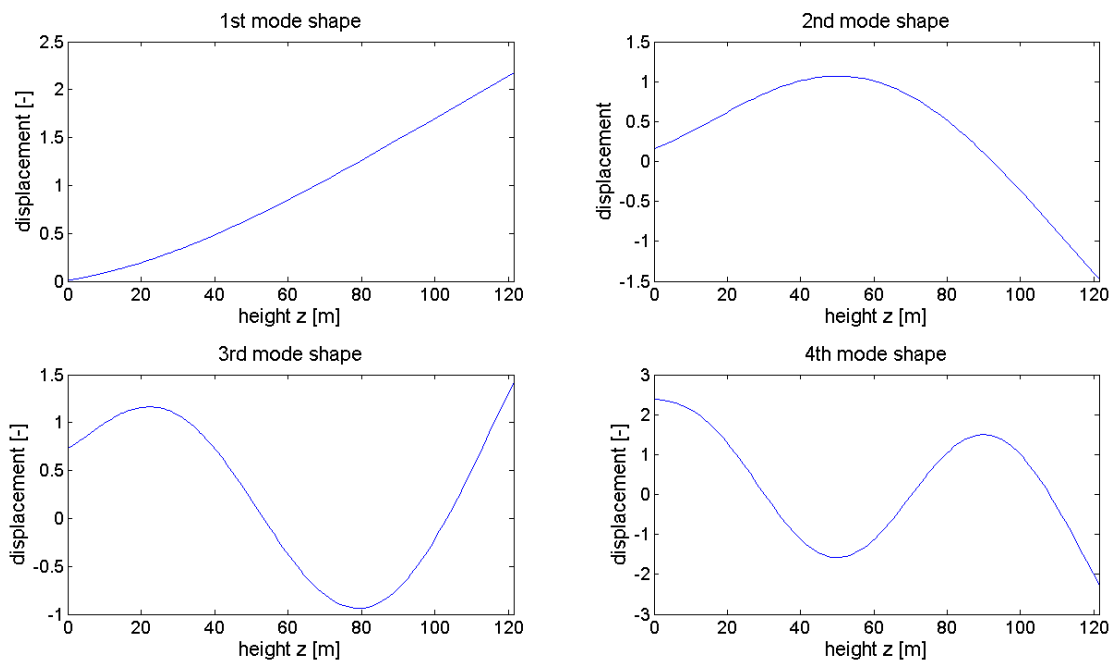


Figure 89 – the shape of the first four modes of vibration

6.3. Calibration of the mass and stiffness parameters

The first natural frequency predicted by the model depends on the parameters concerning mass and stiffness derived from the design calculations. However, there will be a difference between these values and the actual values. Consequently, the predicted natural frequency of the model doesn't correspond with the measured one. First it will be explained which parameters have been estimated with the least accuracy and with a sensitivity analyse, the influence of the parameters on the natural frequency will be investigated. Based on the results of these two investigations, the mass and stiffness parameters will be adapted to match the predicted and measured natural frequency.

6.3.1. Accuracy of the estimated parameters

The accuracy of the mass can be assumed to be the most accurate because it depends on the accuracy of the density and volume of the permanently present elements, because at the time of measurement no variable loads were present (the interior of the building had not been finished). It can be assumed that both volume and density are known with a little error of about $\pm 1\%$.

The bending stiffness of the building can be assumed to be estimated quite accurately. Its accuracy depends on the moment of inertia and the E-modulus of concrete. The error of the assumed E-modulus can be assumed to be very low because calculation has shown that concrete is un-cracked and most elements have been prefabricated. This results in accurate concrete quality. For the stress distribution it has been assumed that all prefab elements are connected monolithically. This assumption enhances some inaccuracy because in reality some shear deformation can occur at the connections, which can result in about 2-5% less stiffness [Tolsma, 2010, p. 73]. It will be assumed that the error in the estimated bending stiffness is about 5%.

The stiffness of the foundation piles is based on the local measurements [Salemans & Hartman, 2009]. It has been advised to reduce the measured stiffness by multiplication with a factor $1/1,3=0,77$. From this it can be assumed that there is large uncertainty about the stiffness of the piles. The error on the assumed stiffness will be about $\pm 25\%$.

Furthermore, the accuracy of the assumed translational stiffness is very low, but a sensitivity analysis will show that the predicted natural frequency is very insensitive to variations of this parameter.

6.3.2. Sensitivity analysis of the parameters on the first natural frequency

By variation of the mass and stiffness parameters in x-direction around values based on the design (Table 15), the influence of the parameters on the first natural frequency have been studied.

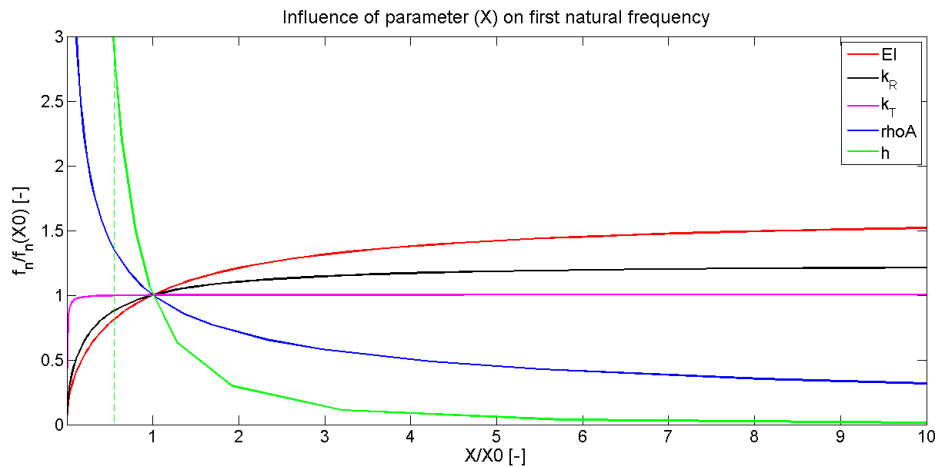


Figure 90 – influence of mass, stiffness and height on the predicted natural frequency.
 $EI_0=2,48 \cdot 10^{13} \text{ Nm}^2$, $k_{R,0}=1,47 \cdot 10^{12} \text{ Nm/rad}$, $k_{T,0}=1,00 \cdot 10^{10} \text{ N/m}$, $\rho A_0=4,30 \cdot 10^5 \text{ kg/m}$, $h_0=121,5 \text{ m}$.

The steepness at $X/X_0=1,0$ has been calculated for all parameters.

Table 17 – steepness of the parameters at $X/X_0=1$

X	ρA	EI	k_R	k_T	h
steepness	-0,72	0,46	0,26	0,005	-2,61

Calibration of the parameters to the measurements.

From the sensitivity analysis it can be concluded that the influence of k_T is negligible, thus difference between the predicted and real values can be neglected. The mass has the largest influence but because its value has been determined with high accuracy, it can be assumed that the difference between the predicted natural frequency and the measured natural frequency will not be caused by a different mass. In reality, the bending stiffness and rotation stiffness can be significantly different. Also the influence is significant.

- The measured natural frequency in x-direction is: 0,536 Hz.
- The natural frequency derived in the design calculations: 0,23 Hz [Ruijter & Splinter, 2009, p. 75]
- The predicted natural frequency in x-direction is: $1,44/2\pi=0,230 \text{ Hz}$. (see Table 16)

Thus the combination of increasing k_R and EI must lead to an increase of $0,536/0,229=2,34$ times the predicted natural frequency. Because the bending stiffness has been determined about 5 times more accurate than the rotation stiffness, it will be assumed that if the bending stiffness is increased 2 times, the rotation stiffness is increase 10 times. The influence of this combined increase on the natural frequency can be found in the following figure.

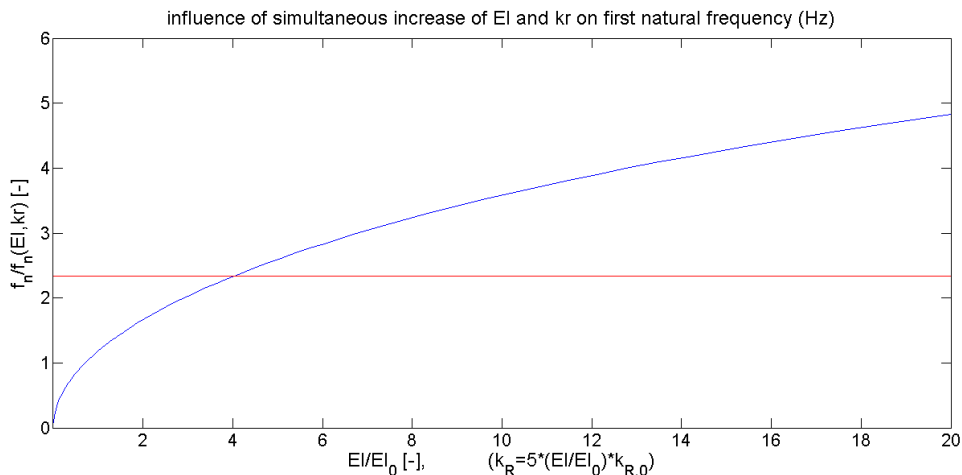


Figure 91 – influence of coupled increase of the bending stiffness and the rotation stiffness.

In order to achieve an 2,34 times larger natural frequency, the bending stiffness has to be at least 4 times larger, which implies that the rotation stiffness has to be $4 \times 5 = 20$ times larger! This is not realistic. Something else must have caused the difference between the predicted and measured natural frequency.

Changing schematization

No mistake has been made in the method to predict the natural frequency with our model because it corresponds to the natural frequency given in the design calculations. But in the design calculation, the tower has been assumed to stand alone. Actually there is a sliding connection up to a height of 56 m between the tower and the low-rise building.



Figure 92 – overview of the New EMC and connection between tower and low-rise part. [Bam & Ballast_Nedam, 2012]

This could be the explanation for the difference, because when the building is supported over 56 m, only 65,5 m is left free to move. In Figure 90 it can be found that the natural frequency is about 2,8 times larger as the height of the building is reduced to $65,5/121,5 = 0,54 \cdot h_0$. However, because there is a slide connection, the building won't be fully supported. New spring and/or sliding connectors have to be taken into account to model this situation. Smooth materials have been applied at the interfaces to avoid large resistance as the building moves [B. Splinter, 2012]. The friction force that

has been developed at the interface will probably be too low to actually have supported the building. Still no explanation for the larger natural frequency has been found.

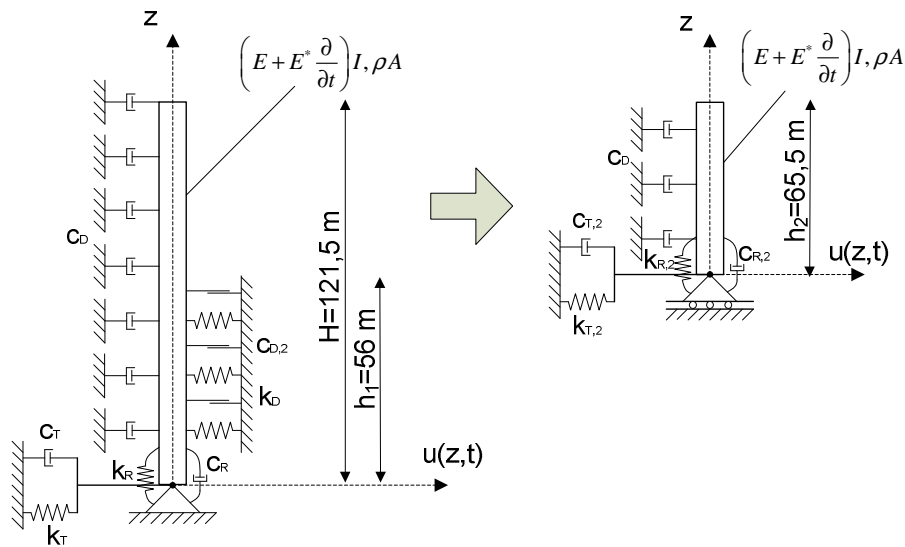


Figure 93 – schematization with new spring and/or sliding connectors

6.3.3. Conclusion

The method to predict the natural frequency of our model has been presented. Two possible explanations for the difference between the predicted and measured natural frequency have been given. But both don't seem to be realistic. It needs to be investigated if the connection won't actually provides some support to the building. Then it can be judged to what extend the connection influences the natural frequency and if the schematization needs to be adapted. The difference between the measured natural frequency and the predicted natural frequency of the building will probably have been caused by a combination of an underestimation of the bending and rotation stiffness and because the sliding connection will provide some support.

It is not wished to completely adapt the schematization because it is preferred to keep a simple model that can be applied on multiple buildings. It is also wished to keep the proposed damping values in the model. Therefore the mass and stiffness parameters will be adapted to fit the natural frequency. This will make it possible to continue and focus on the aspect of damping. After all, the purpose of this investigation is to investigate the damping.

The adapted model parameters can be found below. The predicted natural frequency is now equal to: $3,39/2\pi=0,540$ Hz, which is almost equal to the measured natural frequency (0,536 Hz).

Table 18 – adapted model parameters for the New EMC in x-direction

ρA [kg/m]	EI [Nm ²]	k_R [Nm/rad]	k_T [N/m]	h [m]
2,30E+05	7,44E+13	4,42E+12	1,00E+11	121,5

Table 19 - predicted natural frequencies and constants for the New EMC in x-direction, adapted model parameters

mode	ω_n [rad/s]	C1	C2	C3	C4
1	3,39	0,93	-0,58	-0,90	1
2	19,96	0,58	-0,60	-0,14	1
3	47,84	1,02	-1,02	1,04	1

7. Simulated dynamic behaviour

In chapter 6 a model has been presented and it has been explained how appropriate mass and stiffness parameters can be determined. Unfortunately only the modal damping ratio of the first mode has been determined from measurements. This is insufficient to find the four unknown damping parameters (c_D , c_R , c_T and E^*I). Therefore it is needed to simulate the dynamic behaviour at the top of the building and compare this with the actual measured displacement in time. This method will be illustrated with the New EMC case. Since the response is caused by a random wind load, it is convenient to work with spectra as has been explained in §3.4. The method has been illustrated in the following figure.

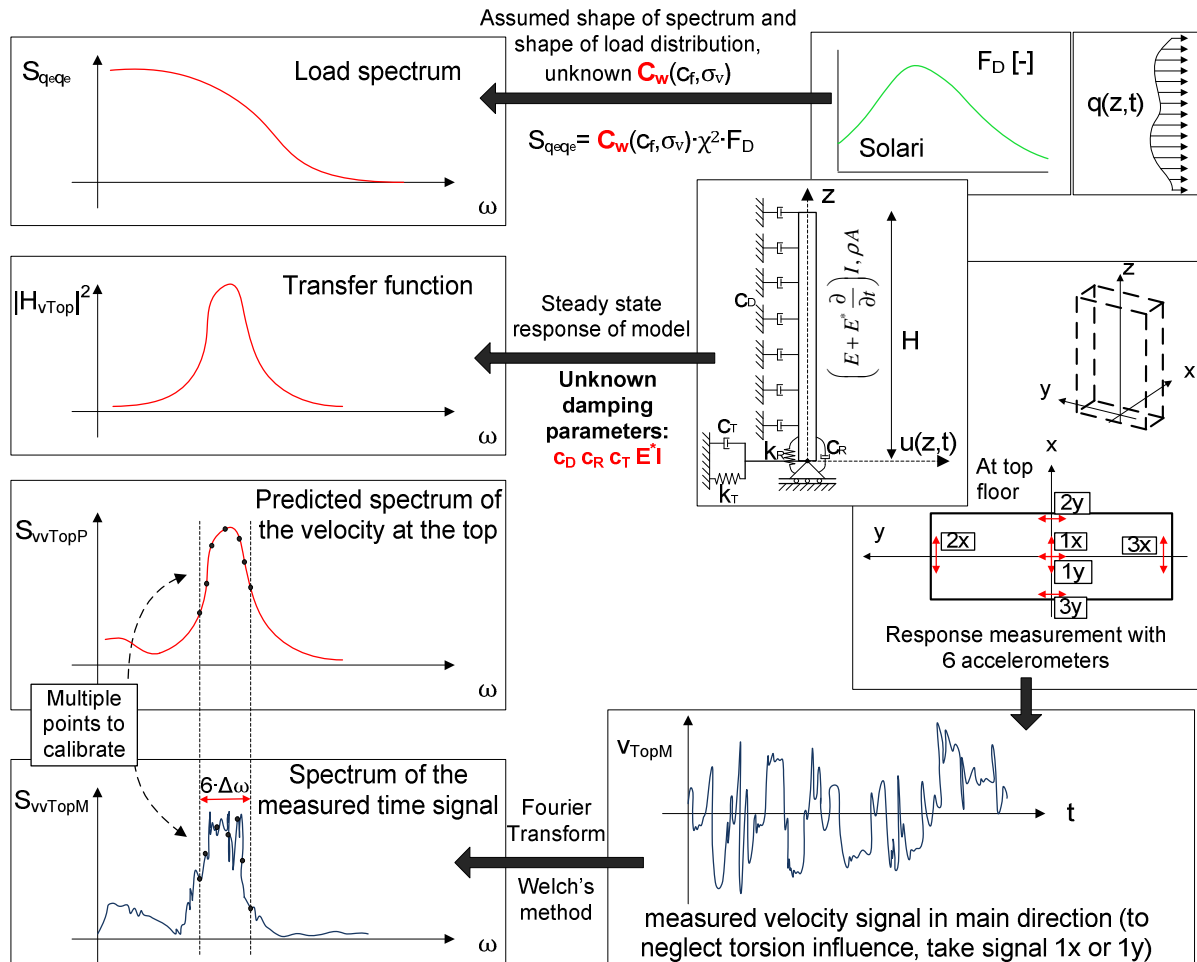


Figure 94 – overview of method to obtain a spectrum of the predicted and measured velocity

In the first section it will be explained how the load spectrum can be obtained. The second section will describe how the transfer function can be derived from the model presented in chapter 6. From these two spectra, the spectra of the velocity at the top can be predicted. The points of this spectra will depend on the unknown damping parameters (c_D , c_R , c_T and E^*I) and the unknown load factor C_w . By comparison of the predicted spectrum with the spectrum of the measured time signal, the model can be calibrated with a least square fit and the unknown parameters can be found.

The method and results of calibration of the load and damping parameters will be presented in the third section. In the conclusion the results will be discussed.

7.1. Assumed wind loading spectrum

In the model, the wind load has been represented by a distributed load as function of height and time. The wind pressure at height z is the summation of the mean and the fluctuating part. The fluctuating part has been measured around the mean deflection of the building, thus only the fluctuating wind pressure has to be modeled. The distributed wind load is equal to the wind pressure multiplied with the width of the building and a shape factor:

$$p_w(z, t) = \frac{1}{2} \rho_{air} \bar{v}(z)^2 + \rho_{air} \cdot \bar{v}(z) \cdot \tilde{v}(z, t) \quad (7.1)$$

$$\tilde{q}(z, t) = B \cdot C_f \cdot \rho_{air} \cdot \bar{v}(z) \cdot \tilde{v}(z, t) \quad (7.2)$$

For constant cross section over height, B and C_f are assumed to be constant. The mean wind velocity can be described by a logarithmic wind profile. It can be concluded that at every height, there is a linear relation between the fluctuating wind velocity and wind load. Therefore the Fourier Transform of the fluctuating wind load (S_q) and the variance spectrum of the fluctuating wind load (S_{qq}) are equal to [Vrouwenvelder, 2004, Ch 4]:

$$S_q(z, \omega) = B \cdot C_f \cdot \rho_{air} \cdot \bar{v}_0 \ln\left(\frac{z}{z_0}\right) \cdot S_v(z, \omega) \quad (7.3)$$

$$S_{qq}(z, \omega) = \left[B \cdot C_f \cdot \rho_{air} \cdot \bar{v}_0 \ln\left(\frac{z}{z_0}\right) \right]^2 S_{vv}(z, \omega) \quad (7.4)$$

The shape of the Solari wind spectrum (F_D) as given in the Eurocode (see appendix E) has been adopted for the wind velocity spectrum, the total variance (σ_v^2) is unknown. This spectrum is a function of the height, but will be assumed constant over height. The shape of the spectrum has been determined at $z=0,6h$ because this has been prescribed in the Eurocode. Using the shape (F_D) of the Solari spectrum, the following expression for the load spectrum can be derived:

$$S_{qq}(z, \omega) = \left[B \cdot C_f \cdot \rho_{air} \cdot \bar{v}_0 \ln\left(\frac{z}{z_0}\right) \right]^2 \cdot \frac{\sigma_v^2}{\omega} F_D\left(z = 0,6h; f = \frac{\omega}{2\pi}\right) \quad (7.5)$$

On a large surface, the peaks of the wind velocity velocity at different places won't occur at exactly the same time. Thus the total wind load on a larger surface shows less variance. Therefore the spectrum has to be multiplied with the aerodynamic admittance to take this into account.

$$S_{q_e q_e}(z, \omega) = \chi(\omega)^2 S_{qq}(z, \omega) \quad (7.6)$$

$$S_{q_e q_e}(z, \omega) = \chi(\omega)^2 \left[B \cdot C_f \cdot \rho_{air} \cdot \bar{v}_0 \ln\left(\frac{z}{z_0}\right) \right]^2 \cdot \frac{\sigma_v^2}{\omega} F_D\left(z = 0,6h; f = \frac{\omega}{2\pi}\right)$$

The expression for the wind loading spectrum at different heights consists out of a constant part with unknown magnitude, a coordinate related part and a frequency dependent part.

$$S_{q_e q_e}(z, \omega) = C_w \cdot Q_z(z) \cdot Q_\omega(\omega) \quad (7.7)$$

$$S_{q_e q_e}(z, \omega) = \left[B \cdot C_f \cdot \rho_{air} \cdot \bar{v}_0 \cdot \sigma_v \right]^2 \cdot \left[\ln\left(\frac{z}{z_0}\right) \right]^2 \frac{\chi(\omega)^2 F_D\left(z = 0,6h; f = \frac{\omega}{2\pi}\right)}{\omega}$$

7.2. The steady state response

The steady state response of the system due to the wind load is the solution to the inhomogeneous equation of motion:

$$\rho A \frac{\partial^2 u}{\partial t^2} + EI \frac{\partial^4 u}{\partial z^4} + E^* I \frac{\partial^5 u}{\partial t \partial z^4} + c_d \frac{\partial u}{\partial t} = q(z, t) \quad (7.8)$$

For which $q(z, t)$ has been defined in the former section (Eq. (7.2)) and the boundary conditions of the system at $z=0$ and $z=H$ have been derived (see appendix F.4.2):

$$\left(E + E^* \frac{\partial}{\partial t} \right) I \frac{\partial^2 u}{\partial z^2} \Big|_{z=0} = k_R \frac{\partial u}{\partial z} \Big|_{z=0} + c_R \frac{\partial^2 u}{\partial z \partial t} \Big|_{z=0} \quad (7.9)$$

$$-\left(E + E^* \frac{\partial}{\partial t} \right) I \frac{\partial^3 u}{\partial z^3} \Big|_{z=0} = k_T u(0, t) + c_T \frac{\partial u}{\partial t} \Big|_{z=0} \quad (7.10)$$

$$\left(E + E^* \frac{\partial}{\partial t} \right) I \frac{\partial^2 u}{\partial z^2} \Big|_{z=H} = 0 \quad (7.11)$$

$$\left(E + E^* \frac{\partial}{\partial t} \right) I \frac{\partial^3 u}{\partial z^3} \Big|_{z=H} = 0 \quad (7.12)$$

7.2.1. Solution in the frequency domain, Fourier Transform

Because next to the convenient distributed damping c_D the equation contains another damping term ($E^* I$) and the boundary conditions also contain two additional damping terms (c_R and c_T) the equations are coupled and can't be solved according to the modal analysis. Therefore the equation of motion and the boundary conditions have been transformed to the frequency domain by making use of the Fourier Transform (see appendix F.4.4). The equation of motion becomes:

$$U(z, \omega)^{IV} - \beta^4 U(z, \omega) = \frac{Q(z, \omega)}{EI + i\omega E^* I} \quad \text{in which} \quad \beta^4 = \frac{\rho A \omega^2 - i\omega c_d}{EI + i\omega E^* I} \quad (7.13)$$

And the boundary conditions in the frequency domain become:

$$(EI + i\omega E^* I) \cdot U'' - k_R \cdot U' - i\omega c_R \cdot U' = 0 \quad \text{for } z = 0 \quad (7.14)$$

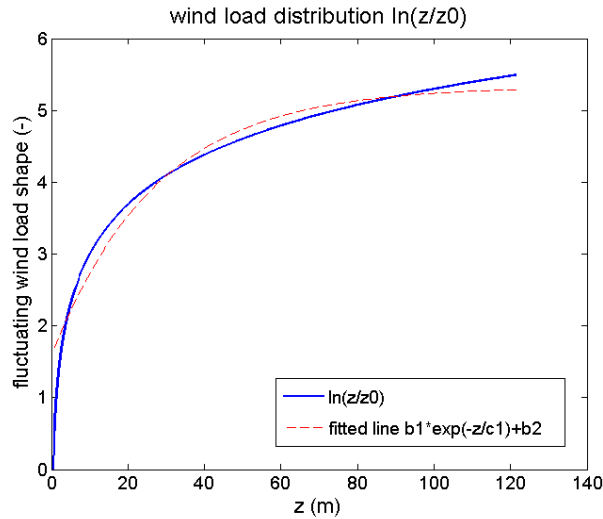
$$(EI + i\omega E^* I) \cdot U''' + k_T U(0) + i\omega c_T U(0) = 0 \quad \text{for } z = 0 \quad (7.15)$$

$$(EI + i\omega E^* I) \cdot U'' = 0 \quad \text{for } z = H \quad (7.16)$$

$$(EI + i\omega E^* I) \cdot U''' = 0 \quad \text{for } z = H \quad (7.17)$$

The Fourier Transform of the load, $Q(z, \omega)$ is comparable to S_q as has been defined in (7.3). The load changes over height according to the logarithmic distribution. To simplify calculations, the logarithmic function is fitted by an exponential functional.

$$Q(z, \omega) = Q_0(\omega) \ln\left(\frac{z}{z_0}\right) \rightarrow Q_0(\omega) (b_2 + b_1 \cdot e^{-z/c}) \quad (7.18)$$


 Figure 95 – fitted exponential function to the logarithmic wind distribution, with $z_0=0,5$ m

The general solution to Eq. (7.13) has been derived in appendix F.4.4:

$$U(z, \omega) = U_{\text{hom}}(z, \omega) + U_{\text{part}}(\omega)$$

$$U(z, \omega) = C_1 \cosh(\beta z) + C_2 \sinh(\beta z) + C_3 \cos(\beta z) + C_4 \sin(\beta z) + C_0(\omega) + C_z(\omega) e^{-z/100}$$

in which

$$C_0(\omega) = \frac{-b_2 Q_0(\omega)}{\beta^4 (EI + i\omega E^* I)} \quad \text{and} \quad \beta^4 = \frac{\rho A \omega^2 - i\omega c_d}{EI + i\omega E^* I} \quad (7.19)$$

$$C_z(\omega) = \frac{b_1 Q_0(\omega)}{EI + i\omega E^* I} \frac{1}{\left[\left(-\frac{1}{c} \right)^4 - \beta^4 \right]}$$

The constants C_1 to C_4 can be calculated from the 4 equations found by substitution of the general solution into the boundary conditions:

$$(EI + i\omega E^* I) \beta^2 \begin{bmatrix} 1 & -\frac{k_R + i\omega c_R}{(EI + i\omega E^* I) \beta} & -1 & -\frac{k_R + i\omega c_R}{(EI + i\omega E^* I) \beta} \\ \frac{k_T + i\omega c_T}{(EI + i\omega E^* I) \beta^2} & \beta & \frac{(k_T + i\omega c_T)}{(EI + i\omega E^* I) \beta^2} & -\beta \\ \cosh(\beta H) & \sinh(\beta H) & -\cos(\beta H) & -\sin(\beta H) \\ \beta \sinh(\beta H) & \beta \cosh(\beta H) & \beta \sin(\beta H) & -\beta \cos(\beta H) \end{bmatrix} \begin{bmatrix} C_1 \\ C_2 \\ C_3 \\ C_4 \end{bmatrix} = \begin{bmatrix} F_{0,1} \\ F_{0,2} \\ F_{0,3} \\ F_{0,4} \end{bmatrix}$$

in which

$$F_{0,1} = - \left[(EI + i\omega E^* I) \cdot \left(-\frac{1}{c} \right)^2 + k_R \cdot \frac{-1}{c} + i\omega c_R \cdot \frac{-1}{c} \right] C_z(\omega) \quad (7.20)$$

$$F_{0,2} = - \left[(EI + i\omega E^* I) \cdot \left(-\frac{1}{c} \right)^3 - k_T - i\omega c_T \right] C_z(\omega) - [k_T + i\omega c_T] C_0(\omega)$$

$$F_{0,3} = - (EI + i\omega E^* I) \cdot \left(-\frac{1}{c} \right)^2 C_z(\omega) e^{-H/c}$$

$$F_{0,4} = - (EI + i\omega E^* I) \cdot \left(-\frac{1}{c} \right)^3 C_z(\omega) e^{-H/c} \quad \text{and} \quad \beta^4 = \frac{\rho A \omega^2 - i\omega c_d}{EI + i\omega E^* I}$$

7.2.2. The Transfer function

Looking at (7.19) and (7.20) it can be observed that there is a linear relation between the loading spectrum $Q_0(\omega)$ and C_1 - C_4 , C_0 and C_z . Thus the response is linearly dependent on the load. The transfer function for the velocity at the top is the response to a unit load with magnitude 1, so $Q_0(\omega)=1$. The velocity response can be obtained by multiplication of U with $i\omega$ (see Eq. (F.221))

$$H_{vTop}(\omega) = i\omega \cdot U(H, \omega) \quad \text{with } Q_0(\omega) = 1 \quad (7.21)$$

The matlab script to generate the transfer function can be found in appendix L.2 and for certain damping values the absolute value to the power two has been plotted. The peaks at the first 2 natural frequency can clearly be observed.

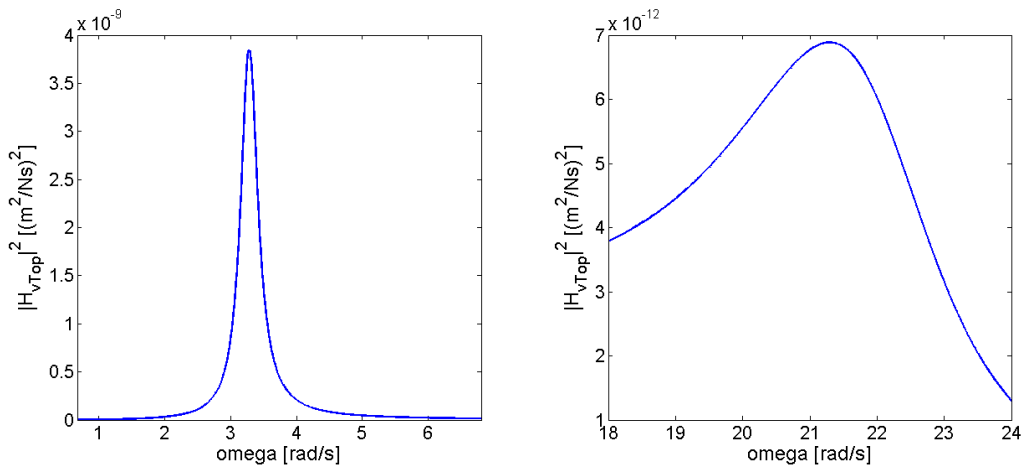


Figure 96 – transfer function at the first natural frequency and the second natural frequency

7.2.3. The steady state response at the top

The spectrum of the velocity at the top due to the assumed load is equal to:

$$S_{vvTopP} = |H_{vTop}(\omega)|^2 S_{q_e q_e}(\omega) \quad (7.22)$$

In which the load spectrum does not contain the logarithmic distribution because this is already incorporated in the transfer function.

$$S_{q_e q_e}(\omega) = [B \cdot C_f \cdot \rho_{air} \cdot \bar{v}_0 \cdot \sigma_v]^2 \chi(\omega)^2 \frac{F_D \left(z = 0, 6h; f = \frac{\omega}{2\pi} \right)}{\omega} \quad (7.23)$$

For chosen damping and load parameters, the predicted spectrum can be obtained.

7.3. Calibration of the damping and load parameters

To illustrate the calibration method, the case of the New EMC in x-direction will be used. First, it will be explained how the spectrum of the measured time signal has been obtained. Secondly the minimum, maximum and initial guess of the unknown parameters will be given. In the third and fourth subsection the results of the calibration will be presented.

7.3.1. The spectrum of the measured signal

The single sided variance spectrum of the measured signal has been obtained using Welch’s method [Welch, 1967]. In this method the measured signal is divided in multiple segments that partly overlap (50%). The single sided variance spectrum of each segment is obtained using a Fast Fourier Transform and the end result is the average of all segments.

In Figure 94 the location of the different accelerometers has been indicated. To avoid the influence of torsion effects, the measured signal of accelerometer 1x has been used. The response has been measured with a sampling frequency (f_s) of 50 Hz during 2 hours (360448 data points).

The length of the segments has been chosen at $N_{FFT}=65536$ points, such that the result is averaged over 10 segments. Because the Fourier transform of a signal is symmetric around $f_s/2$, the Nyquist frequency, the variance spectrum is obtained up to half of the sampling frequency [Hansen, 2011].

$$\omega_{Nyquist} = \Delta\omega(N_{FFT} / 2) = 0.0048(65536/2) = 157rad / s \quad (= f_s / 2 = 25Hz) \quad (7.24)$$

To check the statistical properties of the spectrum, the standard deviation of the time signal has been compared with the area under the single sided variance spectrum, they correspond well enough. The resolution of the obtained spectrum is equal to:

$$\Delta\omega = \frac{f_s \cdot 2\pi}{N_{FFT}} = \frac{50 \cdot 2\pi}{65536} = 0.0048rad / s \quad (\rightarrow \Delta f = 0.00076Hz) \quad (7.25)$$

The matlab script to obtain the spectrum can be found in appendix L.2.

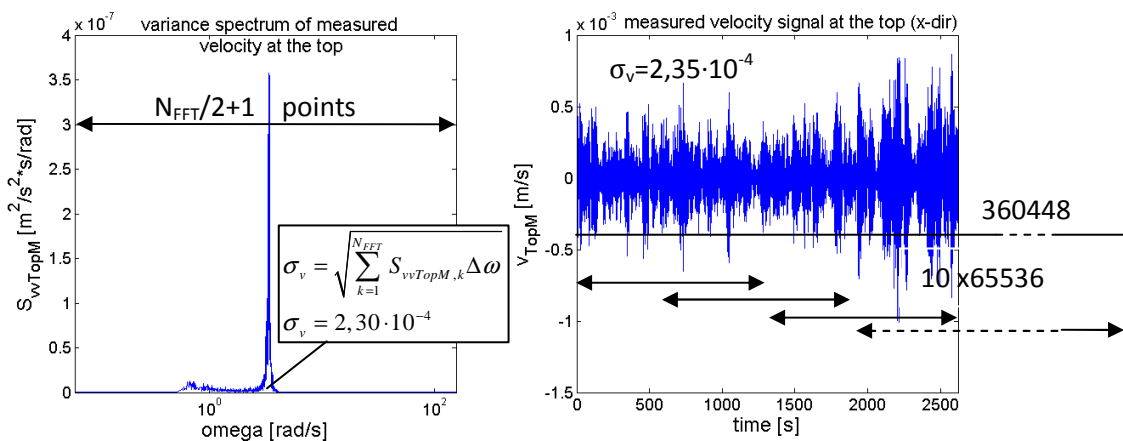


Figure 97 – variance spectrum of the measured velocity and part of the measured time signal

7.3.2. Initial, minimum and maximum values of unknown parameters

The mass and stiffness parameters have already been calculated to correspond with the natural frequency, that has been measured ($f_n=0,536$ Hz). In appendix F.3.6 the c_d has been calculated for a clamped beam model to correspond with the measured modal damping ratio ($\zeta_1=1,63\%$). On the

basis of this it will be assumed that c_d has a value between 10^2 - 10^6 . Based on the magnitude of the mass and stiffness parameters, it will be assumed that the values of the other unknown damping parameters are of the same order of magnitude and will lie between 10^4 and 10^{15} .

Concerning the load, the initial values for σ_v , C_f and the \bar{v}_0 are unknown. C_f mainly depends on the shape and the surroundings. 1,45 is taken as the initial value for C_f because this has been derived for the New EMC (see appendix C). In line with the Eurocode (appendix B.3), it will be assumed that the minimum of C_f is 1 and the maximum is 2,4.

The measurement have been performed under wind with an maximum 1-hour-average wind speed of 12 m/s and a maximum peak-wind speed of 22 m/s [KNMI, 2011]. Assuming that the difference between the peak and the average wind speed is equal to 3,5 times the standard deviation, the initial guess is $\sigma_v=2,9$ m/s. The average wind speed has been measured in the open field at an height of 10 m. Assuming the logarithmic wind profile ($z_0=0,5$ m) for the mean wind velocity results in $\bar{v}_0=4,0$ m/s. However, due to local influences and randomness of the wind load, the actual standard deviation of the wind and mean wind load could have been different at the time of measurement. It will be assumed that both can be 2 times smaller or 2 times bigger. The limits of the wind load constant C_w have been calculated from these values.

Table 20 – initial guess of values and their assumed minimum and maximum values

	c_D [Ns/m ²]	c_R [Nms/rad]	c_T [Ns/m]	$E^* I$ [Nm ² s]	C_w [N ² /m ²]	σ_v [m/s]	C_f [-]	B [m]	ρ_{air} [kg/m ³]	\bar{v}_0 [m/s]
initial guess	1,00E+04	1,00E+10	1,00E+10	1,00E+10	8,70E+05	2,90	1,45	44,30	1,25	4,00
min	1,00E+02	1,00E+04	1,00E+04	1,00E+04	2,60E+04	1,45	1	-	-	2
max	1,00E+06	1,00E+15	1,00E+15	1,00E+15	3,80E+07	5,8	2,4	-	-	8

7.3.3. Rough Calibration

In section 3.4 it has been explained that the response of the structure consists out of a dynamic and quasi static response. The peak of the dynamic response is most dominant, as is clearly visible in the obtained spectrum in Figure 97, but a quasi static peak is also visible. The height of the dynamic peak is mostly influenced by damping. The peak of the quasi static response is mainly influenced by the magnitude of the load and the stiffness of the system.

The effect of the load

The effect of the load on the response has been illustrated for cases of low and high damping values according to Table 20. The figures on the following page indicate the linear relation between the magnitude of the load and the response. For low damping, the absolute effect of the load on the response around the natural frequency is much larger than for the quasi static response, for high damping it is vice versa. As the load increases, the top of the resonance peak will be higher and the peak gets more narrow.

The effect of the damping

Figure 100 shows a reasonable fit of the predicted spectrum with the measured spectrum. This fit has been obtained by assuming C_w , c_R , c_T and $E^* I$ to have their minimum values according to Figure 21 and c_D has been increased until it gives a comparable resonance peak. The influence of variations of c_D around this value has been plotted.

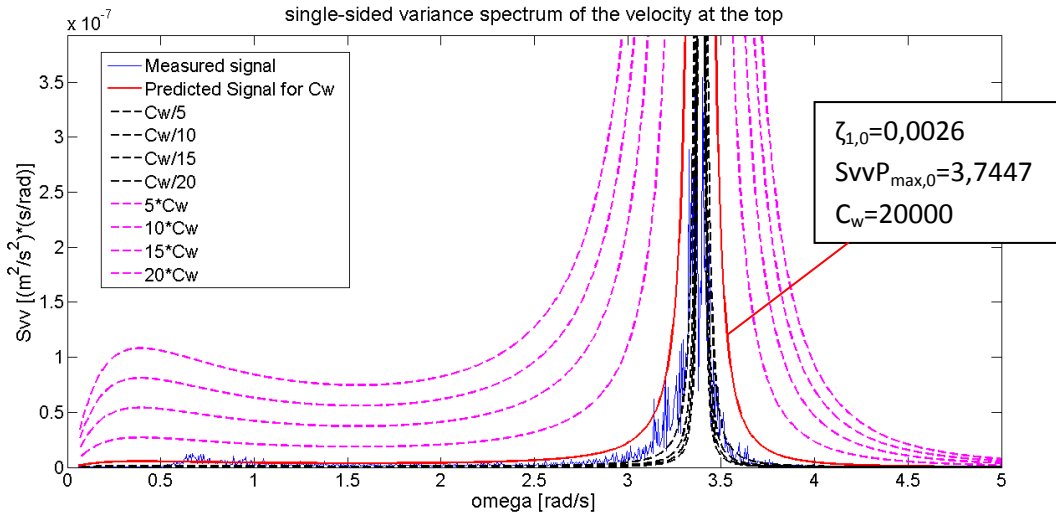


Figure 98 – influence of load under low damping

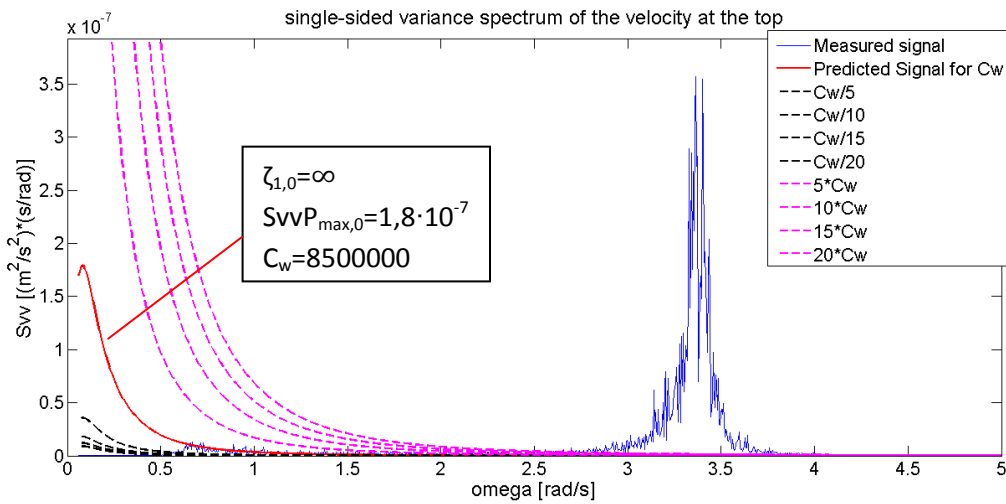


Figure 99 – influence of the load under high damping

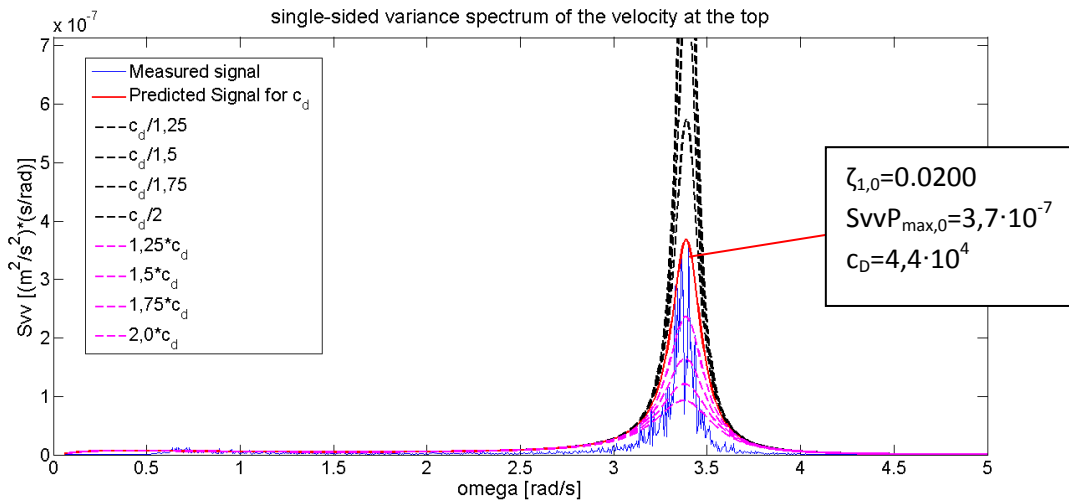


Figure 100 – influence of c_D for minimum load and minimum c_R c_T and E^*

As c_D decreases, the peak increases more than linear and gets more narrow. The height of the quasi static response doesn't depend on the damping parameters. The same behaviour has been observed for c_R and E^*I . For $c_R=2,16 \cdot 10^{11}$ and $E^*I=2,03 \cdot 10^{12}$ a resonance response with comparable height and width has been found.

It has been found that the influence of c_T is too small to reduce the resonance peak to match the measured spectrum when the other damping parameters are low. This is probably caused by the large stiffness of k_T as has been described in appendix G.2.3. Therefore the contribution of this damping term will be neglected and c_T will be assumed to have its minimum value of 10^4 .

Order of magnitude

The load will mainly influence the height at the quasi static response and it will also affect the peak value and the wideness of the resonance peak at the base. The damping parameters will mainly influence the resonance peak. To take these 3 point into account, and to reduce the calculation time, 6 small areas have been selected to calibrate the load and damping parameters. The quasi static part is noticeable from 0.65 rad/s and continues to about 2,0 rad/s, where the wind loading spectrum has become zero (see 3.2.5). Area 1 and 2 take into account the influence of the load on this response. Area 3 and 6 take into account the width of the resonance peak and area 4 and 5 both take the height of the resonance peak into account.

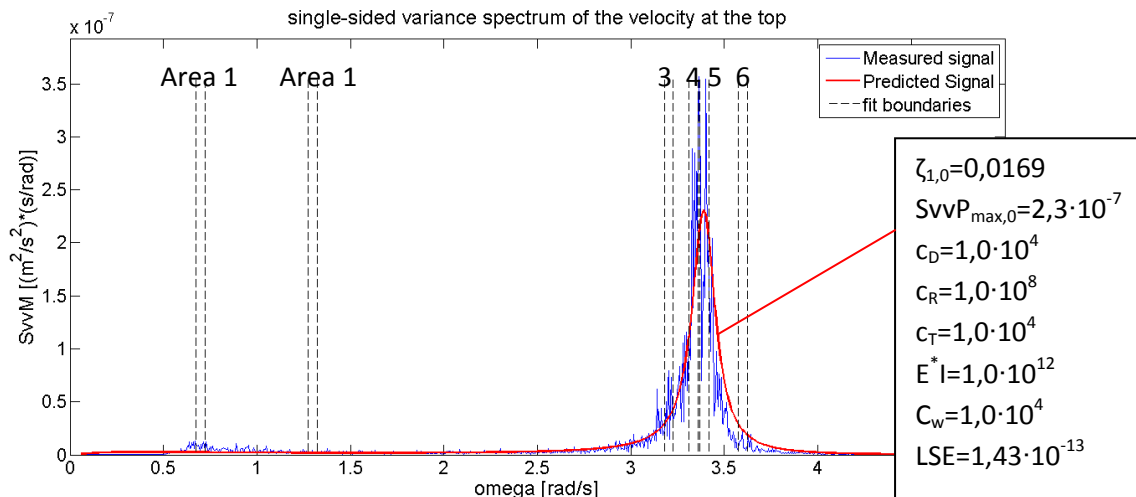


Figure 101 – predicted response from best fitted combination

The least square error has been calculated for combinations of the parameters in the following table. The combinations with the lowest error can be found in appendix M.1, Figure 101 is the best fit.

Table 21 – values used to create all combinations

c_D [Ns/m ²]	c_R [Nms/rad]	c_T [Ns/m]	E^*I [Nm ² s]	c_w [N ² /m ²]
1,00E+02	1,00E+04	1,00E+04	1,00E+04	1,00E+04
1,00E+03	1,00E+05	1,00E+04	1,00E+05	1,00E+05
1,00E+04	1,00E+06	1,00E+04	1,00E+06	1,00E+06
1,00E+05	etc.	etc.	etc.	1,00E+07
1,00E+06	1,00E+15	1,00E+04	1,00E+15	1,00E+08
5	12	1	12	5

When looking at the combinations with the lowest error it can be concluded that the load will have order of magnitude 10^4 . The other combinations (1-17) with low error also show some interesting aspects because three ranges can be distinguished. In each range, one of the three relevant damping parameters (c_D , c_R and E^*I) can vary a lot without influencing the result a lot. The upper values correspond with order of magnitude of the values that have already been found. (Figure 100)

Figure 102 – overview of the results for the combinations with the lowest error

	c_D [Ns/m ²]	c_R [Nms/rad]	c_T [Ns/m]	E^*I [Nm ² s]	C_w [N ² /m ²]	Δ Error
comb 1-8	10000	up to 10^{11}	10000	10^{11} or 10^{12}	10000	1-3%
comb 9-15	10000	10^{11}	10000	up to 10^{10}	10000	10-12%
comb 16-17	up to 1000	10^{11}	1,00E+04	10^{12}	1,00E+04	87-100%

Conclusion

The order of magnitude for the parameters that give the best fit has been derived:

Table 22 – order of magnitude for the parameters to obtain the best fit

c_D [Ns/m ²]	c_R [Nms/rad]	c_T [Ns/m]	E^*I [Nm ² s]	C_w [N ² /m ²]
1,00E+04	1,00E+11	-	1,00E+12	1,00E+04

7.3.4. Finer calibration

In order to find a better fit, the same procedure as in the last paragraph has been repeated, only now for values around the found order of magnitude. For each parameter 19 values have been assumed. For example for c_D these values are: $1 \cdot 10^3$, $2 \cdot 10^3$, $3 \cdot 10^3$, ... $8 \cdot 10^4$, $9 \cdot 10^4$. The error of each combination of these values has been calculated. The combinations with the error lower than the lowest error found with the rough calibration, can be found in appendix M.2. A better fit has been obtained, but the difference in error between the different combinations is much smaller. It can only be concluded that the load is most probably: $C_w=1.2 \cdot 10^4$ N²/m². Combinations with very different damping values have comparable errors, thus nothing can be concluded about the relative contribution of each damping source.

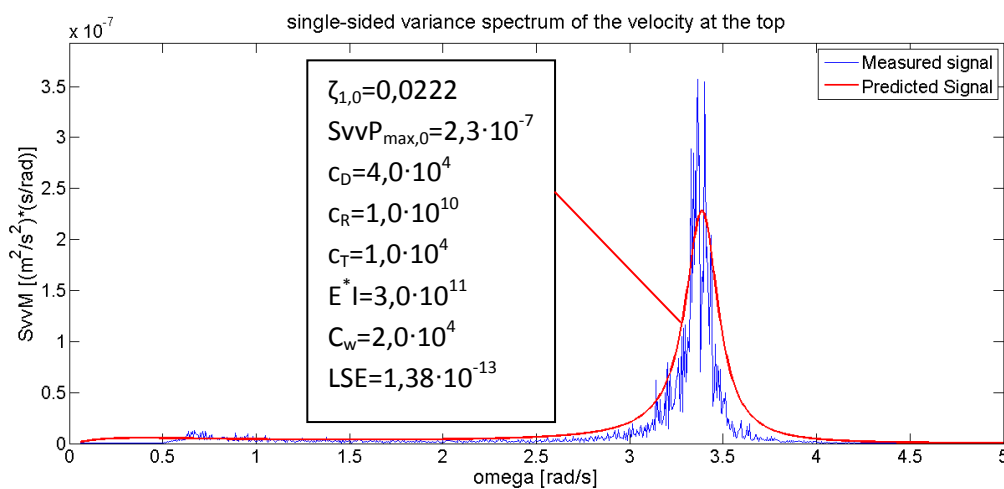


Figure 103 – best fitted spectrum obtained from finer calibration

7.4. Conclusion

Many different combinations of values for the three damping parameters can lead to a best fit. With a rough calibration method, the order of magnitude of the parameters has been determined and can be found in Table 22. These results are considered quite reliable because other combinations show a much larger error. A finer calibration method has indicated that the load is most probably $C_w=1\cdot 2\cdot 10^4$ N^2/m^2 , since the best fits have been obtained with these values.

However the relative contribution of each damping source to the total damping can't be determined from this method. Combinations with very different damping values have comparable errors. Thus the relative contribution of c_D , c_R and E^*I to the total damping can't be obtained.

The best fitted spectrum obtained from the finer calibration is even worse than obtained with the rough calibration. The base of the resonance peak is too wide because of $C_w=20000$. So actually the positions of the calibration areas need to be adapted such that this is solved. The load of the best fit will lie more close to 10000.

The relative contribution of each damping source to the total damping can't be determined from this model because c_D , c_R and E^*I influence the resonance peak in the same way and many different combinations can lead to a best fit.

8. Conclusions and recommendations

The results of the investigation of damping characteristics of high-rise buildings have been reported in the former chapters, this chapter contains the conclusions and recommendations based on these results. First the problem will be described to repeat the relevance of the obtained results.

8.1. Problem description

Traditionally the design of high-rise buildings is dominated by a restriction on the horizontal displacement under a peak wind velocity. However, the new generation of high-rise buildings will become higher and lighter, which makes them more vulnerable to wind-induced vibrations. As a consequence comfort criteria concerning accelerations will become more governing in the future design.

Damping is the most important parameter concerning the acceleration while it is the most uncertain parameter. Structural designers normally use the damping values for reinforced concrete and steel buildings that have been prescribed in the Eurocode (steel: $\delta=0,05$ / $\zeta=0,8\%$, concrete: $\delta=0,10$ / $\zeta=1,6\%$) but they are not aware that the actual damping values can deviate a lot (steel up to $\zeta=2-3\%$ and a minimum of 1,0% for concrete buildings). The uncertainty around the damping value can lead to a reduced factor of safety or an economical inefficient design. To solve this problem a better identification and prediction of damping is needed.

8.2. Conclusions

Investigation of damping from buildings all around the world, has revealed that multiple aspects can influence the damping. In general a downward trend is visible as damping is plotted against the height. At larger heights (>250 m), there seems to be a lower bound of 1% of damping. It has also been observed that the damping ratio of concrete buildings is higher than for steel buildings and the damping depends on the amplitude. This is in accordance with Jeary's theoretical model; the increase of damping at higher amplitudes can be explained by the activation of energy dissipation in more and smaller cracks at higher amplitudes.

Lagomarsino's formula gives an estimation of the damping based on the natural period and the building material. Based on the Japanese damping database (AIJ2000) the damping can be predicted by a formula that takes building material, building height and the amplitude dependency into account. But still many data points deviate a lot from the predicted line. It has been concluded that structural characteristics such as type and material of the main load bearing structure (MLBS), type of foundation and non structural fit-out are also aspects that will probably influence the amount of damping. To get a better estimation of the damping, the influences of these structural characteristics have been investigated by literature study. As the damping values of 11 Dutch buildings have been compared with their structural characteristics. The following has been concluded:

- Higher damping can be expected in buildings with a steel MLBS with bolted connections and in buildings with a concrete MLBS in which cast in-situ stabilizing elements have been combined with prefab elements. Probably more energy will be dissipated due to friction because in these systems, more relative movement between structural elements is possible.
- Also in buildings stabilized by rigid frames, higher damping can be expected than buildings stabilized by shear walls, a central core or a tube structure. This has been observed at the studied cases. This relation is also supported by a comparison between the damping of two

directions of one building where larger damping ratios have been observed in modes of vibration with significant ‘frame action’ in comparison with ‘cantilever/axial shortening action’. [Kijewski-Correa & Pirnia, 2007]

- Concerning the non structural fit out of the building, no clear relation between type, weight and material of the façade has been found. The amount of separation walls has little influence; slightly higher/lower damping ratios can be expected in buildings with many/few separation walls.
- Concerning radiation of energy to the underground, observations support the theoretical formula for rocking. The influence of the rocking ratio is a good explanation for the downward trend of the damping ratio with increasing slenderness of the building. The mass density of the structure seems to have a significant influence on the damping. Higher damping ratios have been observed at low mass density and lower damping ratios at higher mass density.

Three damping classes have been defined: a high, normal and low damping class. It is proposed to classify a building according to the following table and estimate the damping with the corresponding empirical fitted formula.

Table 23 –classification of a building

Main Load bearing Structure	Foundation	Non Structural Elements	Class	formula
steel structure with bolted braced/rigid frames	low rocking ratio (< 3,5)	many separation walls	high	$\zeta=3,24 \cdot (h/d)^{-0,31}$
(partly) prefabricated structure with rigid frames	low struct. Mass density (< 225 kg/m ³)			
other combinations			normal	$\zeta=2,32 \cdot (h/d)^{-0,22}$
cast in-situ, monolithic concrete, core/shear walls (coupled)	high rocking ratio (≥3,5) high struct. Mass density (≥ 225 kg/m ³)	few separation walls	low	$\zeta=1,76 \cdot (h/d)^{-0,31}$

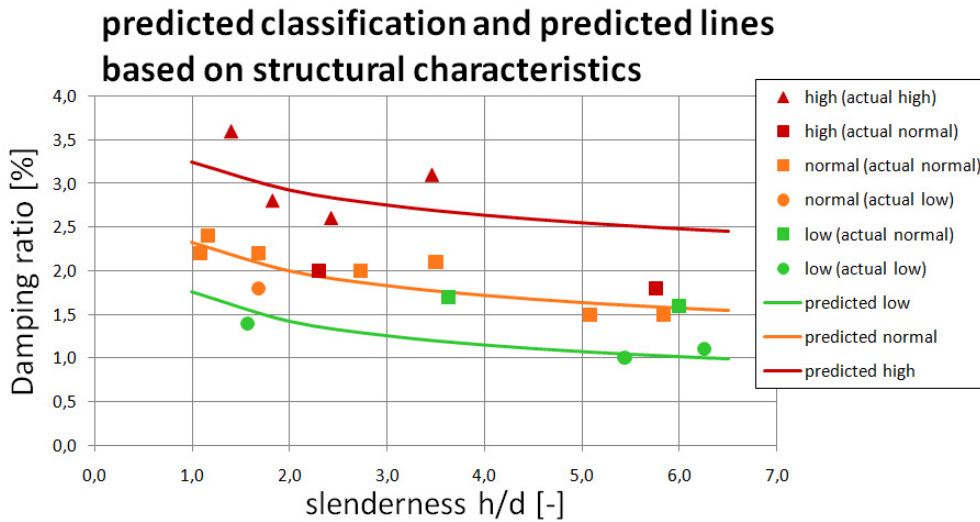


Figure 104 – predicted classification and line based on Table 13 in relation to the actual damping values

This method which gives a prediction based on structural characteristics (called vdBerg) gives a better prediction than other predictors. On average the empirical formula’s of Lagmarsino and AIJ2000 underestimate the damping (15% and 44%) while vdBerg on average doesn’t deviate ($\mu=1,0$ see Table 13). The difference is visualized in Figure 105.

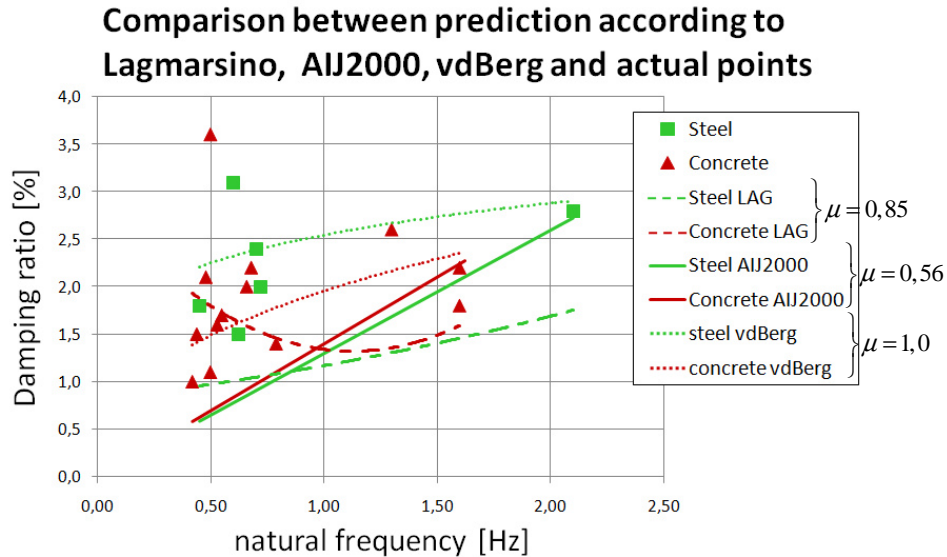


Figure 105 – predicted lines according to Lagmarsino, AIJ2000 (without amplitude dependency) and vdBerg (Table 13)

This investigation has given insight into the influence of diverse structural characteristics. Structural engineers can use Table 23 to estimate the damping. However the relations found between the structural characteristics and damping have to be used with care because they have been based on a very small database. The influence of purely one aspect has not been observed because higher/lower damping ratios are the result of a combination of multiple aspects. Also the influence of the amplitude has not been taken into account, because it has not been given at which amplitude the measured damping ratios have been obtained.

Model

A simple mathematical model has been developed to identify the amount of damping in different parts of the building. By comparison of the structural characteristics of many buildings with the found damping per part, structural characteristics can be linked to low/high values of damping in a specific part. With this information, the model can be used to optimize the design by a prediction of the total damping based on the damping of 4 parts.

In this model the building has been represented by an Euler Bernouilli beam with distributed mass (ρA) elastically supported at its base (k_T and k_R). The internal material damping in the MLBS (E^*), damping due to frictional forces between structural and non-structural elements (c_D) and damping in the foundation (c_R and c_T) have been represented by 4 viscous damping parameters. The beam is subjected to a load $q(z,t)$.

The damping and load parameters can be calibrated by comparison of the measured spectrum and the predicted spectra of the velocity at the top of the building (see Figure 106). The spectrum of the measured velocity signal can be obtained with the Fast Fourier Transform according to Welch’s method.

The magnitude of the variance of the wind load at time of measurement was unknown. Therefore only the shape of the wind loading spectrum according to Solari (F_D) has been adopted. This has to be multiplied with the aerodynamic admittance function and an unknown load parameter C_w to obtain the load spectrum. Via partial differential equations of the model and by making use of the Fourier transform, the transfer function can be obtained. This function depends on the unknown

parameters: c_D , c_R , c_T and E^*I . For many combinations of values for C_w , c_D , c_R , c_T and E^*I , the predicted spectrum can be obtained by multiplication of the load spectrum with the transfer function.

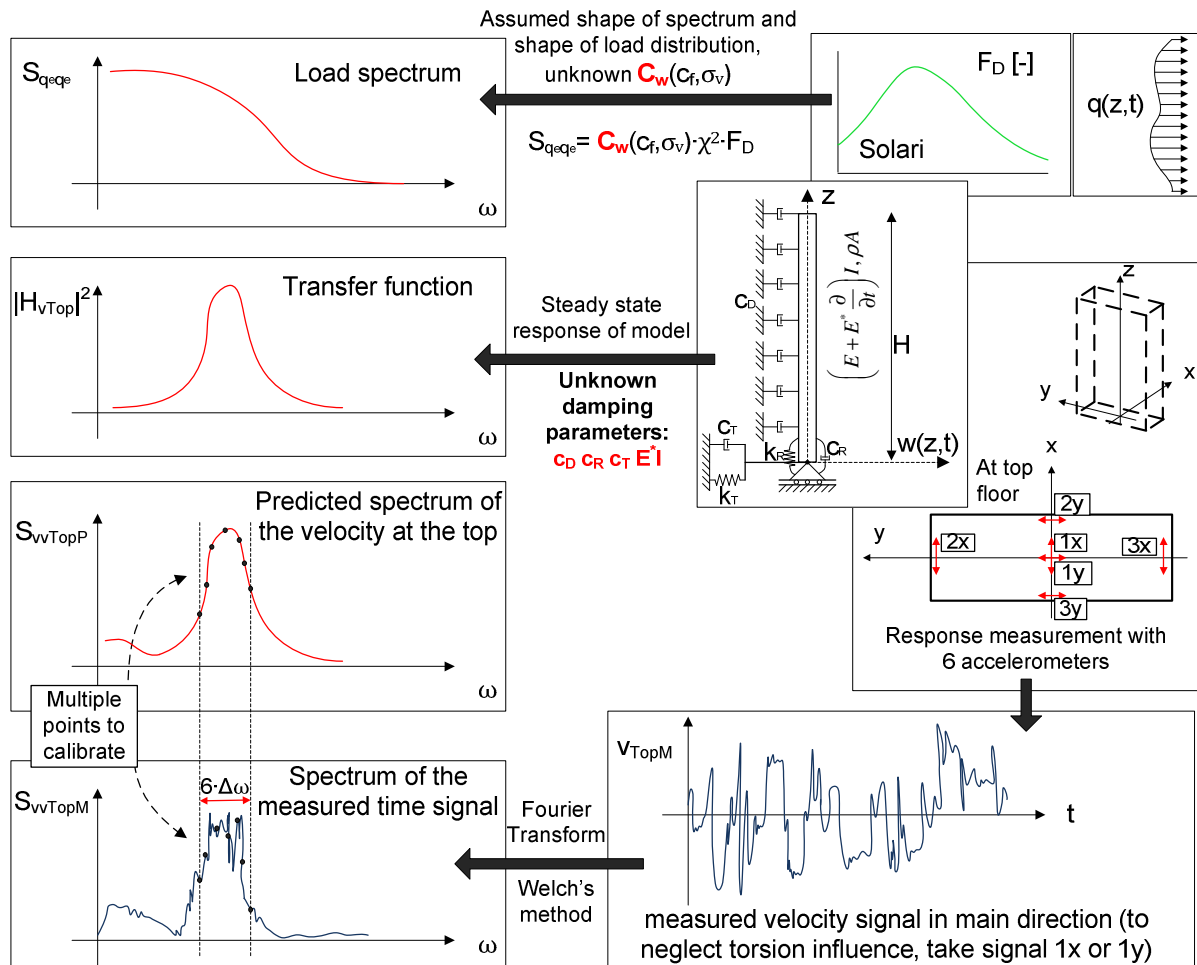


Figure 106 – overview of the method to obtain a spectrum of the predicted and measured velocity

Best fit values for C_w , c_D , c_R , c_T and E^*I can be found by taking the combination that gives the least square error between the predicted and measured spectrum at the quasi static peak and the resonance peak of the first natural frequency (see following figure)

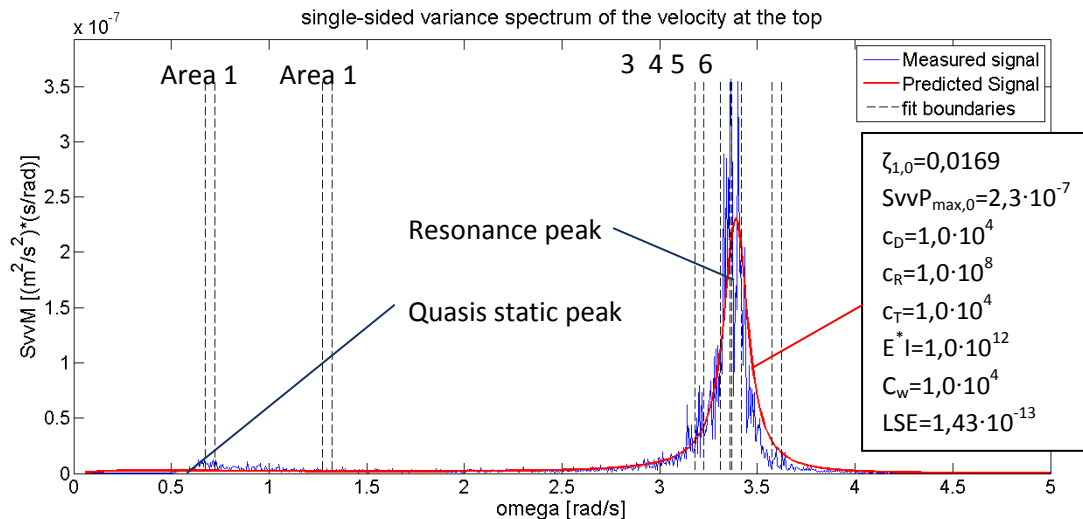


Figure 107 – predicted response from best fitted combination for the New EMC in x-direction

It is possible to give a reliable estimation of the load factor C_w but it is only possible to estimate the order of magnitude of the damping parameters. It has however been concluded that the influence of c_T can be neglected. The relative contribution of each damping source to the total damping can't be determined with this method because c_D , c_R and E^*I influence the resonance peak in the same way and many different combinations can lead to a best fit. The measured response at the top is insufficient to determine the contribution of each damping source with this model.

8.3. Recommendations

For the design of future high-rise building I recommend structural engineers to not simply use the prescribed damping values as given in the Eurocode. It is recommended to also estimate the damping with the empirical fitted formula of Lagomarsino, AIJ2000 and the proposed method based on structural characteristics (vdBerg). By comparing these values, it is up to the structural engineer to assume a damping value that leads to a safe and comfortable building.

For better identification of structural characteristics that are of influence and better prediction of damping, further verification of the proposed classification method and better calibration of the mathematical model is needed. Therefore especially the measurements need to be improved:

- More high-rise buildings need to be monitored.
- Especially the newest, most slender buildings must be monitored because they will give the best reference for the design of future high-rise buildings.
- It took a lot of research to gather information about the structural characteristics of buildings as is presented in Table 10 and Table 11. This information should always be gathered when a building is monitored and must be collected in a large damping database, to establish better relations between the structural characteristics and the damping.
- The amplitude dependency should always be determined when a building is monitored (for example with the random decrement technique). This allows comparison of damping values under equal amplitude conditions.
- In order to investigate the contribution of the non-structural elements to the total damping, the damping of the casco of the building and the finished building needs to be determined.

- It needs to be investigated if the contribution of damping in the foundation can be derived by comparison of the damping in modes of vibration with large and small rotation at the base. Therefore the rotation at the base needs to be monitored simultaneously with the response at the top. It has to be investigated if the response due to the second mode can be identified and used. It can be expected that the second mode shows less rotation at the base, but the resonance peak of the second natural frequency is very small.

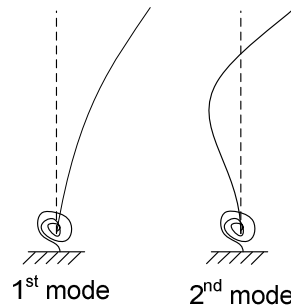


Figure 108 – larger rotation at the base in the first mode

- Besides the response, also the wind load needs to be monitored to diminish inaccuracy due to assumptions about the wind load.
- Because it takes a lot of time and money to perform measurements on full scale buildings, I also suggest to set up an investigation program with scale models of high-rise buildings. It must be possible to vary diverse structural characteristics in such model. The effect of one aspect can be determined by variation of one aspect, under equal circumstances.

Literature list

- Balendra, T. (1993). *Vibration of Buildings to Wind and Earthquake Loads*. London: Springer-Verlag.
- Bam & Ballast_Nedam (2012). *De Nieuwbouw in 4 Dimensies (Film)* Retrieved 10-03-2012, from <http://www.erasmusmc.nl/nieuwbouw/>
- Blaauwendraad, J. (2006). *Plate Analysis, Theory and Application, Lecture Notes Ct4180*. Delft: Faculty of Civil Engineering and Geosciences.
- Ellis, B.R. (1996). *Full-Scale Measurements of the Dynamic Characteristics of Buildings in the UK*. *Journal of Wind Engineering and Industrial Aerodynamics*, 59, 35-382.
- Fu, J.Y., Li, Q.S., Wu, J.R., Xiao, Y.Q. & Song, L.L. (2008). *Field Measurements of Boundary Layer Wind Characteristics and Wind-Induced Responses of Super Tall Buildings*. *Journal of Wind engineering and Industrial Aerodynamics*, 96, 1332-1358.
- Galanti, F.M.B. & Oostvogels, J.M.J. (2006). *Metingen Van De Beweging Van Twee Hoge Gebouwen Bij Wind: TNO bouw en ondergrond*.
- Hansen, J. (2011). *Fft Tutorial* Retrieved 12-02-2012, from <http://www.ele.uri.edu/courses/ele436/labs/fft.pdf>
- Hayden, T. (2009). *Crowding Our Planet, . National Geographic: earth pulse, a visual almanac*.
- Hoenderkamp, J.C.D. (2007). *High-Rise Structures, Preliminary Design for Lateral Load*. Eindhoven: TUEindhoven.
- Jeary, A.P. (1986). *Damping in Tall Buildings - a Mechanism and a Predictor*. *Earthquake engineering and structural dynamics*, 14, 733-750.
- Jeary, A.P. (1996). *The Description and Measurement of Nonlinear Damping in Structures*. *Journal of Wind Engineering and Industrial Aerodynamics*, 59, 103-104.
- Jeary, A.P. (1997). *Designer's Guide to the Dynamic Response of Structures*. London: E & FN Spon.
- Kijewski-Correa, T. & Pirnia, J.D. (2007). *Dynamic Behavior of Tall Buildings under Wind: Insight from Full Scale Monitoring*. *The Structural Design of Tall and Special buildings*, 16, 471-486.
- KNMI (2011). *Uurgegevens Van Het Weer in Nederland, Rotterdam, 06-09-2011, 18:00* Retrieved 07-10-2011, from http://www.knmi.nl/klimatologie/uurgegevens/select_uur.cgi?language=nl
- Koten, H. van (1977). *Cur Rapport 75, Demping Van Bouwconstructies: TNO*.
- Li, Q.S., Fang, J.Q., Jeary, A.P. & Wong, C.K. (1998). *Full Scale Measurements of Wind Effects on Tall Buildings*. *Journal of Wind Engineering and Industrial Aerodynamics*, 74-76, 741-750.
- Li, Q.S., Wu, J.R., Liang, S.G., Xiao, Y.Q. & Wong, C.K. (2004). *Full-Scale Measurements and Numerical Evaluation of Wind-Induced Vibration of a 63-Story Reinforced Concrete Tall Building*. *Engineering structures*, 26, 1779-1794.
- Lijst Van Hoogste Gebouwen Ter Wereld* (2012). Retrieved 20-01-2012, from http://nl.wikipedia.org/wiki/Lijst_van_hoogste_gebouwen_ter_wereld
- Marukawa, H., Kato, N., Fujii, K. & Tamura, Y. (1996). *Experimental Evaluation of Aerodynamic Damping of Tall Buildings*. *Journal of Wind Engineering and Industrial Aerodynamics*, 177-190.
- Metrikine, A. *Dynamics, Slender Structures and an Introduction to Continuum Mechanics, Lecture Notes Ct4145*. Delft: Faculty of Civil Engineering and Geosciences.
- NNI (2005). *Nen-En 1991-1-4: General Actions - Wind Actions*. Delft.
- NNI (2007). *Nen-En 1991-1-4/Nb: General Actions - Wind Actions*. Delft.
- Oosterhout, G.P.C. van (1996). *Thesis: Wind-Induced Dynamic Behaviour of Tall Buildings*. TUDelft, Delft.
- Oosterhout, G.P.C. van & Geurts, C.P.W. (2001). *Trillingen En Hoogbouw: Comfort En Demping. cement, 2001-2, 73-75*.
- Ruijter, J.J. de & Splinter, H. (2009). *Nieuwbouw Erasmus Mc, Rotterdam Tranche 1, Oost, Hoogbouw: Aronsohn Constructies raadgevene ingenieurs B.V.*

- Salemans, J.W.M. & Hartman, A.D. (2009). *Nieuwbouw Erasmus Medisch Centrum: Geotechnisch Advies*: Deltares.
- Satake, N., Suda, K., Arakawa, T., Sasaki, A. & Tamura, Y. (2003). *Damping Evaluation Using Full-Scale Data of Buildings in Japan*. *Journal of structural engineering*, 470-477.
- Simone, A. (2009). *An Introduction to the Analysis of Slender Structures, Lecture Notes Ct4190*. Delft: Faculty of Civil Engineering and Geosciences.
- Smith, B.S. & Coull, A. (1991). *Tall Building Structures, Analysis and Design*: John Wiley & sons, inc.
- Smith, R.J., Merello, R. & Willford, M. (2010). *Intrinsic and Supplementary Damping in Tall Buildings. Structures and Buildings*, 163(SB2), 111-118.
- Smith, R.J. & Willford, M.R. (2008). *Damped Outriggers for Tall Buildings. The Arup Journal*, 3, 15-21.
- Spijkers, J.M.J., Vrouwenvelder, A.C.W.M. & Klaver, E.C. (2005). *Structural Dynamics, Part 1: Structural Vibrations. Lectures Notes Ct4140*. Delft: Faculty of Civil Engineering and Geosciences.
- Splinter, B. (2012) [Personal Communication].
- Steenbergen, R.D.J.M. & Geurts, C.P.W. (2011). *Praktische Handvatten Voor Eigenfrequentie. Bouwen met staal*, 219, 46-47.
- Tamura, Y. (2005). *Lecture 10: Damping in Buildings [Lecture Slides]* Retrieved 02-08-2011, 2011, from http://www.wind.arch.t-kougei.ac.jp/info_center/ITcontent/tamura/10.pdf
- Taranath, B.S. (1998). *Steel, Concrete and Composite Design of Tall Buildings*: Mc graw Hill.
- Tolsma, K. (2010). *Precast Concrete Cores in High-Rise Buildings*. TU Delft.
- Vrouwenvelder, A.C.W.M. (2004). *Random Vibrations, Lecture Notes Ct5145*: Faculty of Civil Engineering and Geosciences.
- Vrouwenvelder, A.C.W.M. & Geurts, C.P.W. (2006). *Dynamica, Windbelasting En Voorschriften. Cement*, 2006-1, 20-24.
- Watanabe, Y., Isyumov, N. & Davenport, A.G. (1997). *Empirical Aerodynamic Damping Function for Tall Buildings. Journal of Wind Engineering and Industrial Aerodynamics*, 72, 313-321.
- Welch, P.D. (1967). *The Use of Fast Fourier Transform for the Estimation of Power Spectra: A Method Based on Time Averaging over Short, Modified Periodograms. IEEE Trans. Audio and electroacoust*, AU-15, 70-73.
- Woudenberg, I.A.R. & Vambersky, J.N.J.A. (2003). *Windbelasting Hoogbouw En Regelgeving. Cement*, 2003-6, 89-94.

